Mechanics and Dynamics of Liposomes and Cells Studied by QCM and ECIS

Dissertation zur Erlangung des Grades
"Doktor der Naturwissenschaften"

am Fachbereich

Chemie, Pharmazie und Geowissenschaften

der Johannes Gutenberg-Universität in Mainz

vorgelegt von

Angelika Sapper

geboren in Fulda

Mainz, 2006

Dekan:	Prof. Dr. Langguth
1. Berichterstatter:	Prof. Dr. A. Janshoff
2. Berichterstatter:	HD Dr. M. Maskos

Tag der mündlichen Prüfung: 24. Juli 2006

Meiner Mutter

Der Weg ist das Ziel.

(*Konfuzius)*

Contents

Introduction

Locomotion is a fundamental and fascinating property of cells and essential for all kind of life. Cell motility plays a central role in a variety of biological processes, including embryonic development and woundhealing, tissue maintaince, and immune system functions in the adult animal.[1] But it is also associated with many diseases such as metastatic cancer, neurological birth defect and arthritis. Investigations into this highly complex field of cell migration are not only important for basic research, but also significant to the clinical sector as invasive and metastatic behavior of malignant cells is the major cause of mortality in all cancer patients. An important prerequisite for cell movement is cell attachment, in which the cytoskeleton connects across the plasma membrane to the substratum. Cell attachment attributes to the so called focal adhesion complexes and is mediated by integrins, the major family of cell surface adhesion receptors. As cell-substrate interactions play a pivotal role in cell movements surface-physical techniques are well suited tools to investigate cell motility. Several recent studies showed that quartz crystal microbalance (QCM),[2, 3, 4, 5, 6, 7, 8] electrical cell-substrate impedance sensing (ECIS)[9, 10, 11, 12] and optical methods[13, 14, 15, 16, 17] are powerful tools to monitor the kinetics of cell attachment. However, detection of fluctuations in cell shape requires a more sensitive device. Only a few studies based on optical methods has picked up cell shape fluctuations in the area of the cell-to-substrate adhesion,[18, 19] while ECIS has demonstrated sufficient sensitivity to detect so-called micromotion of cells with a time resolution of 1 second.[20, 21, 22]

The objective of this study was the establishment of a new approach to gauge the dynamics of adherent cells by measuring the fluctuations that are imposed on the resonance frequency of a thickness shear mode (TSM) resonator that is covered by a monolayer of cells. The dynamic behavior of cells is mainly determined by the dynamic properties of the cytoskeleton. This cellular "scaffold" contains actin filaments, microtubules and intermediate filaments. Hence, interfering with actin polymerization and the dynamic instability of microtubules results in changes of cell motility.[23] From

this point of view, QCM-based fluctuation measurements were scrutinized whether the new method provides sufficient sensitivity to observe alterations in cell motility due to specific changes of the cytoskeleton. Besides the effects of cytoskeleton-interacting drugs the impact of osmotic stress, changes of the metabolic rate and the activation of integrin-induced transmembrane signals to cell motility were examined.

Ultimately the new technology would enable a direct quantification of the motility of tumor cells derived from biopsy material. With respect to this aspect the motility of two pancreatic carcinoma cell lines (derived from the same original tumor, but known to possess different metastatic potential) were studied.

Results gained from QCM-based frequency fluctuation measurements were compared with resistance fluctuations obtained from ECIS analysis. As the origin of QCM-based signal differs from the source of ECIS-based signal, combination of the two methods provides complementary information about the dynamics of adherent cells.

Among other things, the observed dynamics of cells are related to surface undulation of the plasma membrane. Several recent studies reported about this "flickering" phenomenon in erythrocytes[18] and lymphocytes, monocytes, fibroblast and cardiomyocytes.[24] In order to reduce the manifold interactions of the complex biological structure it is useful to imitate the plasma membrane by artificial systems like simple lipid bilayers.

From this point of view dynamics of giant unilamellar vesicles were studied by QCM and ECIS measurements. The aspiration of this investigations was the quantification of liposome adsorption as well as the detection of shape fluctuations and electrically induced deformation of giant unilamellar vesicles. Those measurements permit the determination of elastic properties of lipid bilayers, which are extremely soft with respect to bending but essential incompressible under lateral tension. Furthermore, the combination of ECIS-based adsorption measurements and dynamic Monte Carlo Simulations allows to estimate the rate constant of vesicle adsorption.

Bibliography

[1] Alberts, B.; Johnson, A.; Lewis, J.; Raff, M.; Roberts, K.; Walter, P. *Molecular Biology of the Cell* Garland Science 2002.

[2] Wegener, J.; Seebach, J.; Janshoff, A.; Galla, H.-J. *Biophys. J.* 2000, 78, 2821-2833.

[3] Wegener, J.; Janshoff, A.; Galla, H.-J. *Eur. Biophys. J.* 1998, 28, 26-37.

[4] Reiss, B.; Janshoff, A.; Steinem, C.; Seebach, J.; Wegener, J. *Langmuir* 2003, 19, 1816-1823.

[5] Marx, K. A.; Zhou, T.; Montrone, A.; Schulze, H.; Braunhut, S. *Biosensors and Bioelectronics* 2001, 16, 773-782.

[6] Marx, K. A.; Zhou, T.; Warren, B.; Braunhut, S. *Biotechnol. Prog.* 2003, 19, 987-999.

[7] Rodahl, M.; Höök, F.; Fredriksson, C.; Keller, C. A.; Krozer, A.; Brzezinski, P.; Voinova, M.; Kasemo, B. *Faraday Discuss.* 1997, 107, 229-246.

[8] Fredriksson, C.; Kihlman, S.; Rodahl, M.; Kasemo, B. *Langmuir* 1998, 14, 248-251.

[9] Wegener, J.; Keese, C. R.; Giaever, I. *Exp. Cell Res.* 2000, 259, 158-166.

[10] Lo, C.-M.; Keese, C. R.; Giaever, I. *Biophys. J.* 1995, 69, 2800-2807.

[11] Lo, C.-M.; Ferrier, J. *Phys. Rev. E* 1998, 57, 6982-6987.

[12] Lo, C.-M.; Keese, C. R.; Giaever, I. *Exp. Cell Res.* 1999, 250, 576-580.

[13] Gingell, D.; Heavens, O. *J. Microsc.* 1996, 182, 141-148.

[14] Todd, I.; Mellor, J. S.; Gingell, D. *J. Cell Sci.* 1988, 89, 107-114.

[15] Marchi-Artzner, V.; Lorz, B.; Hellerer, U.; Kantlehner, M.; Kessler, H.; Sackmann, E. *Chemistry* 2001, 7, 1095-1101.

[16] Parak, W. J.; Domke, J.; George, M.; Kardinal, A.; Radmacher, M.; Gaub, H. E.; de Roos, A. D.; Theuvenet, A. P., Wiegand, G.; Sackmann, E.; Behrends, J. C. *Biophys. J.* 1999, 76, 1659-1667.

[17] Giebel, K.-F.; Bechinger, C.; Herminghaus, S.; Riedel, M.; Leiderer, P.; Weiland, U.; Bastmeyer, M. *Biophys. J.* 1999, 76, 509-516.

[18] Fricke, K.; Sackmann, E. *Biochem. Biophys. Acta* 1984, 803, 145-152.

[19] Geggier, P.; Fuhr, G. *Appl. Phys. A* 1999, 68, 505-513.

[20] Lo, C.-M.; Keese, C. R.; Giaever, I. *Exp. Cell Res.* 1993, 204, 102-109.

[21] Pei, Z.; Keese, C. R.; Giaever, I.; Kurzawa, H.; Wilson, D. E. *Exp. Cell Res.* 1994, 212, 225-229.

[22] Giaever, I.; Keese, C. R. *Proc. Natl. Acad. Sci. USA* 1991, 88, 7896-7900.

[23] Ballestrem, C.; Wehrle-Haller, B.; Hinz, B.; Imhof, B. A. *Mol. Biol. Cell* 2000, 11, 2999-3012.

[24] Krol, A. Y.; Grinfeldt, M. G.; Levin, S. V.; Smilgavichus, A. D. *Eur. Biophys. J.* 1990, 19, 93-99.

Chapter 1

Biological Systems

1.1 Biological Cells

The smallest viable, breeding unit is the biological cell. Each cell stems from another cell.[1] The sentence is of universal validity and is among the few dogmata of biology. Some organisms, such as bacteria, consist of a single cell. Besides those unicellular organism, multicellular organisms contain as many as trillion and more cells. The human corpus, for example consists of more than 10^{14} cells, with a typical cell size of 10 μm and a typical cell mass of 1 nanogram. Each cell of an organism is somewhat self-maintaining and self-contained and serves several abilities, such as cell division (mitosis or meiosis), metabolism, traffic of vesicles and response to external and internal stimuli.

There are two cell types, prokaryotic and eukaryotic cells. Prokaryotic cells are mostly found in bacteria and archaea, while eukaryotic cells mostly form multicellular organism. Eukaryotic cells are about 10 times the size of a typical prokaryotic cell. The major difference, however, between the two cell types is that in eukaryotic cells the genotype is stored in the nucleus, while in prokaryotic cells the DNA is formed to a plasmid laying in the cytoplasm. Table 1.1 summarizes the differences between prokaryotic and eukaryotic cells.

1.1.1 Subcellular Components

A basic characteristic of a living cell, whether prokaryotic or eukaryotic, is the cell membrane, forming a semipermeable barrier, which on the one hand shields the interior of the cell from the exterior and on the other hand realizes

[1] "Omnis cellula e cellula" R. Virchow, 1855

	Prokaryotes	Eukaryotes
Typical organism	bacteria, archaea	fungi, plants, animals
Typical size	$\sim 1 - 10\ \mu m$	$\sim 10 - 100\ \mu m$
Type of nucleus	no real nucleus; nucleoid region	real nucleus with double membrane
DNA	circular	linear molecules (chromosomes) with histone proteins
RNA-/protein-synthesis	coupled in cytoplasm	RNA-synthesis inside the nucleus protein-synthesis in cytoplasm
Ribosomes	50S+30S	60S+40S
Cytoplasmatic structure	very few	highly structured by endo-membranes and cytoskeleton
Cell movement	flagella	flagella and cilia
Mitochondria	none	one to several dozen
Chloroplast	none	in plants and algae
Organization	usually single cells	single cells, colonies, higher multicellular organism
Cell division	binary fission	Mitosis and Meiosis
Cell cycle	none	existing

Table 1.1: Comparison of features of prokaryotic and aukaryotic cells. S is the sedimentation-coefficient.

controlled metabolism pathway and maintains the electric potential of the cell. This membrane is formed by a double layer of lipids and hydrophilic molecules. Embedded within this membrane are various other molecules such as proteins which are acting as channels and pumps.

Inside, the cell is filled with a salty, colorless, mucous cytoplasm, which takes up the most cell volume. The shape of the cell is organized and maintained by the cytoskeleton, an important, complex and dynamic cell component, consisting of microfilaments. Additionally, the cytoskeleton is responsible for the movement of the whole cell and further for the movement and the transport inside the cell. Each cell contains desoxyribonucleinacid (DNA), which offers the genotype of the cell, and ribonucleinacid (RNA), which is necessary to build proteins and enzymes. Furthermore cells possess various organelles, that maintain its vital functions. Figure 1.1A shows a schematic drawing of an eukaryote with its various organelles while figure 1.1B illustrates the much simpler structure of a prokaryotic cell.

The nucleus, where almost all DNA replication and RNA synthesis occur, is the information center of eukaryotic cells containing the DNA. It is

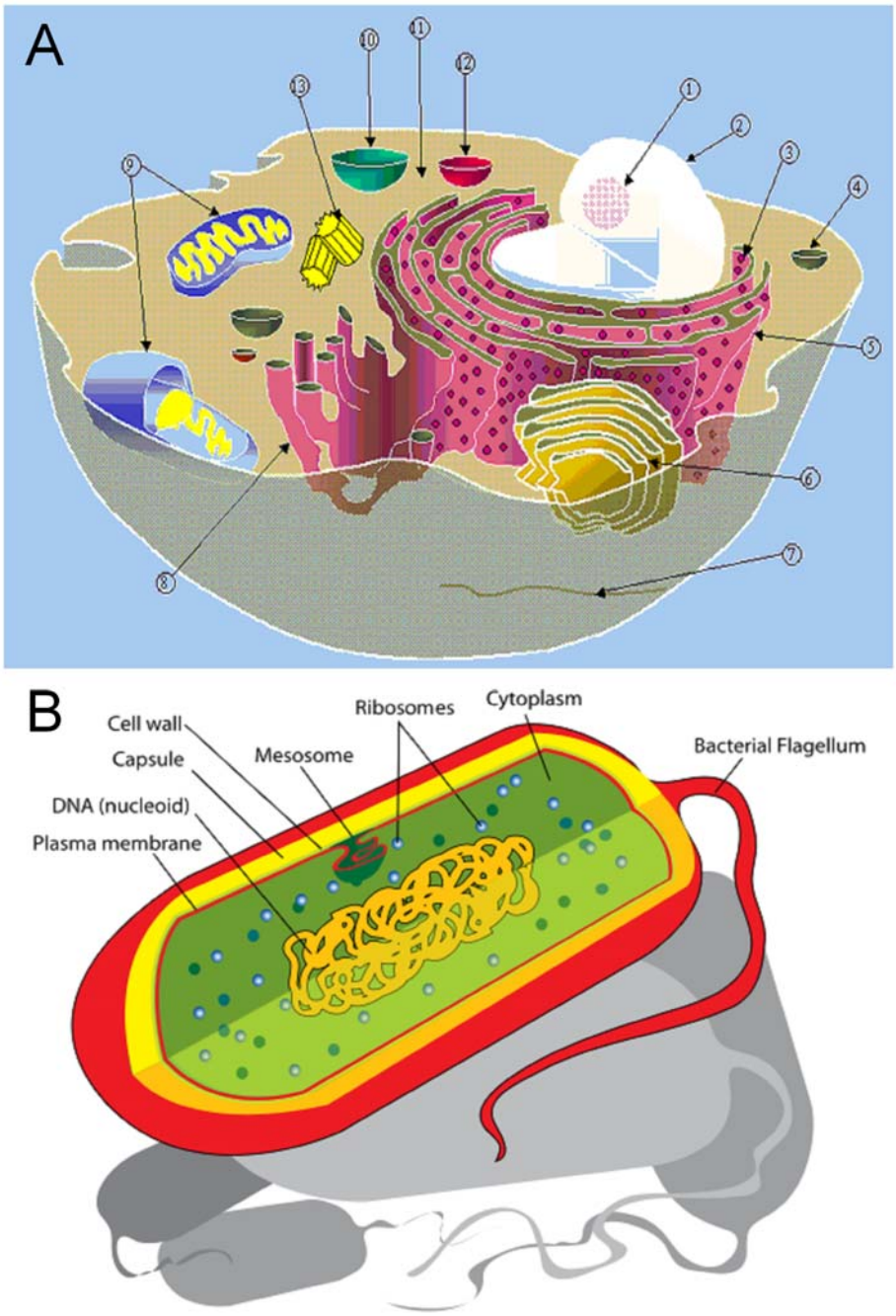

Figure 1.1: Schematic drawing of a typical animal cell (A) and a prokaryote (B). Subcellular components of the eukaryote (A): (1) nucleolus, (2) nucleus, (3) ribosome, (4) vesicle, (5) rough endoplasmic reticulum (ER), (6) Golgi apparatus, (7) cytoskeleton, (8) smooth ER, (9) mitochondria, (10) vacuole, (11) cytoplasm, (12) lysosome, (13) cenrioles.

enveloped by a double membrane, which was built in the endoplasmic reticulum. Like the cell membrane the envelope of the nucleus is semipermeable, thus it's permeable for RNA and macromolecules but not for the much larger DNA. Prokaryotes have no distinct nuclear compartment to house their DNA. The power generators of the cells are mitochondria and chloroplast, which generate energy by oxidizing organic substances (mitochondria) or by using solar energy (chloroplast). Protein synthesis takes place in ribosomes, which occurs hundred or thousand fold in cells due to the importance of protein synthesis. They are embedded in the endoplasmic reticulum (ER), which forms together with the Golgi apparatus the macromolecule manager. The ER is the transport network for molecules targeted for certain modification and specific destinations, while the Golgi apparatus delivers proteins to the organelles. The cellular digestive system is formed by peroxisomes and lysosomes, which contain more than three dozen enzymes for degrading proteins, nucleic acids, and polysaccharides. Food, waste and water is stored in vacuoles. Centrioles help in the formation of the mitotic apparatus and are found in animal cells as well as in some fungi and algae cells.

1.1.2 The Eukaryotic Cytoskeleton

The cytoskeleton is the cellular "scaffold", consisting of dynamic, thin, protein filaments, contained within the cytoplasm and attached to the plasma membrane. This dynamic filament network is responsible for the mechanic stability and the shape of the cell. Furthermore, the cytoskeleton is important for the active movement of the whole cell as well as the movement and transport inside the cell. Figure 1.2 shows an eukaryotic cytoskeleton. Although the complex system of protein filaments is called "cell skeleton", it can be considered as an extremely flexible network, containing three kinds of cytoskeletal filaments: actin filaments, microtubules and intermediate filaments (figure 1.3). However, the three cytoskeleton filaments would be ineffective on their own. A set of accessory proteins, that control assembly of the filaments, and motor proteins, that either move organelles along the filaments or move the filaments themselves, is essential for the usefulness of the cytoskeleton.

Actin Filaments

Actin filaments, also known as microfilaments, are two-stranded helical polymers of the protein actin, with a diameter of 7 nm, being in a dynamic state of polymerization and depolymerization of globular g-actin (figure 1.3A). They are mostly concentrated beneath the plasma membrane, as they maintain cel-

lular shape, form cytoplasmatic protuberances (like microvilli and pseudopodia), hold membrane-spanning proteins in their place and participate in some cell-to-cell or cell-to-matrix junctions. Furthermore the interaction of actin and it's motorprotein myosin provides the mechanism of muscle contraction.

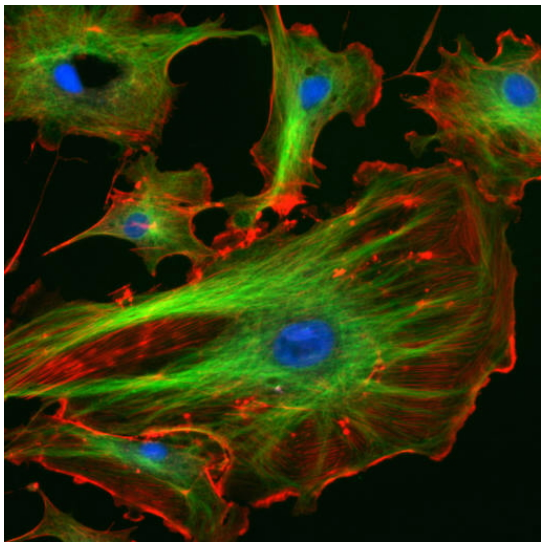

Figure 1.2: The eukaryotic cytoskeleton. Actin filaments are shown in red, microtubules in green, and the nuclei are in blue.[1]

Microtubules

Microtubules are long hollow cylinders of about 25 nm, formed by 13 protofilaments which are polymers of alpha and beta tubulin (figure 1.3B). They are much more rigid than actin filaments. However, microtubules possess a dynamic instability, i.e. individual microtubules exhibit alternating phases of elongation and rapid shortening. These long and straight bundles of protofilaments are organized by a single microtubule-organizing center (MTOC), also know as centrosome, where one end of each microtubule is attached. Together with the motor proteins dynein and kinesin, microtubules are responsible for intracellular transport of organelles like vesicles or mitochondria. Furthermore, microtubules can quickly rearrange themselves to form bipolar mitotic spindle during cell division and form motile whips called cilia and flagella on the surface of the cell.

Intermediate Filaments

Intermediate filaments, 8 - 10 nm in diameter, are ropelike fibers made of intermediate filament proteins, which constitute a large and heterogeneous family (figure 1.3C). As intermediate filaments are more stable than actin filaments and microtubules, they act mainly as a mechanic support for the cell. Furthermore, they play a role in some cell-cell and cell-matrix junctions. In epithelial cells, for example, they span the cytoplasm from one cell-cell junction to another, thereby strengthening the entire epithelium. Different intermediate filaments exist, one type is made of vimentins, being the common structural support of many cells. Other types are made of keratin, found in hair, nails and skin cells, or of laminin, giving structural support to the nuclear envelope.

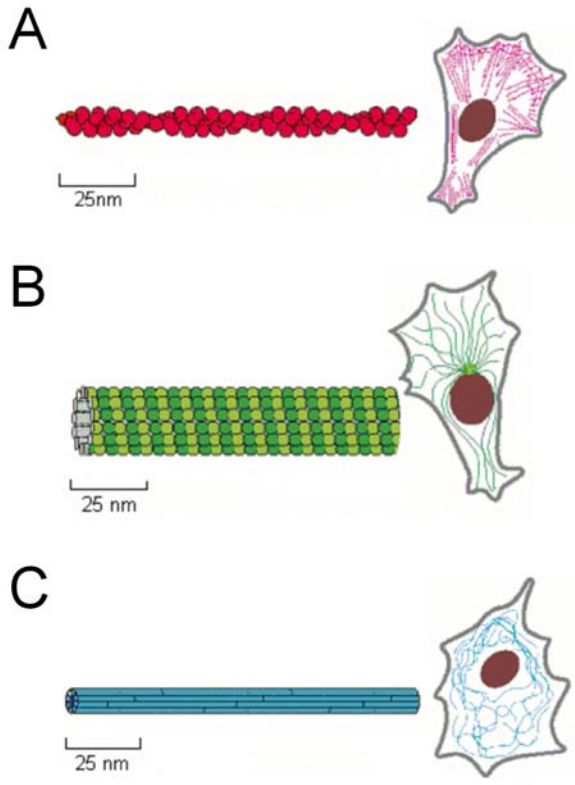

Figure 1.3: The three major types of protein filaments that form the cytoskeleton. *(A)* Actin filaments. *(B)* Microtubules. *(C)* Intermediate filaments.[2]

1.1.3 Cell Mechanics

An essential property of cells is their ability to sense mechanical signals and transduce them into biological response. So, it is well established that mechanically induced alteration of cell shape effect several cellular functions including locomotion, growth differentiation and proliferation. During the last decade many studies reported that the cytoskeleton plays a pivotal role in transmitting mechanic stress from cell surface, across the cytoplasm and into the nucleus.[3, 4] Thus various types of models of cytoskeleton mechanics were introduced like *open cell foams*, *the cortical membrane model* or *tensed cable networks.*[6, 5] The latter is most appropriate to describe the central role of the cytoskeleton prestress in determining the behavior of adherent cells at the steady state. This internal prestress, which is analogous to the stress within a tensed bow, is found in all living cells.

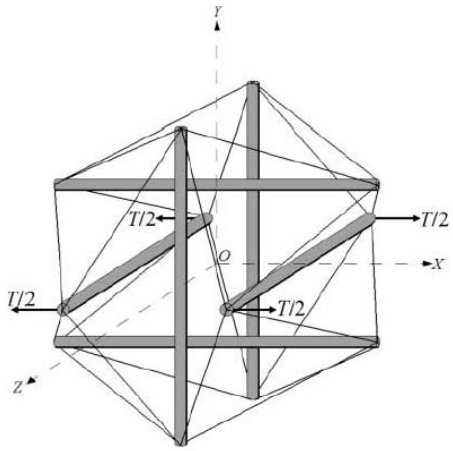

Figure 1.4: A six-strut tensigrity model. The cables (thin lines) carry pre-existing tension that is balanced by compression in the struts (gray columns).[6]

A special case of the *tensed cable networks* is the *tensigrity model* which is composed of tensile elements (cables) as well as compressive elements (struts), which balance tension in the cables (figure 1.4). This model is suitable as a description of actin filament, microtubules and intermediate filaments. In adherent cells, actin filaments and intermediate filaments exist as tensile elements whereas microtubules and thick, cross-linked actin bundles are envisioned as compression elements.

1.1.4 Cell Motility

When Anthony van Leeuwenhoek, in 1674, looked through a glass bead that served him as a simple microscope, at a drop of water from a pool, he was astonished about the small particles moving in the fluid.[2] Leeuwenhoek saw probably ciliated protozoa swimming by the agitated, but coordinated motion of thousands of hairlike cilia on their surface. Later, it was found out, that Leeuwenhoek observed an exception, thus most cells crawl upon surfaces as for example in animals all cells crawl, excluding sperms. The most prominent crawling cell are amoeba and listeria monocytogenes. Cell crawling plays an important role in many fields like the embryonic development and also in wound healing, tissue maintenance and immune system functions in the adult animal. Besides these benefits of cell crawling, the motility of cells provides a disadvantage with regard to the spreading of cancer cells from an initial focal tumor to multiple sites within the body. As most of the cells crawl and only a view cell types, like protozoas and sperms, have the ability to swim, the following section gives a brief overview about the complex mechanism of cell crawling.

Cell Crawling

The complex process of cell crawling, which depends on the actin-rich cortex beneath the plasma membrane, comprises three different activities: protrusion, in which actin-rich structures are pushed out at the front of the cell, attachment, in which the cytoskeleton bonds to the substratum via the plasma membrane and traction, in which the retracing cytoplasm is pulled forward.

Figure 1.5 depicts a model of cell crawling over a surface. At the plus end, i.e. the leading edge of the cell, the lamellipodium is protruded by actin polymerization (the newly polymerized cortical actin is shown in red), thus the edge moves forward (green arrows at front) and the actin cortex gets stretched. At the rear of the cell, contraction moves the cell forward (green arrow at the back) to relax some of the tension. Due to the protrusion of lamellipodium, new focal contacts, containing integrins, are produced at the plus end, while focal contacts at the rear of the cell are disassembled as the cell crawls forward. Repetition of the distinct steps makes the cell move forward in a stepwise fashion. Otherwise the cell can move forward smoothly, glide over the surface, when the steps are tightly coordinated.

As shown in figure 1.5 protrusion is driven by actin polymerization, pushing the plasma membrane outward. The structure of the protrusion depends

[2] He wrote:"...the motion of these animalcules in the water was so swift and various, upwards, downwards and round about, that 'twas wonderful to see..."

on the cell type, as there are filopodia, lamellipodia and pseudopodia. All three structures are filled with filamentous actin, which excludes membrane-enclosed organelles. Filopodia, lamellipodia and pseudopodia differ mainly in the way the actin filaments are organized, simply spoken, filopodia are one-dimensional, lamellipodia are two-dimensional and pseudopodia are three-dimensional. Filopodia containing a core of long, bundled actin filaments are formed by migrating growth cones and some types of fibroblasts. Epithelial cells, fibroblasts and some neurons generate the two-dimensional sheet-like structure of lamellipodia. Pseudopodia, generated by amoebae and neutrophils, are three-dimensional projections filled with an actin filament gel. Due to the two-dimensional appearance, lamellipodia are easier to observe in living cells than the two other structures, thus we know more about the dynamic structure and protrusion mechanism of lamellipodia than we do for either filopodia or pseudopodia.

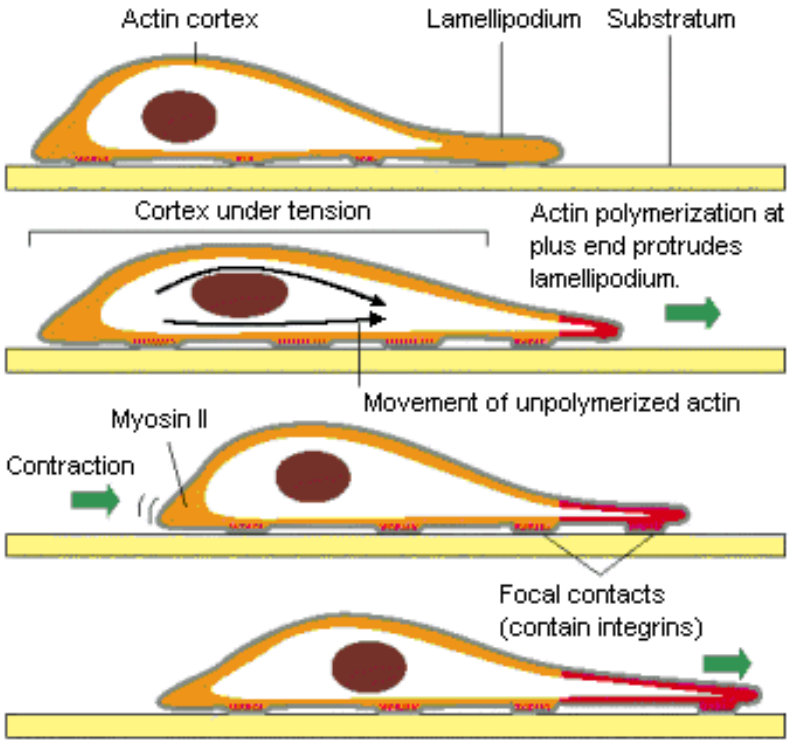

Figure 1.5: Schematic drawing of a cell crawling over a substrate. The movement is driven by forces generated in the actin rich cortex.[2]

Besides actin polymerization, attachment of the cell to the substratum plays a pivotal role in the mechanism of cell crawling. Thus, a migrating

cell forms specialized focal adhesions where the plasma membrane is held approximately 15 nm from the substratum. These focal adhesion enables the cell to attach to the extracellular matrix[3] through integrins, a large family of transmembrane proteins, that link intracellularly to actin filaments. One side of the integrins, that serves as an anchor, is exposed on the cell surface and binds to molecules such as fibronectin and vitronectin in the extracellular space. The cytoplasmatic domain of the integrin is connected with a cluster of proteins, like α-actinin, tensin or vinculin. Figure 1.6 summarizes known interactions between various constituent of cell matrix adhesion.[7]

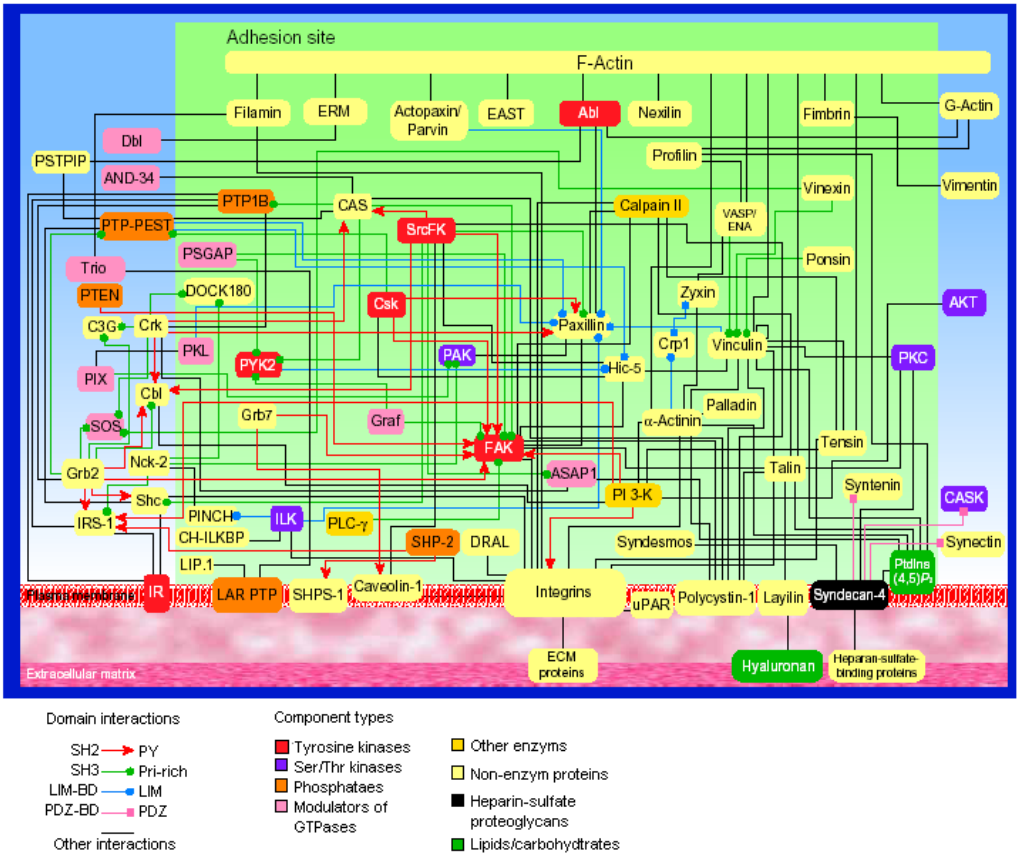

Figure 1.6: Schematic diagram summarizing known interactions between various constituents of cell matrix adhesion.[7]

Focal contacts are more than a mechanical anchorage of the cell, they also

[3]The extracellular matrix is composed of various proteins and polysaccharides that are secreted locally and assembled into an organized meshwork in close association with the surface of the cell that produces them.

serve as a transmitter of signals from the extracellular matrix to the inside of the cell. The focal adhesion kinase (FAK), for example, is an enzyme that binds to structural components of the focal adhesion such as integrins and the tyrosine kinase Src or the adapter protein Grb2. Phosphorylation of tyrosines in various proteins by FAK, induces clustering of other proteins with binding domains for phosphorylated tyrosines in this region. This complex sends and receives signals.

1.2 Artificial Biomembranes

The biological membrane serves as a semipermeable barrier between the intracellular and extracellular side. The greater part of it consists of lipids and proteins. Furthermore it contains steroids and small amounts of carbohydrates, mostly found tethered to proteins and lipids. Figure 1.7 presents the fluid mosaic model for the biological membrane as proposed by S. Jonathan Singer and Garth Nicolson in 1972.

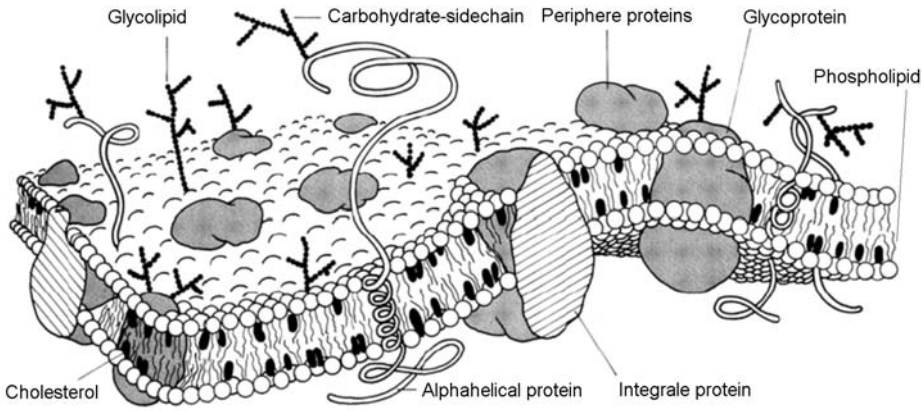

Figure 1.7: Fluid mosaic model of the biological membrane as proposed by Singer and Nicolson.[8] The fluid membrane contains mainly lipids and proteins.

The essence of their model is that biological membranes serve as a two-dimensional fluid, consisting of oriented lipids and globular proteins.[8] Due to the amphiphatic nature[4], lipids readily form bimolecular sheets, 5 - 10 nm thick bilayer, in aqueous media. These bilayers provide, as the temperature

[4]Amphiphatic lipids contain a hydrophilic headgroup and a hydrophobic hydrocarbon tail.

is high enough, a fluid, for most ions and molecules impermeable matrix, in which proteins are embedded. The physical and chemical properties of the membrane are mainly characterized by different headgroups and tails of the lipids, thus big differences occur in diverse cell types, i.e. membrane types. The biological character is mainly given by proteins, occurring in various manner. Nowadays the model described by Singer and Nicolson (figure 1.7) is not longer valid as there are recent studies concerning the structure of biological membranes. Instead of forming a homogeneous phase of sphingo- and glycerophospholipids, membrane lipids are supposed to form a manifold mosaic of domains called *rafts.*[9, 10, 11, 12] In order to reduce the complexity of biological membranes, it is helpful to examine isolated components like simple structured artificial membranes.

1.2.1 Lipidmembranes

The repertoire of membrane lipids is extensive, but each lipid possesses a critical common structural theme: these amphipatic molecules contain both a hydrophilic and a hydrophobic moiety as shown in figure 1.8.

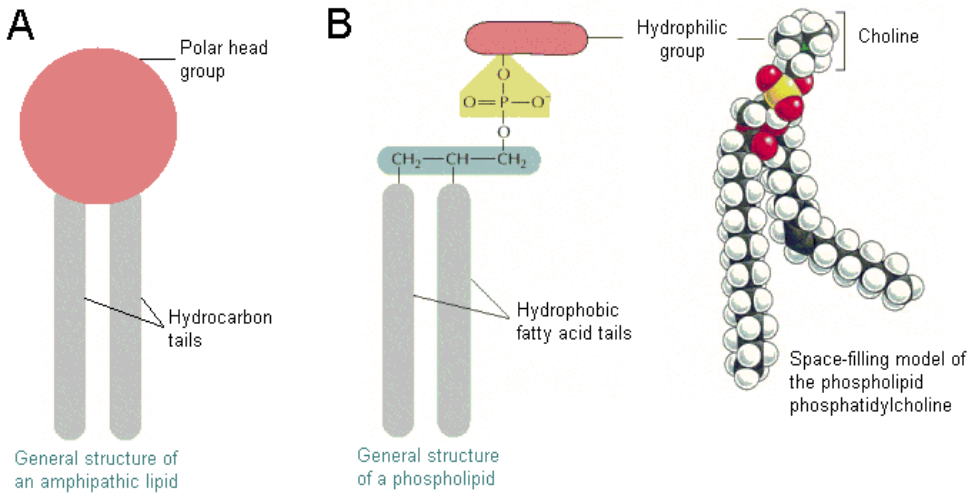

Figure 1.8: (A) Simplified structure of a phospholipid or glycolipid molecule. (B) More detailed structure of the phospholipid phosphatidylcholine.[2]

The major constituents of cell membranes are phospholipids (figure 1.8B). In the hydrophilic head region the glycerol is attached to two fatty acid chains. The "third" site on the glycerol is linked to a hydrophilic phosphate group, which is attached to a small hydrophilic group such as choline (figure

1.8B). Besides choline the hydrophilic group can be formed by ethanolamine, serine or glycerine. The hydrophobic tail of the lipid holds saturated or unsaturated fatty acids with a typical length of 14, 16 or 18 hydrocarbons. The length of the fatty acid chains and the number of double bounds influence the fluidity of the lipid bilayer, thus prokaryotes can regulate the fluidity of their membranes by varying its composition. For example, the ratio of saturated and unsaturated fatty acid chains in the *Escherichia coli* membrane decreases from 1.6 to 1.0 as the growth temperature is lowered from 42 °C to 27 °C. Eukaryotes use cholesterol, containing a bulky steroid nucleus with a hydroxyl group at one end and a flexible hydrocarbon tail at the other end, to regulate the fluidity of their membrane. Still, the impact of cholesterol on membrane fluidity is not completely understood , thus it is only known that cholesterol modulates the fluidity of membranes.

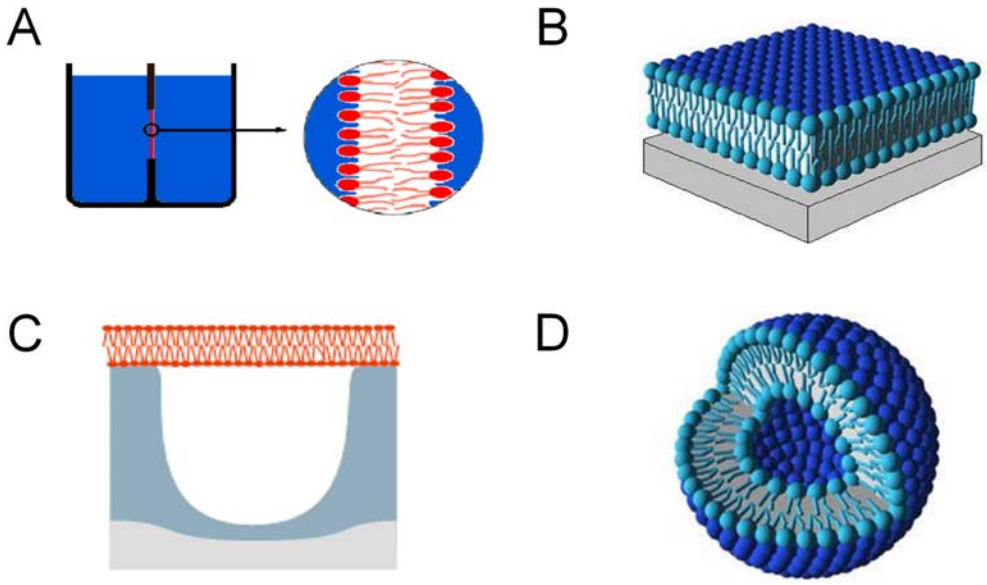

Figure 1.9: Widespread artificial lipid membranes. (A) Black lipid membrane.[13] (B) Solid supported phospholipid bilayer.[14] (C) Pore spanning lipid membrane. (D) Unilamellar phospholipid vesicle.[14]

The formation of lipid bilayers is a self-assembly process in water, i.e. it is a rapid and spontaneous process. The major driving forces for the formation of a lipid bilayer are hydrophobic interactions. Furthermore, there are van der Waals attractive forces between the hydrocarbon tails as well as electrostatic and hydrogen-bonding attractions between the polar head groups and water molecules. Different preparations of lipid bilayers are used

to examine the physical, chemical or biological nature of artificial membranes: *black lipid membranes* (BLMs), *solid supported phospholipid bilayers* (SPBs), *pore spanning lipid membranes* and *unilamellar phospholipid vesicles* (figure 1.9).

BLMs, the first model system enabling the examination of transport processes,[15, 16] are nowadays a well established system to study single channel events. A drawback of BLMs is their poor stability of only a few hours. However SPBs, lipid bilayers supported by a solid substrate are more stable than BLMs and therefore more suitable for longtime studies. Due to the given property of SPBs, a wide range of surface sensitive methods such as *atomic force microscopy* (AFM), *surface plasmon resonance spectroscopy* (SPR), *impedance spectroscopy, optical microscopy* or *quartz crystal microbalance* (QCM) are available to study the nature of solid supported membranes. Pore spanning phospholipid bilayers combine the benefits of BLMs and SPBs, as they are supported by a porous solid substrate and both sides of the bilayer face an aqueous solution providing sufficient space to host large integral proteins.

The common nature of these three artificial membranes is that they are all planar. However, in nature, the biological cell is enveloped by a spheric shell. Thus, the biological membrane is more comparable with unilamellar phospholipid vesicles, also known as liposomes, with respect to its shape (figure 1.9D). Membrane lipids exposed to an aqueous solution form vesicles, spheric shells containing one or multiple bimolecular sheets.[5] By diverse preparations like sonification or extrusion, vesicles of different sizes are available. It is distinguished between *small unilamellar vesicle* (SUVs) with a diameter up to 50 nm, *large unilamellar vesicles* (LUVs), with a diameter between 50 to 1000 nm and *giant unilamellar vesicles* (GUVs), with a diameter comparable to the size of prokaryotic or eukaryotic cell.

Beside the observation of transport phenomenons and diffusion processes, unilamellar phospholipid vesicles can be used to study mechanical properties of lipid membranes.[17, 18, 23] Furthermore liposomes are nowadays a versatile tool to mimic cell adhesion and membrane-membrane interactions by adsorption of liposomes to a functionalized surface.[19, 20, 21, 22] However unilamellar vesicles, specially SUVs are often used to prepare planar lipid bilayers like SPBs or pore spanning membranes. As a liposome adsorbs to a surface, deformation due to an attractive contact potential might occur. The complex kinetic of vesicle adsorption, spreading and rupture leading to the formation of a solid supported planar lipid bilayers had been widely stud-

[5] Vesicles containing a singel bilayer a called *unilamellar*, while those, containing multiple bilayer are called *multilamellar*.

ied by various scientist.[24, 25, 26, 27] However the entire process of bilayer formation is still unknown.

Bibliography

[1] http://rsb.info.nhi.gov/ij/

[2] Alberts, B.; Johnson, A.; Lewis, J.; Raff, M.; Roberts, K.; Walter, P. *Molecular Biology of the Cell* Garland Science, 2002.

[3] Ingber, D. E. *J. Cell Sci.* 1993, 613-627.

[4] Wang, N.; Butler, J. P.; Ingber, D. E. *Science* 1993, 26, 1124-1127.

[5] Ingber, D. E. *Annu. Rev. Physiol.* 1997, 59, 575-599.

[6] Stamenovic, D.; Ingber, D. E. *Biomechan. Model Mechanobiol.* 2002, 95-108.

[7] Zamir, E.; Geiger, B. *J. Cell Science* 2001, 114, 3577-3579.

[8] Singer, S. J.; Nicolson G. L. *Science* 1972, 175, 720-731.

[9] Simons, K.; Ikonen, E. *Nature* 1997, 387, 569-572.

[10] Brown, D.A.; London, E. *Annu. Rev. Cell Dev. Biol.* 1998, 14 111-136.

[11] Brown, D.A.; London, E. *J. Bio. Chem.* 2000, 275(23), 17221-17224.

[12] Fantini, J.; Garmy, N.; Mahfoud, R.; Yahi, N. *Rev. Mol. Med.* 2002, www.expertreviews.org

[13] Hennesthal, C. *Inaugural-Dissertation* 2003, Fachbereich Chemie und Pharmazie, Westfälische-Wilhelms-Universität, Münster.

[14] http://bunshi3.bio.nagoya-u.ac.jp/bunshi3/students/yohko/CG.html

[15] Müller, P.; Rudin, D. O.; Tein, H. T.; Wescott, W. C. *Nature* 1962,194(4832), 979-980.

[16] Müller, P.; Rudin, D. O.; Tein, H. T.; Wescott, W. C. *J. Phys. Chem.* 1963, 67, 534-535.

[17] Evans, E. *J. Phys. Chem.* 1987, 91, 4219-4228.

[18] Evans, E.; Rawicz, W. *Phys. Rev. E* 1997, 79, 122379-122382.

[19] Reiss, B.; Janshoff, A.; Steinem, C.; Seebach, J.; Wegener, J. *Langmuir* 2003, 19, 1816-1823.

[20] Kastl, K.; Herrig, A.; Lüthgens, E.; Janshoff, A.; Steinem, C. *Langmuir* 2004, 20, 7246-7253.

[21] Faiss, S.; Lüthgens, E.; Janshoff, A. *Eur. Biophys. J.* 2004, 33, 555-561.

[22] Keller, C. A.; Kasemo, B. *Biophys. J.* 1998, 75, 1397-1402.

[23] Kummrow, M.; Helfrich, W. *Phys. Rev. A* 1991, 44, (12), 8356-8360.

[24] Seifert, U.;Lipowsky, R. *Phys. Rev. A* 1990, 42, (8), 4768-4771.

[25] Keller, C. A.; Glasmästar, K.; Zhdanov, V. P.; Kasemo, B. *Phys. Rev. Lett.* 2000, 84, 5443-5446.

[26] Zhdanov, V. P.; Keller, C. A.; Glasmästar, K.; Kasemo, B. *J. Chem. Phys.* 2000, 112, 900-909.

[27] Reimhult, E.; Höök, F.; Kasemo, B. *Langmuir* 2003, 19, 1681-1691.

Chapter 2

Methods and Instrumentation

2.1 The Quartz Crystal Microbalance (QCM)

The quartz crystal microbalance technique has been used to measure deposition of thin films for over 40 years. This technique is based on the changes of the resonance frequency of an oscillating quartz crystal, when small masses are deposited homogeneously on its surface. Sauerbrey showed, that deposition of rigid mass under vacuum or in air provokes a change of the resonance frequency Δf. This proportionality is given by the well-known Sauerbrey equation

$$\Delta f = -\frac{2f_0^2}{A\sqrt{\rho_q \mu_q}}\Delta m = -S_f \Delta m, \tag{2.1}$$

with f_0 the fundamental resonance frequency of the quartz resonator, ρ_q is its density and μ_q is the shear modulus of the quartz crystal. A is the electrode area and S_f the integral mass sensitivity, also known as the Sauerbrey coefficient.[1]

Almost 20 years ago it was shown that the quartz crystal microbalance can be operated in liquids as well as in vacuum. Thus it became a new sensitive tool in bioanalytical research.[2] Working in fluids, the change of the resonance frequency Δf depends on the viscosity η_l and the density ρ_l of the liquid:[3]

$$\Delta f = -f_0^{3/2}\sqrt{\frac{\eta_l \rho_l}{\pi \rho_q \mu_q}}. \tag{2.2}$$

For a better understanding of these phenomena the following sections give a brief overview about the general properties of thickness shear mode oscillators.

2.1.1 General Properties

Basis of the quartz crystal microbalance is the inverse piezoelectric effect, which is only found in crystals without any center of inversion. The piezoelectric effect, found by the Curies in 1880, describes the appearance of electric charge on the surface of a crystal due to mechanical deformation. Inversely, application of an electric voltage provokes a mechanical deformation (figure 2.1B). Thus, an alternating voltage leads to a periodic alternating deformation, i.e. an oscillation of the piezoelectric crystal. The oscillation mode depends on the orientation of the cut. In this work, AT-cut quartz crystals were used possessing a thickness shear mode oscillation. A benefit of these resonators is their small temperature-frequency-correlation. Figure 2.1 shows the lateral deformation and oscillation of such a quartz when a direct or alternating voltage is applied.

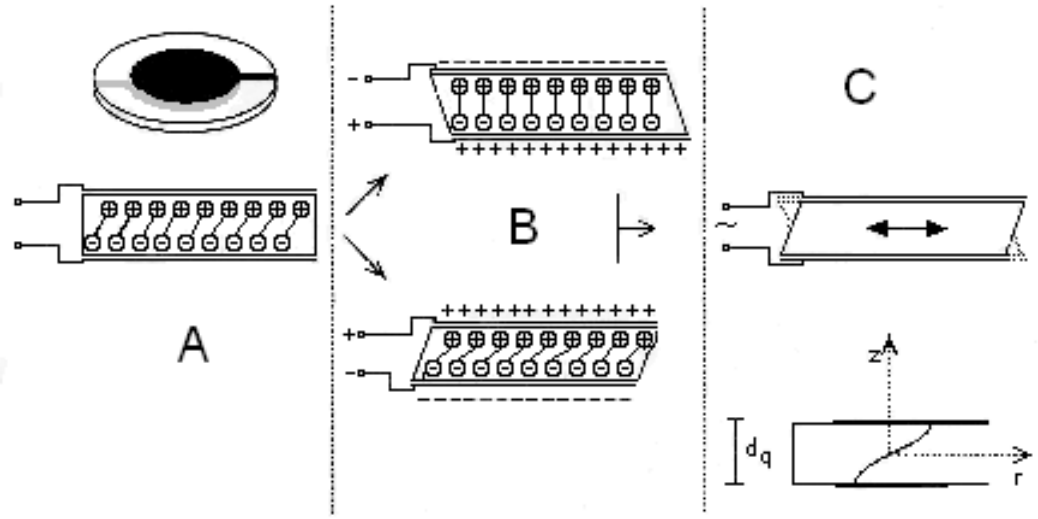

Figure 2.1: Schematic diagram of a piezoelectric quartz crystal in the unperturbed state (A) and during application of a direct (B) or an alternating (C) voltage. Excitation with the resonance frequency provokes a standing acoustic wave across the quartz disc (C, bottom).

Application of an alternating voltage to the electrodes on the quartz surfaces leads to a shear oscillation of the quartz crystal (figure 2.1C top). This oscillation causes an acoustic transversal wave propagating through the resonator (figure 2.1C bottom). By tuning the frequency of the applied alternating voltage a resonance frequency can be found. In this case the wavelength

(or an odd number of the wavelength) is exactly the double of the thickness of the quartz disc d_q, resulting in a standing acoustic wave (figure 2.1C, bottom). The fundamental resonance frequency of the quartz crystal is given by:[4]

$$f_0 = \frac{1}{2d_q}\sqrt{\frac{\mu_q}{\rho_q}}. \tag{2.3}$$

In the present study thickness shear mode resonators with a fundamental resonance frequency of 5 MHz were used. The thickness of these quartz crystals is 330 μm, the shear modulus μ_q and the density ρ_q are $\mu_q = 2.93 \cdot 10^{10}$ N/m^2 and $\rho_q = 2650$ kg/m^3.

To provide stability of the resonance frequency a high quality-factor and minimized electromechanical coupling are needed. The quality-factor Q is defined by

$$Q = 2\pi \frac{\text{energy stored per cycle}}{\text{energy dissipated per cycle}}. \tag{2.4}$$

The quality-factor of the shear mode oscillation in air of an AT-cut quartz is around 10^5. The electromechanical coupling-factor K is determined by the resulting piezo-coefficient $e_q = 9.65 \cdot 10^{-2}$ C/m^2, the actual dielectric constant $\epsilon_q = 4.54 \cdot \epsilon_0$, where $\epsilon_0 = 8.854 \cdot 10^{-12}$ C/(Vm) is the dielectric constant, and the shear modulus $\mu_q = 2.93 \cdot 10^{10}$ N/m^2:[4]

$$K = \sqrt{\frac{\text{stored elastic energy}}{\text{stored electrical energy}}} = \sqrt{\frac{e_q}{\mu_q \varepsilon_q}} \approx 0.091. \tag{2.5}$$

2.1.2 Electromechanical Coupling

For a detailed specification of the oscillation of a quartz crystal and the effect of mass load on the surface, the oscillation can be described by a mechanical model.[5] This model can be easily transformed in an electric model due to the electromechanical coupling in piezoelectric materials. The mechanical model of the oscillating crystal consists of a dashpot r, a mass m and a spring, which possesses a spring constant k (figure 2.2A).[6] Moving the mass m by an external force $\widetilde{F}$ provokes an oscillation.

Transforming the mechanical model into an electric model, the electric properties of the oscillation can be described by the Butterworth-van-Dyke (BVD) equivalent circuit as depicted in figure 2.2B.[4] This circuit contains a resistance, a capacity and an inductance connected in series and an additional capacity connected parallel to the series circuit. Comparing figure 2.2A and

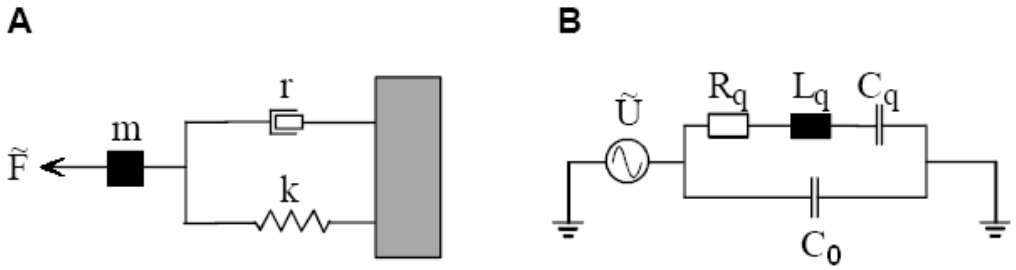

Figure 2.2: (A) Mechanical model of the damped oscillator. (B) Corresponding electric equivalent circuit of the piezoelectric oscillation, the Butterworth-van-Dyke equivalent circuit.

2.2B, the oscillating mass m is equivalent to the inductance L_q, the dashpot r is represented by the resistance R_q, the spring constant k corresponds to the capacity C_q and the external force $\widetilde{F}$ is equivalent to the alternating voltage $\widetilde{U}$. Far away from the resonance frequency the quartz crystal between behaves like a capacity determined by the dielectric property of the resonator. This behavior is represented by the capacity C_0. The individual parameters can be calculated by the following equations:[4]

$$C_0 = \frac{\varepsilon_q A}{d_q}, \tag{2.6}$$

$$C_q = \frac{8Ae_q^2}{\pi^2 d_q \mu_q}, \tag{2.7}$$

$$L_q = \frac{d_q^3 \rho_q}{8Ae_q^2}, \tag{2.8}$$

$$R_q = \frac{\pi^2 d_q \eta_q}{8Ae_q^2}, \tag{2.9}$$

where η_q is the viscosity of the resonator.[1]

The BVD equivalent circuit (figure 2.2B) possesses two resonance frequencies, the antiresonance f_A, corresponding to the whole circuit, and the serieresonance f_S, corresponding to the upper serial branch. The two resonance frequencies can be calculated by Kirchhoff's laws:

[1] Note that the BVD equivalent circuit is only valid in the regime of the quartz resonance. For a detailed description and derivation of equation 2.6-2.9 see Mason and Rosenbaum.[7, 8]

$$f_A = \frac{1}{2\pi}\sqrt{\frac{1}{L_q}\left(\frac{1}{C_q}+\frac{1}{C_0}\right)}, \tag{2.10}$$

$$f_S = \frac{1}{2\pi}\sqrt{\frac{1}{L_q C_q}}. \tag{2.11}$$

2.1.3 Impact of Mass Load and Viscoelastic Fluids on the Response of the Resonator

The mechanical properties of the mass load and the viscoelastic fluids determine the impact on the oscillation of the quartz crystal. For a thin and rigid film Sauerbrey's equation 2.1 is still valid. However, for thick layers, viscous liquids, elastic solids or viscoelastic films equation 2.1 is not longer appropriate.[9] In detailed studies it was found that the load can be handled like an additional inductance and resistance in the Butterworth-van-Dyke equivalent circuit (figure 2.2B).[10, 11, 12, 13, 14, 15, 16] Here the additional resistance represents the energy dissipation and the inductance corresponds the kinetic energy of the oscillating mass coupled to the surface. The resulting equivalent circuit is depicted in figure 2.3.

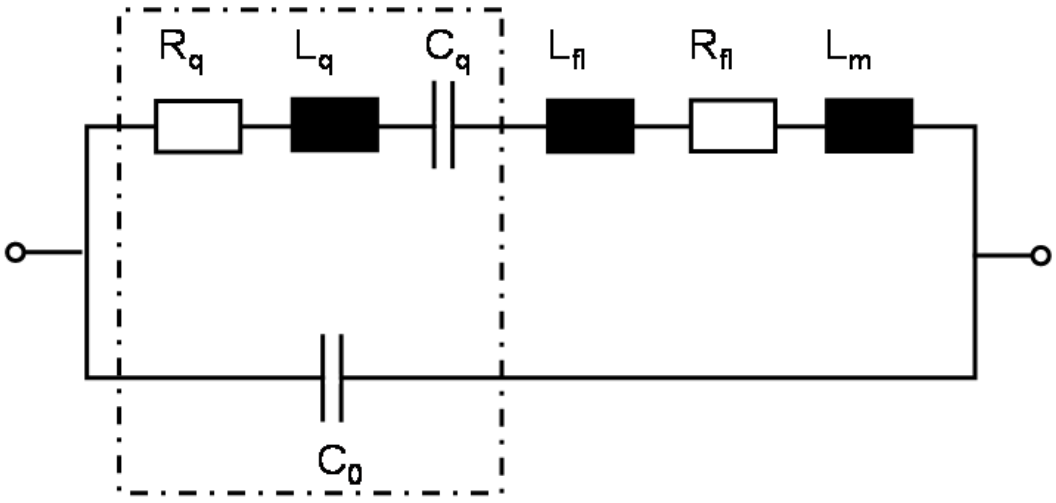

Figure 2.3: BVD equivalent circuit quartz crystal loaded with a rigid mass and a viscous fluid.

The additional inductance L_m due to foreign mass load can be estimated by the thickness of the layer d_m and its density ρ_m:[15]

$$L_m \simeq \frac{1}{8K^2C_0f_0}\frac{d_m\rho_m}{\sqrt{\mu_q\rho_q}}. \tag{2.12}$$

The impact of a thin viscoelastic fluid on the response of the resonator can be described by the additional inductance L_{fl} and resistance R_{fl}:[15]

$$L_{fl} \simeq \frac{1}{8K^2C_0f_0}\sqrt{\frac{\rho_{fl}\eta_{fl}}{4\pi f\mu_q\rho_q}}, \tag{2.13}$$

$$R_{fl} \simeq \frac{1}{8K^2C_0f_0}\sqrt{\frac{\pi f\rho_{fl}\eta_{fl}}{\mu_q\rho_q}}, \tag{2.14}$$

where ρ_{fl} is the density and η_{fl} the viscosity of the fluid.

In the case of a foreign mass and a thin viscoelastic fluid deposited on the surface of a quartz resonator, the inductance L_q and the resistance R_q have to be replaced by

$$L = L_q + L_{fl} + L_m \quad \text{and} \quad R = R_q + R_{fl}. \tag{2.15}$$

Using the inductance L and the resistance R the quality-factor Q (equation 2.4) of the oscillating quartz crystal can be described by the following equation:

$$Q = 2\pi f_0\frac{L}{R}. \tag{2.16}$$

In the present study biological systems such as cells and liposomes, which can not longer treated like a rigid mass due to their high viscoelasticity, were studied. Hence, equation 2.12 is not longer valid. The oscillating crystal provokes a shear stress to the adhering cell or liposome. The strain tensor u_{ik} and the shear stress σ_{ik} are related to the complex frequency-dependent shear modulus $G^*(f) \equiv G'(f) + iG''(f)$ of viscoelastic fluids by the following equation:[17]

$$\sigma_{ik} = 2G^*u_{ik}. \tag{2.17}$$

The real part $G'(f)$ and the imaginary part $G''(f)$ of the complex shear modulus G^* are also known as the storage modulus and the loss modulus. The frequency change can be calculated as:[17, 18]

$$\Delta f = -\frac{2h\rho}{h_q\rho_q} f_0 \left[1 - 2\frac{\pi\rho_{fl}\eta_{fl}f_0}{\rho}\frac{G''}{G'^2 + G''^2}\right], \tag{2.18}$$

where ρ is the density and h the thickness of the viscoelastic layer. Equation 2.18 demonstrates that the fluid provokes a decrease of the frequency change. This effect is known as the *missing mass* effect and can be observed for unilamellar vesicles.[17]

2.1.4 Experimental Setup

QCM provides two operational modes, an *active* and a *passive mode*. Operating in the *active mode* the quartz crystal is connected to a phase-lock oscillator circuit determining the frequency. Here the resonance frequency is measured directly by a frequency counter. Otherwise, in the *passive mode*, an impedance analyzer sweeps the frequency and takes continuously impedance spectra of the oscillating resonator. Analyzing this spectra by means of the BVD-circuit the resonance frequency can be calculated. In contrast to the *active mode,* this method allows the determination of the fundamental resonance frequency and its overtones simultaneously. However, a drawback of the *passive mode* is the poorly time resolution and a reduced signal to noise ratio due to the fact that the frequency can be measured more accurately as the voltage. For all QCM-based measurements in this work a high time resolution is required. Therefore all measurements were carried out in the *active mode* with a time resolution in the millisecond-range.

Besides the time resolution, the sensitivity plays a pivotal role. To monitor small frequency fluctuations occurring with cell migration or deformation of liposomes in the Nanometer-scale, it is essential to provide high sensitivity and prevent electronic noise. For this reason several phase-lock oscillators were probed with regard to their electronic noise. Significant differences were observed (data not shown). To provide high sensitivity the phase-lock oscillator (QCM100, SRS, Inc., Sunnyvale, CA, USA) with the lowest electronic noise, was used in this work.

The experimental setup depends on the system to be studied. In the following sections the setups used for investigating liposomes and cells are described in more detail.

Liposome Measurements

In this work the adsorption of charged giant liposomes and their electrically induced deformation were studied. For vesicle adsorption a flow system (figure 2.4) was used. A pump ensures a constant flow of buffer solution

through the tubes, the reaction chamber and the QCM-cell. The diameter of the tubes and the distance between the electrode and the bottom of the plug were optimized to the size of the liposomes. To study adsorption and deformation of giant liposomes, the diameter of the tubes was about 2 mm and the distance between the electrode on the top of the quartz crystal and the bottom of the plug above the quartz was about 3.2 mm. Deformation of vesicles was induced by an external alternating electric field and read out by the response of the thickness shear mode resonator. The used phase-lock oscillator allows monitoring the resonance frequency and applying an alternating voltage between the upper electrode on top of the quartz crystal and the gold electrode above simultaneously.

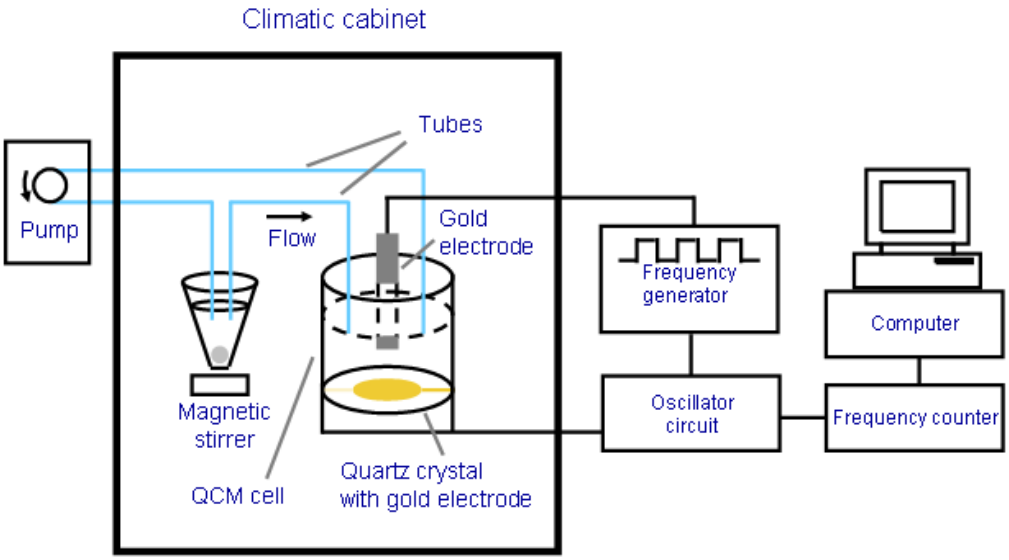

Figure 2.4: Experimental setup used for the observation of electrical induced deformation of charged giant liposomes. In the top of the QCM cell an electrode is placed. Between this electrode and the electrode on the top of the quartz crystal a square wave voltage is applied using a frequency generator.

In order to provide a constant temperature, the crystal holder was placed in a climatic cabinet, which also served as a Faraday cage. The resonance frequency was recorded by a frequency counter (Agilent 53181A, Agilent Technologies, Palo Alto, Calif., USA) and transferred via GPIB to a computer. The voltage supply delivers an alternating voltage without bias.

According to the general procedure, the giant liposomes were injected into the reaction chamber and time course of the resonance frequency was

monitored by the computer as described above. After adsorption process, when the equilibrium condition is reached, the pump was switched off and the alternating voltage was applied across the deposited liposomes while changes in the resonance frequency were monitored.

Cell Measurements - Monitoring Cell Motility

Cell motility was monitored using the setup depicted in figure 2.5. The measurement chamber containing the quartz crystal was connected to the phase-lock oscillator. The resonance frequency of the oscillating quartz crystal was recorded with a sampling rates between 13 and 133 Hz by a frequency counter and transferred via GPIB to a computer. All measurements were carried out in incubators with 5 % (v/v) CO_2 atmosphere at 37 °C, while the incubators also served as a Faraday cage.

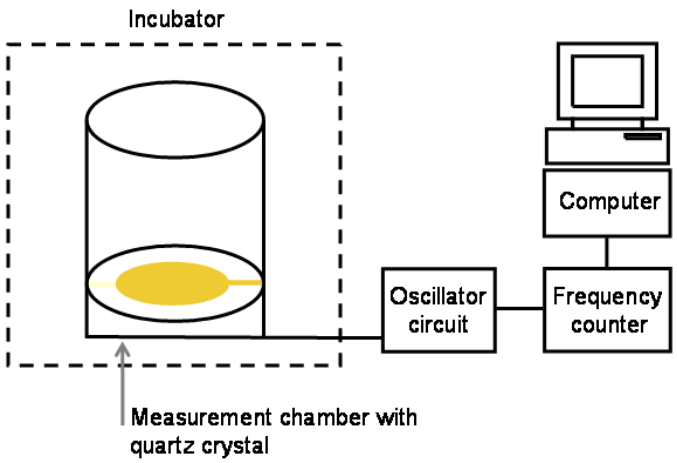

Figure 2.5: Experimental setup to monitor shape fluctuations of mammalian cells.

Cell Measurements - Impedance Analysis in the Regime of the Quartz-Resonance

In order to characterize the mechanical load of the quartz crystal, impedance analysis was used to determine the quality-factor Q given in equation 2.4. Figure 2.6A illustrates the setup used for impedance analysis. The quartz crystal was clamped into the measurement chamber and connected to the continuous-wave impedance analyzer (SI-1260; Solartron Instruments, Farnborough, UK).

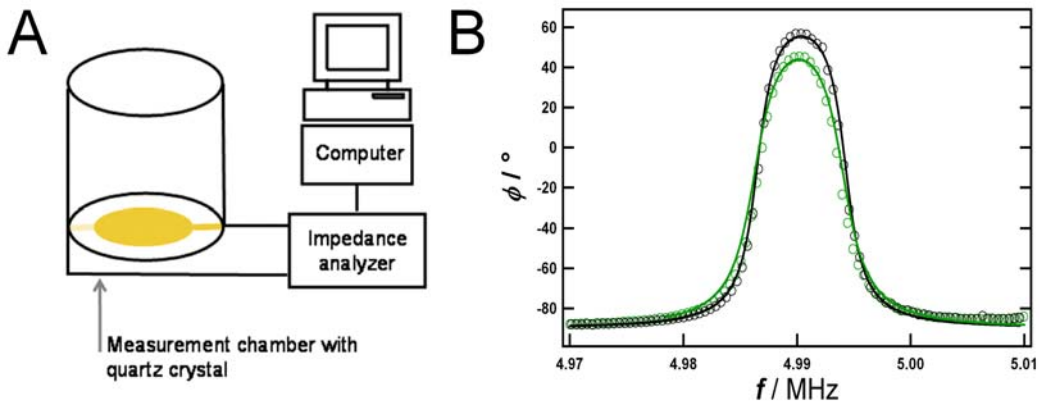

Figure 2.6: (A) Experimental setup to record impedance data of quartz resonators. (B) Phase shift ϕ as a function of frequency for a 5 MHz thickness shear mode resonator near its fundamental resonance. (Black) Resonator immersed in buffer solution. (Green) Resonator covered with vital MDCK-II cells in culture fluid. Solid lines represent the transfer functions of the BVD network after parameter fitting.

Impedance analysis was performed in the frequency regime close to the quartz fundamental resonance (5 MHz). Figure 2.6 B shows typical impedance spectra of a quartz resonator immersed in buffer solution (black) and a resonator covered with vital MDCK-II cells in culture fluid (green). The impedance spectra can be described by the transfer function of the BVD model (see Appendix A). Fitting the impedance spectra to this model (solid lines in figure 2.2B) provides energy storage (inductance) and energy dissipation (resistance), thus the Q-factor.

2.2 Electric Cell-Substrate Impedance Sensing (ECIS)

Electric cell-substrate impedance sensing (ECIS) was introduced in 1984 by Giaever and Keese.[19] By this impedance sensing method morphology of adherent cells as well as their dynamic changes, induced by biological, chemical or physical stimuli, can be monitored.

2.2.1 General Properties

Generally cells are grown on the surface of gold electrodes and the frequency-dependent impedance between the two electrodes, immersed in culture medium to provide electric current,[2] is measured (figure 2.7). It is obvious that the current is hampered by the cell layer, due to the insulating character of cells, and by this the magnitude of the impedance depends on the coverage of the electrode with cells. However, the correlation between the impedance and the surface coverage is quite complicated.

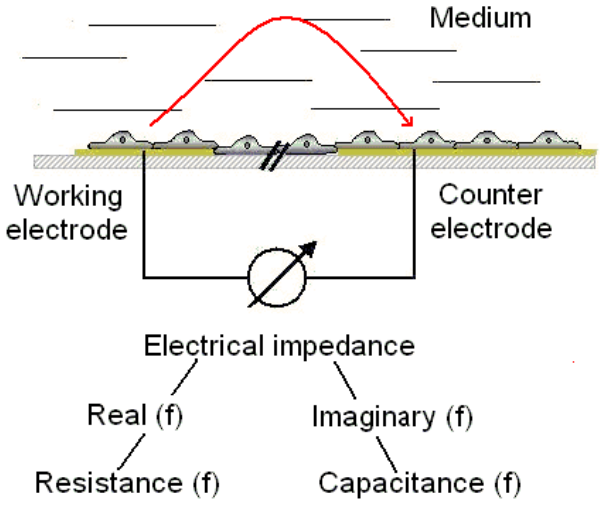

Figure 2.7: Schematic drawing of ECIS-measurements.

Figure 2.7 shows a schematic of ECIS-measurements. In this setup the resistance of the bulk tissue culture medium is in series with the impedance of the electrodes and will dominate the measurement unless an electrode is small. For a circular disc electrode in a conducting medium in infinite extent, the constriction resistance varies as $\rho_{medium}/2d_{electrode}$, where ρ_{medium} is the resistivity of the medium and $d_{electrode}$ is the diameter of the electrode. The capacitance associated with the electrode-electrolyte interface is proportional to the area of the electrode, $(\pi/4)d^2_{electrode}$. Since the impedance is given by the sum of the resistance and the inverse of the capacitance, it can always be dominated by the capacitance by choosing a sufficiently small diameter. For this reason, a small working electrode with an area of about 5×10^{-4} cm^2 is

[2] In addition to its general function of being nutrient for cells, culture medium, possessing high salt concentration, is used as an electrolyte.

used. The counter electrode is about 300-fold larger (0.15 cm^2). Therefore the total impedance of the system is dominated by the impedance of the working electrode.[3]

2.2.2 Electric Model

The model used to calculate the specific impedance (impedance for a unit area) of a cell-covered electrode as a function of frequency is based on the measured values of a cell-free electrode, $Z_n(f)$, the specific impedance, $Z_m(f)$, through the cell layer and the resistivity, ρ_{liq}, of the tissue culture medium. The specific impedance through the cell layer $Z_m(f)$ is mainly determined by capacitance of the upper and lower cell membranes in series. If the capacitance of a single cell membrane is C, then for the intact cell, $Z_m(f) = -i/\pi f C$.[4] Figure 2.8 shows the various current path.

Several assumptions must be made to simplify the calculations. 1) The cells are assumed to have cylindrical shape with radius r_c, 2) the current flows radially in the space formed between the ventral surface of the cell and the substratum, 3) the current density under the cells does not change in the vertical direction, 4) the electrode potential V_n is a constant, being independent of the position and 5) the potential in solution on the dorsal side of the cells is likewise treated as constant.[5] Finally 6) the electrical potential inside the cell V_m is a constant and 7) the presence of the cells does not affect the polarization of the electrode.

Applying Ohm's law to the model in figure 2.8B, the following equations are found:

$$-dV = \frac{\rho_{liq} dr}{h 2\pi r} I \tag{2.19}$$

$$V_n - V = \frac{Z_n(f)}{2\pi r dr} dI_n \tag{2.20}$$

$$V - V_m = \frac{Z_m(f)}{2\pi r dr} dI_m \tag{2.21}$$

$$dI = dI_n - dI_m. \tag{2.22}$$

[3] The impedance of each electrode is dominated by its capacity, which is proportional to the area of the electrode. The total impedance is governed by the total capacity C_{tot}: $C_{tot} = \left(\frac{1}{C_{working}} + \frac{1}{C_{counter}}\right)^{-1} \approx C_{working}$ for $C_{working} \ll C_{counter}$ for. $C_{working}$ is the capacity of the working electrode and $C_{counter}$ of the counter electrode.

[4] As the cell possesses two membranes the total capacity C_{tot} is given by a series circuit of two capacities C, yielding $C_{tot} = \frac{C}{2}$. The capacitance of cell membranes is typically about 1 μF/cm^2.

[5] The potential is set to zero; this doesn't affect the calculated impedance.

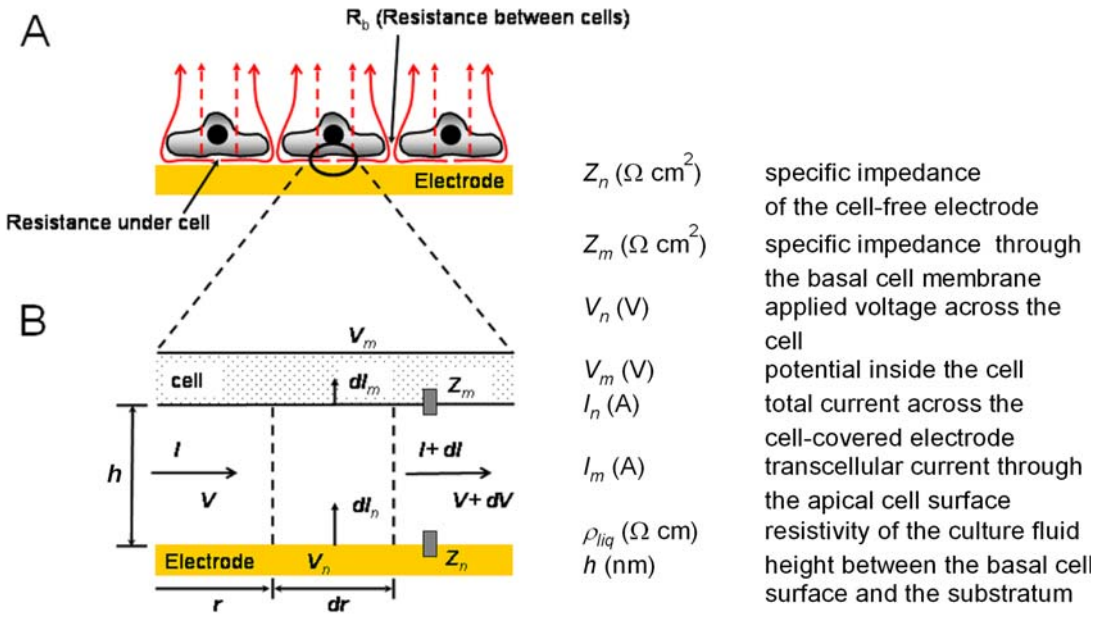

Figure 2.8: (A) Diagram of the cells in tissue culture. Calculated resistance is due to the current flow under the cells and an additional resistance because the current must flow out between the cells. Broken lines represent capacitive flow through the cell membrane. (B) Schematic drawing emphasizing the spaces between the cell and the substrate.

Combining equations 2.19 - 2.22 yields equation 2.23:

$$\frac{d^2V}{dr^2} + \frac{1}{r}\frac{dV}{dr} - \gamma^2 V + \beta = 0, \tag{2.23}$$

where

$$\gamma^2 = \frac{\rho_{liq}}{h}\left(\frac{1}{Z_n} + \frac{1}{Z_m}\right) \quad \text{and} \quad \beta = \frac{\rho_{liq}}{h}\left(\frac{V_n}{Z_n} + \frac{V_m}{Z_m}\right). \tag{2.24}$$

Here, V_n is the potential of the electrode and V_m is the potential measured in the solution just outside the cell layer, and h is the height of the space between the ventral surface of the cell and the substrate.

The solution of equation 2.23 is given by the modified Bessel function of the first kind I_0:[22, 23]

$$V = AI_0(\gamma r) + \frac{\beta}{\gamma^2}, \tag{2.25}$$

$$I_n(\gamma r) = \frac{\left(\frac{\gamma r}{2}\right)^n}{\Gamma(n+1)} + \frac{\left(\frac{\gamma r}{2}\right)^{n+2}}{1!\Gamma(n+2)} + \frac{\left(\frac{\gamma r}{2}\right)^{n+4}}{2!\Gamma(n+3)} + ... \tag{2.26}$$

For the intercellular lateral path (figure 2.9) the two equations related to the

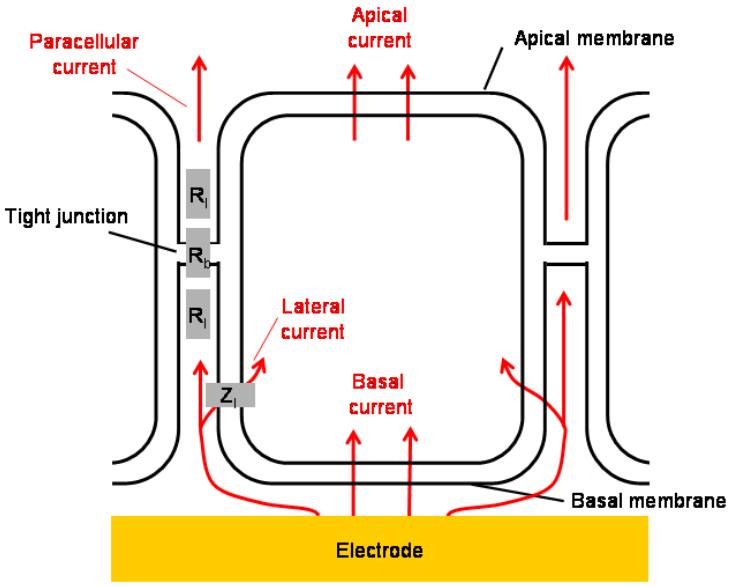

Figure 2.9: Schematic diagram of cells in tissue culture, illustrating the various current paths.

paracellular current can be expressed as

$$\frac{dV_m}{dz} = -2I_l R_l, \tag{2.27}$$

and

$$V_l - V_m = \frac{Z_l}{2\pi r_c dz}(-dI_l), \tag{2.28}$$

where I_l is the paracellular current through the intercellular lateral path, R_l is the paracellular resistance for a unit length, V_l is the potential in the lateral paracellular path, and Z_l is the specific impedance through the lateral path.

Equations 2.27 and 2.28 can be combined to yield the following differential equation:

$$\frac{d^2V_l}{dz^2} - \lambda^2 V_l + \lambda^2 V_m = 0, \tag{2.29}$$

where

$$\lambda = \sqrt{\frac{4\pi r_c R_l}{Z_l}}. \tag{2.30}$$

The solution of equation 2.29 is:

$$V_l = V_i + Ce^{\lambda z} + De^{-\lambda z}. \tag{2.31}$$

Having four constants A, C, D and V_i in equation 2.25 and 2.31 to be determined, four boundary conditions are needed:[23]

$$\begin{aligned} V\left(r = r_c\right) &= V_l\left(z = 0\right), & (2.32)\\ I\left(r = r_c\right) &= I_l\left(z = 0\right), & (2.33)\\ I_l\left(z = l\right) \times R_b^* &= V_l\left(z = l\right), & (2.34)\\ I_n &= I_m + I_l\left(z = l\right), & (2.35) \end{aligned}$$

where R_b^* is the junctional resistance between adjacent cells (R_b is the junctional resistance between adjacent cells over a unit cell area). Solving this equation in closed form is rather complex. By using matrix algebra a numerical solution can be readily obtained. Thus, the four boundary conditions can be written as a matrix equation:

$$\mathbf{MX} = \mathbf{Y}, \tag{2.36}$$

where $\mathbf{M}$ is the matrix:

$$\mathbf{M} = \begin{pmatrix} \frac{-2\pi h\gamma r_c I_1(\gamma r_c)}{\rho_{liq}} & \frac{\lambda}{2R_l} & -\frac{\lambda}{2R_l} & 0 \\ I_0(\gamma r_c) & -1 & -1 & -\frac{Z_m}{Z_n+Z_m} \\ 0 & e^{\lambda l}\left(1+\frac{\lambda R_b}{2R_l}\right) & e^{-\lambda l}\left(1-\frac{\lambda R_b}{2R_l}\right) & 1 \\ -\frac{2I_1(\gamma r_c)}{Z_n\gamma r_c} & \frac{\lambda e^{\lambda l}}{2R_l\pi r_c^2} & -\frac{\lambda e^{-\lambda l}}{2R_l\pi r_c^2} & -\frac{Z_m+Z_n+Z_a}{(Z_n+Z_m)Z_a} \end{pmatrix}, \tag{2.37}$$

and $\mathbf{X}$, $\mathbf{Y}$ being vectors:

$$\mathbf{X}=\begin{pmatrix} A \\ C \\ D \\ V_i \end{pmatrix} \quad \text{and} \quad \mathbf{Y}=\begin{pmatrix} 0 \\ -\frac{Z_m V_n}{Z_n+Z_m} \\ 0 \\ -\frac{V_n}{Z_n+Z_m} \end{pmatrix}, \tag{2.38}$$

where Z_a is the specific impedance through the apical cell membrane, and I_1 is the modified Bessel function of the first kind in order 1 (equation 2.26). The numerical constants A, C, D, and V_i are found by solving equation 2.36, and finally the current flowing out of the electrode under a single cell I_c can be determined by integrating equation 2.20:

$$I_c = \int_0^{r_c} \frac{2\pi r}{Z_n}(V_n - V)dr = -\frac{2\pi r_c^2 A}{Z_n \gamma r_c} I_1(\gamma r_c) + \frac{\pi r_c^2}{Z_n + Z_m}(V_n - V_i). \tag{2.39}$$

The specific impedance for a cell-covered electrode is obtained by dividing V_n by I_c:[23, 24]

$$\frac{1}{Z_c} = \frac{1}{Z_n}\left(\frac{Z_n}{Z_n + Z_m} + \frac{\frac{Z_m}{Z_n+Z_m}}{\frac{\gamma r_c}{2}\frac{I_0(\gamma r_c)}{I_1(\gamma r_c)} + R_b\left(\frac{1}{Z_n}+\frac{1}{Z_m}\right)}\right). \tag{2.40}$$

Note that the solution in equation 2.40 depends on two parameters, R_b the resistance between the cells for a unit area, and α defined by:

$$\gamma r_c = r_c\sqrt{\frac{\rho}{h}\left(\frac{1}{Z_n}+\frac{1}{Z_m}\right)} = \alpha\sqrt{\frac{1}{Z_n}+\frac{1}{Z_m}}. \tag{2.41}$$

Since $Z_n(f)$ is measured and $Z_m(f)$ is basically the impedance of two cell membranes in series (figure 2.8 B), R_b the resistance between two cells for unit area and h the height of the space between the ventral surface of the cell and the substratum are available.

2.2.3 Setup

In this work adsorption and micromotion of giant liposomes and MDCK-II cells were studied. For all experiments a setup as shown in figure 2.10 was used. The measurement system consists of an eight-well dish (figure 2.11) with circular gold-film electrodes ($d = 250\ \mu$m) upon the bottom of each well (Applied Biophysics, Inc., Troy, NY), a lock-in amplifier (SRS830, SRS, Inc.; Sunnyvale, CA, USA) with an internal oscillator, and a personal computer

that controls the measurement and stores the data. The oscillator applies an AC signal of amplitude 1 V through a series 1 MΩ resistor to the two electrode system. Immersing the gold-film electrodes of this setup in a buffer salt solution used as the bulk electrolyte, the current flow is approximately at 1 μA in the frequency regime between 400 and 40 kHz. The in-phase and out-of-phase voltages across the system are measured by the amplifier and converted into real and imaginary parts of the electrode impedance, which are represented formally as resistance and capacitance of a RC series circuit.

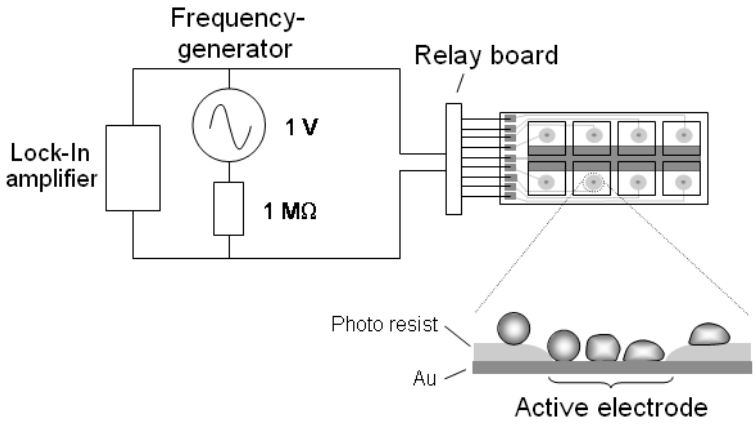

Figure 2.10: Schematic drawing of the experimental setup to follow adsorption and shape fluctuations of liposomes and cells. The size of the electrode is not drawn to scale with respect to the liposomes/cells.

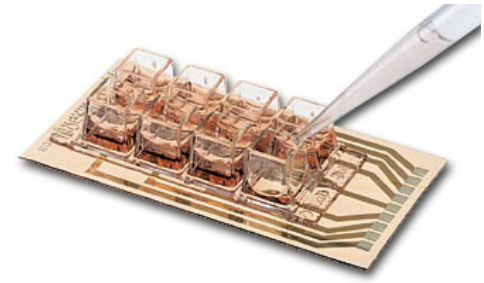

Figure 2.11: Eight-well dish with electrodes deposited upon the bottom of each well. The active electrode area is delineated by circular openings in a photoresist overlayer that insulates the rest of the gold-film electrode from the bulk electrolyte.[25]

2.3 Light Microscopy

2.3.1 Phase Contrast Microscopy

In 1953 the Dutch physicist F. Zernike got the Nobel prize in physics for the invention of the phase contrast microscope. Nowadays, this technique is due to its simplicity and cost-effectiveness widely spread and is one of the basic equipment in each cell laboratory.

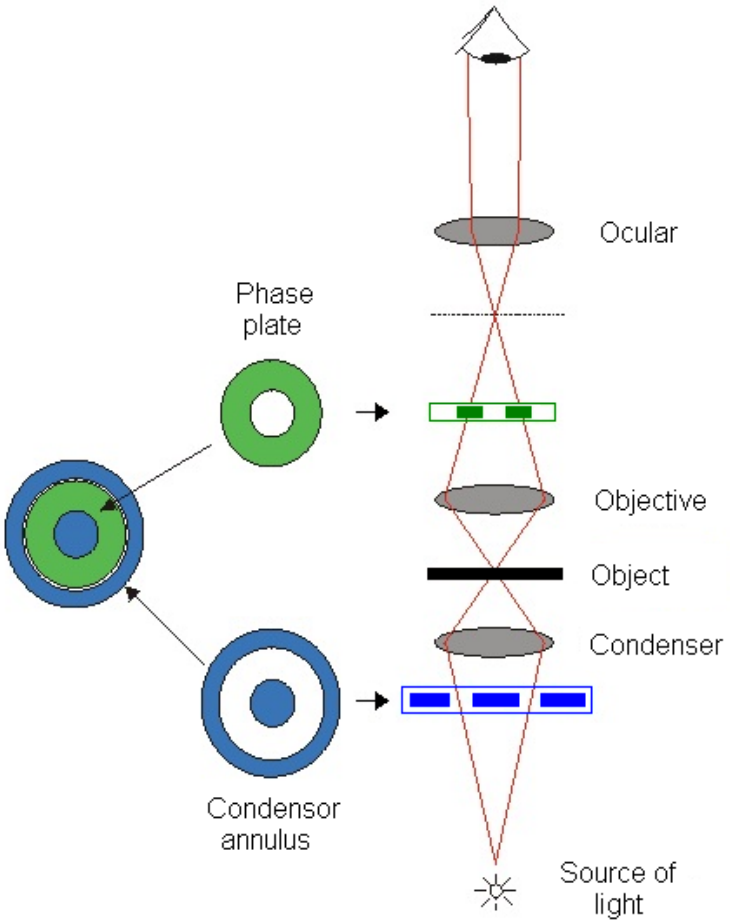

Figure 2.12: Schematic sketch of the optical path of a phase contrast microscope.

An eminent advantage of phase contrast microscopy is the observation of living objects. Using ordinary light microscopy biological objects are nearly invisible to the human eye. As light travels through a medium, interaction

with this medium causes changes of its amplitude and its phase. The human eye measures only the energy of the light arriving at the retina, so changes in phase are not observed, although these changes in phase carry a large amount of information. In 1935 Zernike succeeded in the development of a new technique, the phase contrast microscopy, that transforms changes in the phase into changes in the amplitude and thus makes changes in the phase visible to the human eye.[26, 27, 28] A schematic sketch of the optical path of a phase contrast microscope is depicted in figure 2.12

The principal of phase contrast method is explained considering a transparent object in the form of a one-dimensional phase grating. The transmission function of such an object is given by following equation:[29]

$$F(x) = e^{i\Phi(x)} \tag{2.42}$$

where $\Phi(x)$ is a real periodic function, whose period is equal to the period d of the grating. As the magnitude of Φ is small, equation 2.42 becomes:

$$F(x) \sim 1 + i\Phi(x). \tag{2.43}$$

Developing equation 2.42 into Fourier series results:

$$F(x) = \sum_{m=-\infty}^{+\infty} c_m e^{\frac{2\pi i m x}{d}} \tag{2.44}$$

$$\text{with } c_0 = 1 \text{ and } c_{-m} = -c_m^*. \tag{2.45}$$

The intensity of the mth order is proportional to $|c_m|^2$.

The phase contrast microscope contains a phase plate and a condenser annulus. The dimensions of the phase plate and the condenser annulus are chosen in the way that the light has to pass through a thin annular slit. By means of this slit the ray of light is diffracted. Thus the phase of the central order is retarded or advanced with respect to the diffraction spectra by one quarter of the period. Thus the complex amplitude distribution in the focal plane characterized by the coefficients c_m is altered to a distribution characterized by c'_m, where

$$c'_0 = c_0 e^{\pm i\frac{\pi}{2}} = \pm i \text{ and } c'_m = c_m \qquad (m \neq 0). \tag{2.46}$$

The positive or negative sign refers whether the phase of the central order is retarded or advanced. By this modulation the resulting image in the focus plane represents a fictitious amplitude grating:

$$G(x) = \pm i + i\Phi(x). \tag{2.47}$$

Therefore the intensity in the image plane is now described by the following equation (neglecting Φ^2 in comparison to unity)

$$I(x') = |G(x)|^2 = 1 \pm 2\Phi(x). \tag{2.48}$$

This relation shows that changes in the phase are transformed into changes in the amplitude.

The previous derivation was applied to phase objects with a periodic structure. However, phase contrast method is also valid for non-periodic structures (for a detailed description of this validity see Born and Wolf).[29]

Figure 2.13 shows phase contrast images of giant unilamellar vesicles (A) and MDCK-II cells (B).

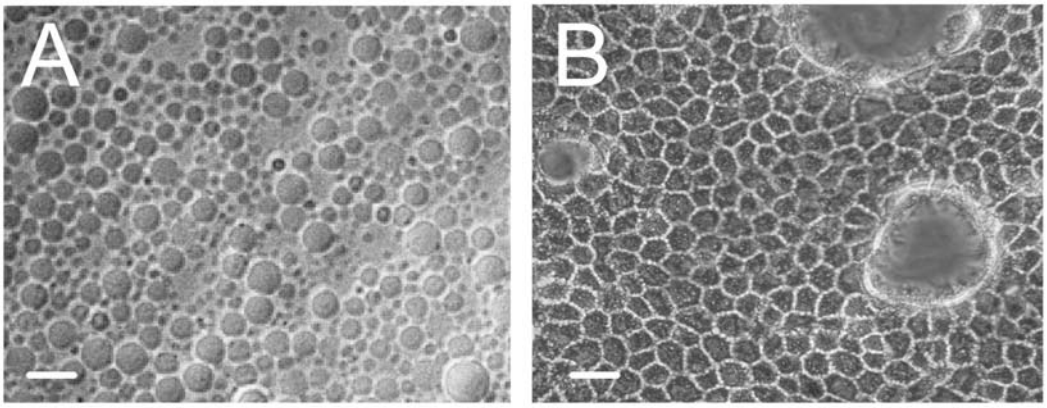

Figure 2.13: Phase contrast images of (A) giant unilamellar vesicles and (B) MDCK-II cells. The scale bar corresponds to 20 μm.

2.3.2 Confocal Laser Scanning Microscopy

Confocal Laser Scanning Microscopy (CLSM), based on wide-field fluorescence microscopy, is a light microscopic method providing high optical resolution. Mostly biologists make use of this novel technique to visualize biological systems, like chloroplast possessing chlorophyll, an autofluorescence molecule. Besides autofluorescence staining vital or dead cells using fluorochromes is used to follow specific processes of the cell's metabolism or to image cellular compounds.

Fluorescence microscopy is based on a physical phenomenon called fluorescence. This phenomenon describes the excitation of molecules, called fluorochromes, by visible light and the entailed emission of the fluorescence

light. This light always possesses a higher wavelength than the excitation light, within nanoseconds. As the adsorbed and emitted light have different wavelength, the fluorescence light can be separated from the excitation light.

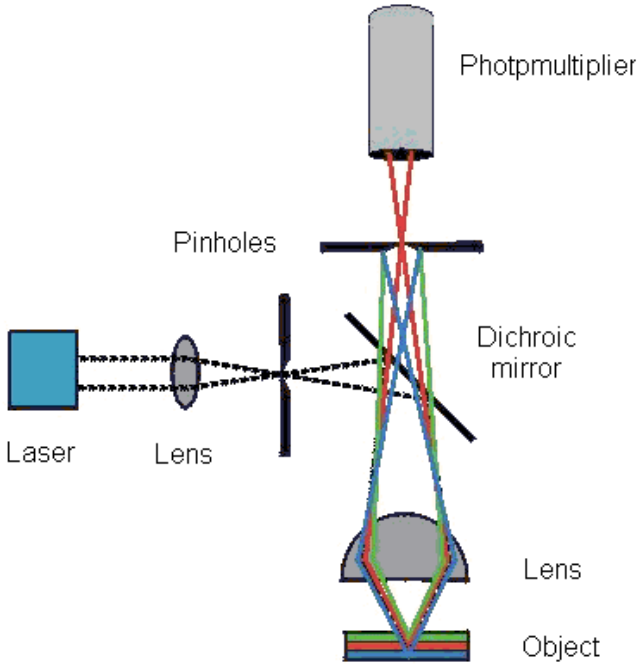

Figure 2.14: Schematic sketch of the optical path of a confocal microscope.

A disadvantage of conventional light microscopy is the detection of unfocused light belonging not to the focus plane in addition to light of the focus plane. This drawback leads to a limited spatial resolution. Thus, elimination of unfocused beams yields a higher spatial resolution. This is realized in confocal microcopy by two pinholes possessing very small diameters. A schematic sketch of the optical path of a confocal microscope is depicted in figure 2.14.

Monochromatic, coherent light generated by a laser and focused by a lens and a pinhole is reflected by a dichroic mirror to the object. The arising fluorescence light of the object, having a higher wavelength than the excitation light, is transmitted by the dichroic mirror and reaches, passing the second pinhole, a photomultiplier which serves as a detector.

Limitation of the emitted light to an individual focus plane and using monochromatic coherent light increase the spatial resolution and the contrast of the image. The symmetric setup of the optical components ensures

that the two pinholes and one point of the objective plane are confocal, i.e. they have the same foci. The signal detected by the photomultiplier belongs exactly to one point of the object. Therefore, the probe has to be scanned pointwise to get the whole image of the object. For this reason scanning mirrors are placed in the optical path to catch all points of the object, which are then detected by the photomultiplier and transferred to a computer which assembles the individual points to a two-dimensional picture. Even three-dimensional pictures can be imaged by variation of the focus plane.

Figure 2.15 shows images of MDCK-II cells (A) and giant unilamellar vesicles (B) taken with a CLSM.

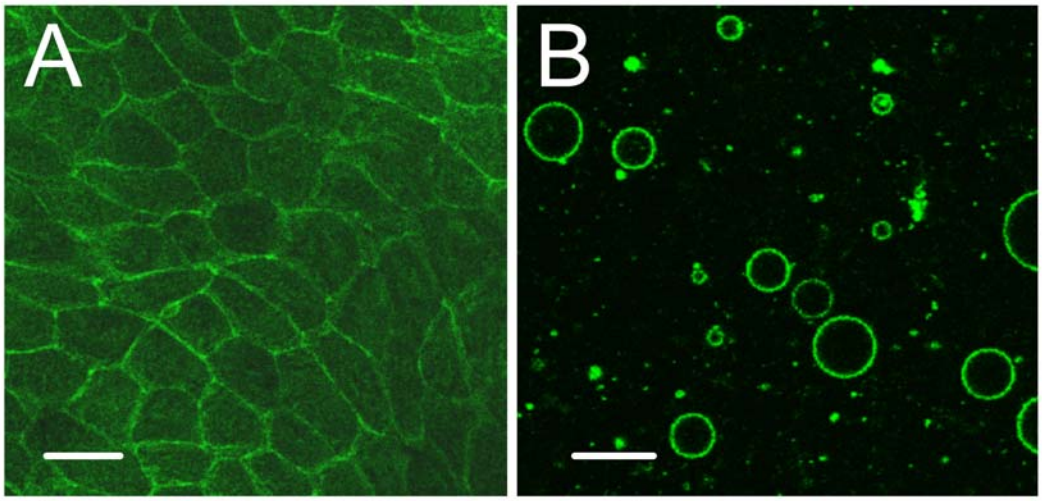

Figure 2.15: Fluorescence images of (A) MDCK-II cells and (B) giant unilamellar vesicles. The scale bar corresponds to 20 μm.

Bibliography

[1] Sauerbrey, G. *Z. Phys.* 1955,155, 206-222.

[2] Nomura, T.; Okuhara, M. *Anal. Chim. Acta* 1982, 142, 281-284.

[3] Kanazawa, K. K.; Gordon, J. G. *Anal. Chem.* 1985, 57,1770-1771.

[4] Bottom, V. E. *Introduction to Quartz Crystal Design*, van Nostrand Reinhold, New York, 1982.

[5] Muramatsu H., Tamiya E., Karube I. *Anal. Chem.* 1988, 60, 2142-2146.

[6] Buttry D., Ward M.D. *Chem. Rev.* 1992, 92, 1355-1379.

[7] Mason, W. P. *Electromechanical transducers and wavefilters* Van Nostrand Company, Princton,1958.

[8] Rosenbaum, J. F. *Bulk acoustic wave theory and devices* Artech House Inc., London, 1988.

[9] Janshoff, A.; Galla, H.-J.; Steinem, C. *Angew. Chem.* 2000, 112, 4164-4195.

[10] Martin, S. J.; Bandey, H. L.; Cernosek, R. W.; Hillman, A. R.; Brown, M. J. *Anal. Chem.* 2000, 72, 141-149.

[11] Granstaff, V. E.; Martin, S. J. *J. Appl. Phys.* 1994, 1319-1329.

[12] Lucklum, R.; Behling, C., Cernosek, R. W.; Martin, S. J. *J. Phys. D* 1996, 30, 346-356.

[13] Lucklum, R.; Hauptmann, P. *Faraday Discuss.* 1997, 107, 123-140.

[14] Rodahl, M.; Höök, F.; Kasemo, B. *Faraday Discuss.* 1996, 107, 229- 246.

[15] Bandey, H. L.; Martin, S. J.; Cernosek, R. W.; Hillman, A. R. *Anal. Chem.* 1999, 71, 2205-2214.

[16] Johannsmann, D. *Macromol. Chem. Phys.* 1999, 200, 501.

[17] Voinova, M. V.; Jonson, M.; Kasemo, B. *Biosensors and Bioelectronics* 2002, 17, 835-841.

[18] Lucklum, R.; Hauptmann, P. *Meas. Sci. Technol.* 2003, 14, 1854-1864.

[19] Giaever, I.; Keese, C. R. *Proc. Nadl. Acad. Sci. USA* 1984, 81, 3761-3764.

[20] Wegener, J.; Keese, C. R.; Giaever, I. *Exp. Cell. Res.* 2000, 259, 158-166.

[21] Wegener, J.; Seebach, J.; Janshoff, A.; Galla, H.-J. *Biophys. J.* 2000, 78, 2821-2833.

[22] Bronstein, I. N.; Semendjajew, A.;Musiol, G.; Mühling, H. *Taschenbuch der Mathematik* Verlag Harry Deutsch, Frankfurt, 1997.

[23] Lo, C.-M.; Keese, C. R.; Giaever, I. *Biophys. J.* 1995, 69, 2800-2807.

[24] Giaever, I.; Keese, C. R. *Proc. Natl. Acad. Sci. USA* 1991, 88, 7896-7900.

[25] www.biophysics.com

[26] Zernike, F. *Z. Tech. Physik* 1935, 16, 454.

[27] Zernike, F. *Phys. Z.* 1935, 36, 848.

[28] Zernike, F. *Physica* 1942, 9, 686, 974.

[29] Born, M.; Wolf, E. *Principales of Optics* Cambridge University Press, 1980.

Chapter 3

Adsorption and Fluctuations of Giant Liposomes Studied by Electrochemical Impedance Measurements

3.1 Introduction

Adsorption and adhesion of liposomes play pivotal roles in many biological processes such as exo- and endocytosis and membrane trafficking. Vesicles also serve as simple model systems for cells. They can be doped with receptor moieties to mimic cell-adhesion, used as targets to screen for membrane-active peptides or proteo-liposomes are used to elucidate transport properties of transmembrane proteins. Moreover, liposomes are frequently used as vehicles for drug delivery or as a reaction compartments on the nanoscale and they provide the starting material for the formation of solid supported lipid bilayers, that are often needed as a matrix for membrane proteins in recent sensor technology.[1, 2]

The kinetics of vesicle adsorption on a surface can be monitored by a variety of different techniques such as ellipsometry, surface plasmon resonance spectroscopy, and most prominently the quartz crystal microbalance (QCM).[3, 4, 5, 6] The QCM allows distinguishing between intact and ruptured vesicles and offers the opportunity to gauge the contact area formed with the quartz crystal similar to optical techniques such as reflection interference contrast microscopy (RICM). For instance, recently we were able to quantify the adhesion energy necessary for liposome rupture by tuning the amount of specific links between support and vesicle.[3, 7, 8] Adhesion of

vesicles as a function of vesicle size and lipid composition has also been studied with the QCM approach.[1, 9] A thorough study on the impact of surface chemistry, vesicle size, temperature and osmotic pressure has recently been provided by Höök and coworkers[1] while Zhdanov and Kasemo were able to simulate the rupture of vesicle by dynamic Monte Carlo simulations.[10] However, despite the usefulness of the quartz crystal microbalance to study the adsorption of vesicles by monitoring both, decrease of the resonance frequency and increase of the viscous energy dissipation of a thickness shear mode resonator, two main drawbacks are related with using the QCM. State-of-the-art sensors need to be organized in arrays of micrometer sized spots to be fast and efficient. However, miniaturizing the active surface of the QCM is limited to the millimeter range due by the accompanying reduction of the quality factor in aqueous solution with decreasing sensing area.[11] The second drawback is the ambiguity in deducing the coverage of the electrode from the frequency shift. This is due to the fact that liposomes represent complex viscoelastic bodies that might cause unpredictable frequency shifts depending on the state of the lipids, their charge and size.[12] In fact, it is even questionable whether the frequency decrease is indeed proportional to an increase in surface coverage. In this paper, we describe a novel means to quantify adsorption of liposomes using electrochemical impedance spectroscopy. The approach is based on sub-millimeter sized electrodes and can in principle be used to study the adsorption and adhesion of single giant liposomes when the electrode area is further reduced in the micrometer range. Moreover, the impedance approach provides a linear correlation between surface coverage and changes in the electrode capacitance recorded at an AC frequency of 40 kHz.[13] The technique also allows distinguishing between intact and disrupted liposomes with the prospect of forming surface bound vesicle-arrays on a micrometer scale well suited to screen for membrane active compounds as demonstrated by the vivid action of melittin, the major constituent of bee venom. So far the technique applied here to monitor liposome adsorption has been widely used to study the adhesion of animal cells and is commonly referred to as electric cell-substrate impedance sensing or short ECIS.[14, 15] We will also show that sensitive impedance readings are well suited to study thermal shape fluctuations of the adsorbed vesicles.

3.2 Material and Methods

3.2.1 Instrumentation

The ECIS device is based on AC impedance measurements using weak and non-invasive AC signals as described in more detail elsewhere.[13, 16] The measurement system consists of an eight-well dish with electrodes deposited upon the bottom of each well, a lock-in amplifier with an internal oscillator, relays to switch between the different wells, and a personal computer that controls the measurement and stores data. The entire system was obtained from Applied Biophysics, Inc. (Troy, NY; www.biophysics.com).

The oscillator applies an AC signal of amplitude 1 V through a series 1 MΩ resistor to the two-electrode system (figure 2.10). With this setup and using physiological buffer solution as the bulk electrolyte, the current flow is approximately constant at 1 μA. The in-phase and out-of-phase voltages across the system are measured by the amplifier and converted to real and imaginary components of the electrode impedance, which are presented formally as resistance and capacitance of a RC series circuit.[14, 16] We acquired impedance data at a fixed frequency of 40 kHz with a time resolution of either 3 min during adsorption of vesicles or 1 second when we monitored shape-fluctuations.

3.2.2 Electrode Arrays

Each electrode well contains a small working electrode (area = $5{\cdot}10^{-4}$ cm^2) and a large counter electrode (area = 0.15 cm^2). Due to the difference in surface area (∼300-fold), the total impedance of the system is determined mainly by the impedance of the small electrode. In addition to this there is a frequency-independent series resistance of roughly 900 ohm due to the solution resistance, especially that immediately next to the small electrode (constriction resistance) as well as a small amount due to leads and contacts. Prior to liposome injection the electrode arrays were treated in an argon-plasma for 10 s, providing an intense cleaning of the electrodes. Directly after plasma cleaning, the electrodes were immersed in an aqueous solution of 1 mM 3-mercaptopropionic acid (Sigma), which self-assembles on the gold surface forming a monomolecular layer. After 30 min, the electrodes were thoroughly washed with water. 1 mM avidin (Sigma) dissolved in buffer solution (150 mM NaCl, 1 mM TRIS-HCl, pH 8) was added and incubated for 60 min. The avidin attaches to the carboxylate group of 3-mercaptopropionic acid via electrostatic interaction.[7] Directly before liposomes were added, the surface was rinsed with buffer solution to remove unbound avidin.

3.2.3 Preparation of Liposomes

Asolectin (Sigma), 1-palmitoyl-2-oleoyl-sn-glycero-3-[phospho-rac-(1-glycerol)] (POPG) (Avanti), 1,2-dipalmitoyl-sn-glycero-3-phosphoethanolamine-N-(CapBiotinyl) (N-biotinyl Cap-PE) (Avanti) and cholesterol (Sigma) were used as purchased and dissolved in chloroform/methanol (1:2, v/v) to prepare films of asolectin/POPG/cholesterol (70:25:5 (w/w)) with variable biotin-content (N-biotinyl Cap-PE) (0, 5, 10, 15 % (w/w) at the cost of asolectin) exhibiting a total weight of 0.2 mg. The lipids were placed at the desired weight ratio in a small glass vial and first dried at 55 °C under a gentle stream of nitrogen and second under vacuum for 3 hours at the same temperature. The films were hydrated in 2 ml of an aqueous solution containing 150 mM sucrose. After an overnight incubation giant unilamellar vesicles (GUVs) were formed spontaneously. The suspension was shaken gently, diluted with 2 ml buffer solution (150 mM NaCl, 1 mM TRIS-HCl, pH 8) and sieved through a polycarbonate membrane (Costar) with pores of 8 μm in diameter.

3.2.4 Monte Carlo Simulation

Kinetics of reversible adsorption on a homogeneous surface can be described by the following rate equation 3.1:

$$\frac{d\Theta}{dt} = k_{on}\pi a^2 \rho(\delta)\Phi(\Theta), \tag{3.1}$$

where Θ denotes the surface coverage, k_{on} is the rate constants of particle adsorption, πa^2 is the area occupied by one vesicle, $\rho(\delta)$ is the number density of vesicles at the interface,[17] and $\Phi(\Theta)$ is the available surface function (ASF), i.e. the area not excluded by adsorbed vesicles. depends on the mass transport of vesicles to the surface. In the simulations below we applied a static method. Mass transport, dominated by sedimentation with the transport rate constant k_{tr} is included by a mean field ansatz as described previously.[8] Assuming linear mass transport to the surface equation 3.2 holds:[18, 19]

$$j = k_{tr}a^2 \left[\rho(\infty) - \rho(\delta)\right], \tag{3.2}$$

with $\rho(\infty)$ being the vesicle number density in the bulk solution and a being the radius of the vesicle. Thus, equation 3.1 becomes equation 3.3:

$$\frac{d\Theta}{dt} = \frac{k_{on}\pi a^2 \rho(\infty)\Phi(\Theta)}{1 + \frac{k_{on}}{k_{tr}a^2}\Phi(\Theta)}. \tag{3.3}$$

Dynamic Monte Carlo simulations are performed as described previously following the RSA-algorithm imposing periodic boundary conditions.8 Adsorption of liposomes, modelled by spheres, normally distributed in size with a mean radius $a = 5\ \mu m$ and a standard deviation of 1 μm, takes place on a square with an edge-length of 1mm. The algorithm comprises the following steps:

- A random place for adsorption of a sphere in the xy plane is chosen and simulation time is incremented by equation 3.4:

$$\Delta t = -\frac{\ln r}{k_{on}\rho(\infty)S}. \tag{3.4}$$

S is the surface area (1 mm^2), and r denotes an evenly distributed random number ($0 < r \leq 1$).

- If the area within a radius of $2a$ around the xy coordinate is empty, adsorption takes place; otherwise the attempt is rejected. If the particle density at the interface is zero, mass transfer is taken into account by adding an increment of time equation 3.5:

$$\Delta t = \frac{1}{k_{tr}a^2\rho(\infty)S} \tag{3.5}$$

consistent with linear transport conditions. The transport rate k_{tr} in equation 3.5 is determined by sedimentation which can be described by Stoke's law equation 3.6:

$$k_{tr} = \frac{2}{9}\frac{g(\rho_{vesicle} - \rho_{H_2O})}{\eta_{H_2O}} \tag{3.6}$$

For $g = 9.81\ ms^{-2}$, viscosity of water $\eta_{H_2O} = 1.002 \times 10^{-2}\ gcm^{-1}$, density of water $\rho_{H_2O} = 0.99823\ gcm^{-3}$, density of liposomes $\rho_{vesicle} = 1.047\ gcm^{-3}$[20] and sedimentation distance $h = 5\ mm$ the transport rate becomes $k_{tr} = 5 \times 10^3\ m^{-1}s^{-1}$.

3.3 Results and Discussion

Electrochemical impedance measurements have been successfully applied in the past to study the time course of attachment and spreading of animal cells to gold-film electrodes that had been pre-coated with various proteins.[13, 21] It has been shown that the total capacitance of the system (imaginary part of the total impedance expressed as capacitance) above a certain threshold frequency (> 10 kHz) is linearly correlated with the coverage of the electrode

with adherent cells. The necessity for the high frequency arises since only at sufficiently high frequencies the current no longer bypasses the cell bodies but flows as displacement current across the cell membranes through the cell interior. The additional capacitance, that is associated with the plasma membranes and that is now in series to the electrode capacitance, reduces the measured overall capacitance accordingly. Thus, it is straightforward that the degree of capacitance reduction is linearly dependent on surface coverage.[13] The size of the electrode is a crucial point for this approach. When the electrode area becomes too large, the resistance of the bulk solution dominates the total impedance of the system and the capacitance of the electrode is hard to determine experimentally at high frequency. Thus, we used the same type of circular gold-film electrodes (d = 250 μm) and the same technical setup as applied for cell adhesion monitoring[13] to follow the adsorption of biotinylated giant liposomes on avidin coated electrodes.

Figure 3.1 compares the time course of the measured capacitance when giant vesicles doped with different mole fractions of biotinylated lipids as well as latex beads of 3 μm diameter were added to the bulk solution. The capacitance values have been normalized to the starting value at time zero. It is evident that the liposomes induce a considerable larger capacitance reduction than latex beads. The reason is that the latex spheres behave like hard particles with only a very limited contact area with the electrode surface. Thus, the current flows predominantly around the particles even at 40 kHz. The giant liposomes, however, spread out to a certain degree on the electrode surface forming an extended area of close contact with the electrode. The biotin-doped liposomes show a faster adsorption kinetic compared to the biotin-free controls. But not only the kinetics are different, we also observed significant differences in the final capacitance which range between 0.6 for the normalized capacitance for the undoped vesicles to 0.4 for the highest biotin doping of 15 % (w/w). We know from preceding SFM studies that the liposomes show a stronger spreading and flattening on avidin-coated surfaces with increasing biotin content.[7] Since adsorption is irreversible the jamming limit, which is the maximal surface coverage, is naturally independent of biotin-content while k_{on} increases with rising content of biotinylated lipids. The contact area with the protein-coated substrate is larger with increasing biotin-content giving rise to a more pronounced capacitance decrease with the same number of vesicles on the surface. Thus, the magnitude of capacitance reduction is assumed to reflect the more sustained spreading of the liposomes with increasing biotin content. Figure 3.1B shows the time dependent increase of the total resistance obtained at a sensing frequency of 40 kHz. Due to the presence of the dielectric particles close to the electrode surface the resistive portion of the impedance is increased as well. Moreover,

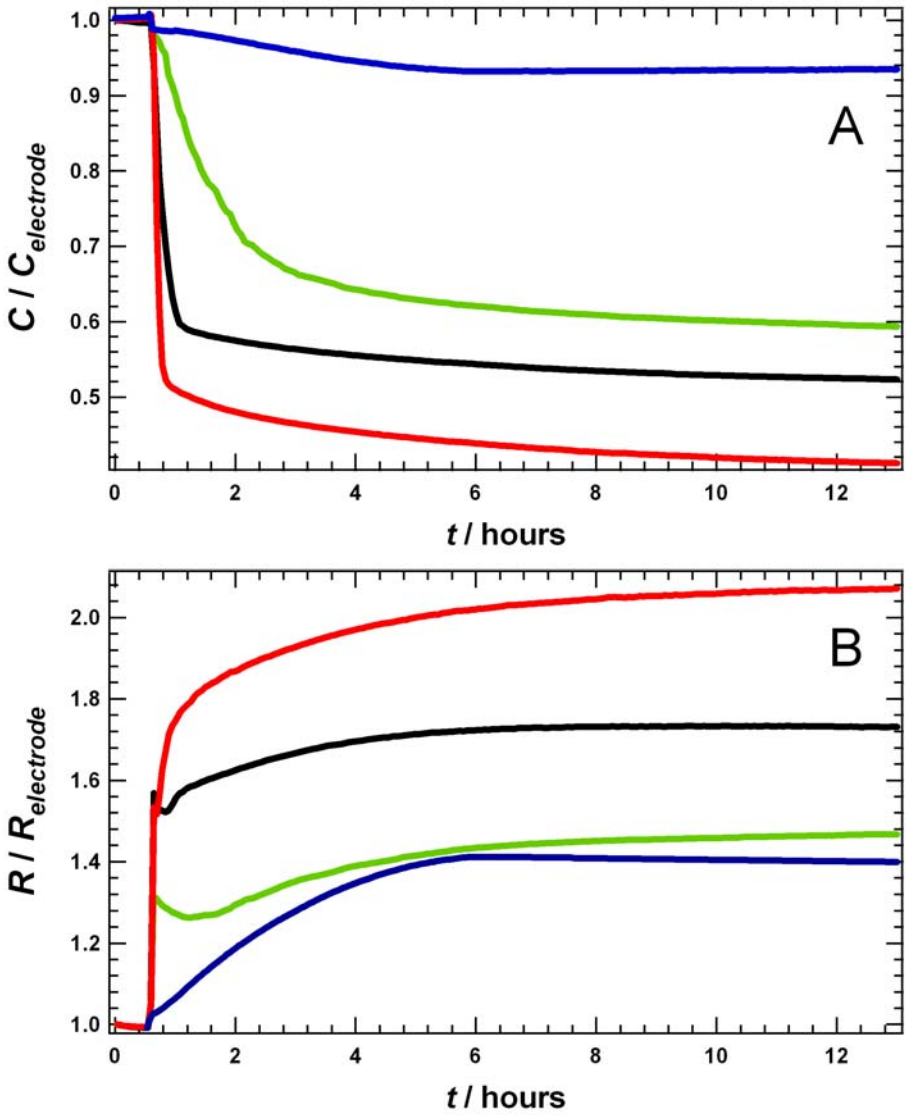

Figure 3.1: Time course of the capacitance (A) and resistance (B) measured at 40 kHz during adsorption of vesicles on the avidin-coated electrodes. Vesicles contain different concentrations of biotinylated lipid, 0 % (green), 5 % (black), 15 % (red). For comparison, the time dependent adsorption of latex beads (blue) on uncoated electrodes is included. For better comparison both quantities are normalized to the starting values at time zero.

with higher biotin concentration the resistance increase is more pronounced but rather low for the hard latex spheres. The resistance readout is, however, more difficult to interpret in terms of surface coverage since the initial jump in resistance is due to the unavoidable change in electrolyte composition associated with vesicle addition to the bathing fluid. Furthermore there is not an easy correlation between surface coverage and magnitude of resistance increase since the latter is also affected by the constriction of current flow between adjacent liposomes.

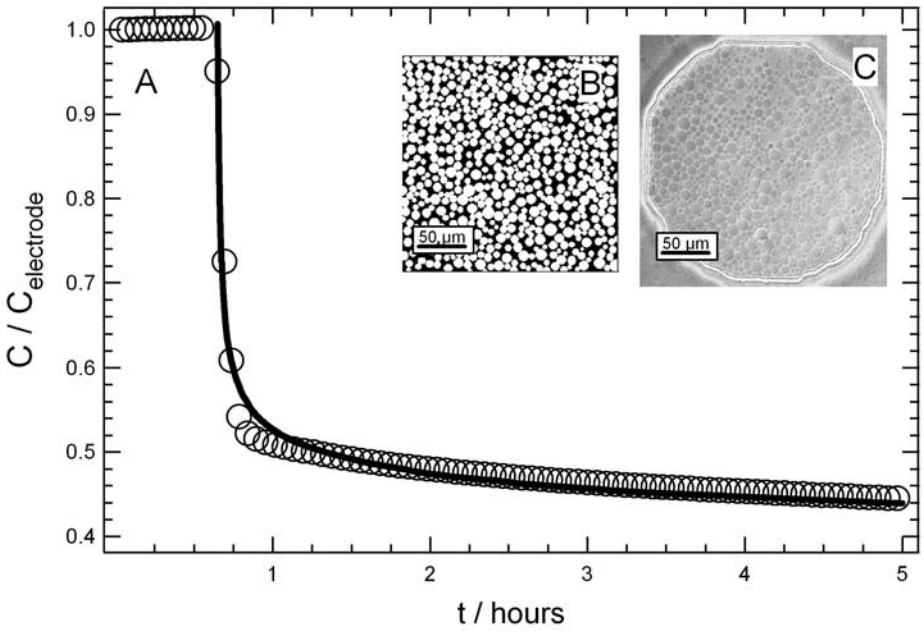

Figure 3.2: Time course of the normalized capacitance measured at 40 kHz when vesicles containing 15 % (w/w) biotinylated lipid adsorb on the functionalized electrode ($\circ\circ\circ$) and values as returned by a dynamic Monte Carlo Simulation (—). The inserts (B) and (C) compare the situation at the electrode surface after vesicle adsorption is complete. (B) visualizes the outcome of the MC calculations close to jamming limit, (C) is a phase contrast micrograph recorded after complete vesicle adsorption.

Figure 3.2 presents the time course of the normalized capacitance for liposomes doped with 15 % (w/w) biotinylated lipids (open symbols) together with the result of a dynamic Monte Carlo simulation (solid line) after optimization of k_{on}. The inserts B and C compare the final situation at the electrode surface as returned by the simulation (B) with a microscopic image

of the vesicles after adsorption was complete (C). The simulated and the experimental situation at the electrode surface compare favorably and from the DMC simulation we could estimate the $\tilde{k}_{on} = k_{on}\pi a^2\rho(\infty)$ value for vesicle adsorption to $(7.0 \pm 0.4)\ \times 10^{-8}\ s^{-1}$. For comparison, the $\tilde{k}_{on}$ value for the undoped liposomes was estimated to $(1.5 \pm 0.5)\ \times 10^{-9}\ s^{-1}$ and is thus, significantly smaller (simulation not shown). The rate constant for mass transport by sedimentation k_{tr} in equation 3.6 was set to $5 \times 10^3\ m^{-1}s^{-1}$ for both doped and undoped vesicles.

We also applied the electrochemical impedance approach to study shape fluctuations of the liposomes adsorbed to the surface. For this purpose we recorded impedance data at fixed AC frequency of 40 kHz with highest sensitivity and a time resolution of 1 s.[12] The resistance at 40 kHz is the most sensitive parameter to monitor shape fluctuations. Figure 3.3 compares the time courses of the fluctuating resistance and the corresponding power spectrum for four different systems: (A) empty electrode just immersed in buffer; (B) 3 μm latex beads; (C) liposomes doped with 15 % (w/w) biotinylated lipids and (D) living MDCK-II cells adherently grown on the electrode surface for comparison. A linear trend was subtracted from the individual datasets prior to the FFT so that the data is now fluctuating around zero. It is apparent that there is a clear difference in the time series recorded for beads and undoped vesicles on the one hand and biotin-doped vesicles as well as living cells on the other hand. To get a more quantitative comparison we have calculated the slopes of the power spectra in the linear regime between 0.1 and 0.01 Hz. For the four different systems we obtained [all $\pm$ 0.1 $(\Omega s)^2$] (A) -0.1 $(\Omega s)^2$; (B) -0.6 $(\Omega s)^2$; (C) -1.9 $(\Omega s)^2$ and (D) -2.7 $(\Omega s)^2$. As expected, the free electrodes just immersed in buffer show the smallest slope of the power spectrum, followed closely by the latex spheres that are unable to pursue form fluctuations by virtue of their construction. Interestingly we observed a slope of approximately $[-2\,(\Omega s)^2]$ for the liposomes which is considered as typical for Brownian motion.[23, 24] Thus, we conclude that it is possible to pick up thermal shape fluctuations of the vesicles by this easy to perform and sensitive electrochemical approach. It is interesting to compare the thermal fluctuations of the liposomes with the form fluctuations performed by living cells in the identical setup. Power spectrum analysis revealed that for living cells we typically find slopes in the range (-2.1 to –2.7), thus, a more sustained frequency dependency than found for Brownian random walk.[23] Consistently, in living cells form fluctuations are not only thermally driven but can be actively pursued by energy consuming activities of the cellular cytoskeleton as has been shown previously.[22]

Taken together, the present study underlines that electrochemical impedance spectroscopy in the way it has been applied here is a powerful

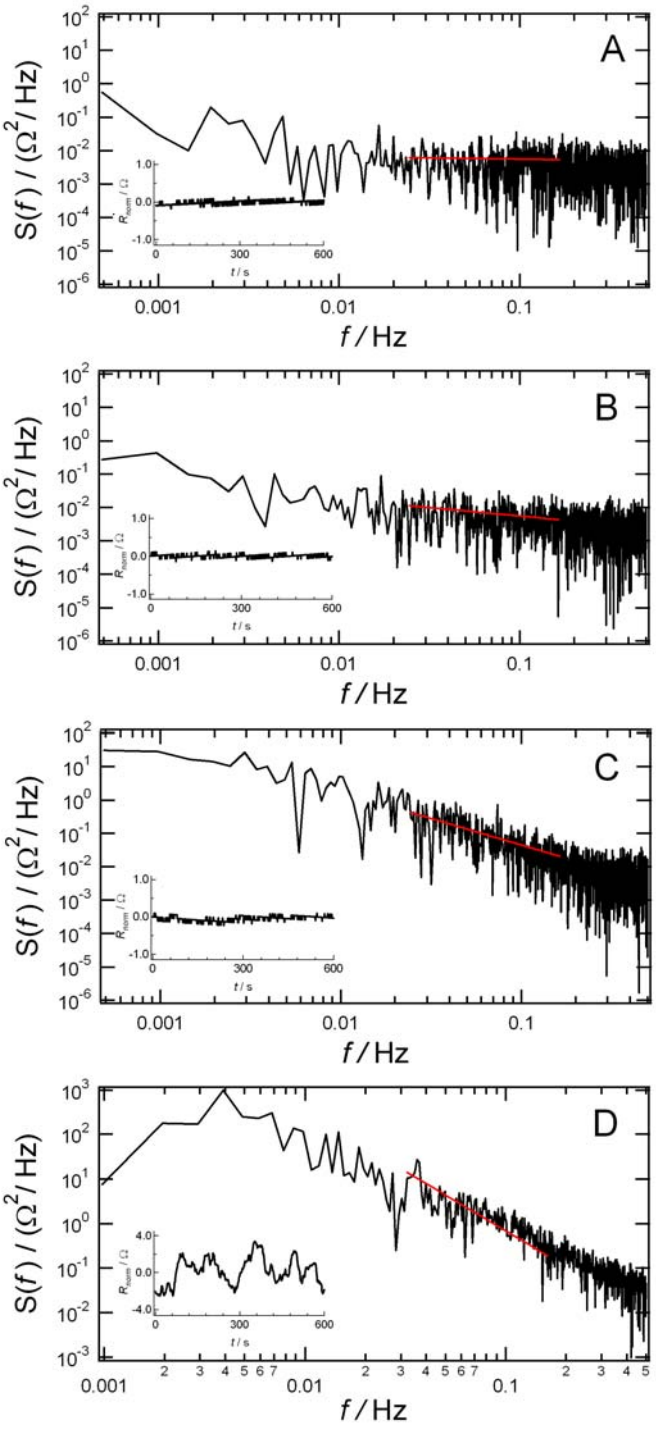

Figure 3.3: Analysis of fluctuations in the resistance measured at a sampling frequency of 40 kHz. To calculate the power spectra we subtracted a linear trend from the raw data and applied an FFT algorithm to subsets of the dataset comprising 2048 s (A-C) and 1024 s (D). The resulting power spectra of the individual subsets were then averaged to yield the spectrum shown in the figure. (A) Empty electrode just immersed in buffer. (B) 3 μm latex beads. (C) Vesicles with 15 % (w/w) biotinylated lipids. (D) Living cells (MDCK-II) in their culture fluid (note the scale).

tool to study the adsorption of giant vesicles to technical surfaces as well as their thermal shape fluctuations and the interference of membrane active compounds. The current device can be further miniaturized to provide the technical basis for screening arrays on the micrometer scale.

Bibliography

[1] Reimhult, E.; Höök, F.; Kasemo, B. *Langmuir* 2003, 19, 1681-1691.

[2] Stamou, D.; Duschl, C.; Delamarche, E.; Vogel, H. *Angew. Chem. Int. Ed. Engl.* 2003, 42, 5580-5583.

[3] Reiss, B.; Janshoff, A.; Steinem, C.; Seebach, J.; Wegener, J. *Langmuir* 2003, 19, 1816-1823.

[4] Keller, C. A.; Glasmästar, K.; Zhdanov, V. P.; Kasemo, B. *Phys. Rev. Letters* 2000, 84, 5443-5446.

[5] Keller, C. A.; Kasemo, B. *Biophys. J.* 1998, 75, 1397-1402.

[6] Lüthgens, E.; Herrig, A.; Kastl, K.; Steinem, C.; Reiss, B.; Wegener, J.; Pignataro, B.; Janshoff, A. *Meas. Sci. Technol.* 2003, 14, 1865-1875.

[7] Pignataro, B.; Steinem, C.; Galla, H. J.; Fuchs, H.; Janshoff, A. *Biophys. J.* 2000, 78, 487-498.

[8] Kastl, K.; Herrig, A.; Lüthgens, E.; Janshoff, A.; Steinem, C. *Langmuir* 2004, 20, 7246-7253.

[9] Faiss, S.; Lüthgens, E.; Janshoff, A. *Eur. Biophys. J.* 2004, 33, 555-561.

[10] Zhdanov, V. P.; Keller, C. A.; Glasmästar, K.; Kasemo, B. *J. Chem. Phys.* 2000, 112, 900-909.

[11] Rosenbaum, J. F. *Bulk acoustic wave theory and devices* Artechhouse: Boston, 1988.

[12] Lucklum, R.; Hauptmann, P. *Meas. Sci. Technol.* 2003, 14, 1854-1864.

[13] Wegener, J.; Keese, C. R.; Giaever, I. *Exp. Cell. Res.* 2000, 259, 158-166.

[14] Giaever, I.; Keese, C. R. *Nature* 1993, 366, 591-592.

[15] Giaever, I.; Keese, C. R. *Proc. Natl. Acad. Sci. U S A* 1984, 81, 3761-3764.

[16] Giaever, I.; Keese, C. R. *Proc. Natl. Acad. Sci. U S A* 1991, 88, 7896-7900.

[17] Adamczyk, Z. *Adv. Colloid Interface Sci.* 2003, 100-102, 267-347.

[18] Adamczyk, Z. *Adv. Colloid Interface Sci.* 2000, 229, 477-489.

[19] Adamczyk, Z.; Siwek, B.; Warszynski, P.; Musial, E. *J. Colloid Interface Sci.* 2001, 242, 14-24.

[20] Goormaghtigh, E.; Scarborough, G. A. *Anal. Biochem.* 1986, 159, 122-131.

[21] Kowolenko, M.; Keese, C. R.; Lawrence, D. A.; Giaever, I. *J. Immunol. Methods* 1990, 127, 71-77.

[22] Lo, C.-M.; Keese, C. R.; Giaever, I. *Exp. Cell Res.* 1993, 204, 102-109.

[23] Giaever, I.; Keese, C. *IEEE Trans Biomed. Eng.* 1986, 33, 242-247.

[24] Marinari, E.; Parisi, G.; Ruelle, D.; Windey, P. *Phys. Rev. Lett.* 1983, 50, 1223-1225.

Chapter 4

Electrically Induced Deformation of Giant Liposomes Monitored by Thickness Shear Mode Resonators

4.1 Introduction

Biological membranes play a pivotal role in living organisms. Mainly composed of phospholipids forming a two-dimensional fluid, biological membranes serve a large variety of functions. They form semipermeable barriers, which are quite permeable for water but impermeable for ions enabling cells to create nano to micrometer sized compartments a prerequisite for providing locally restricted reaction sites and a communication platform based on adsorption, exo- and endocytosis as well as electrical impulses.

From a mere physical viewpoint, thus reducing biological membranes essentially to a lipid bilayer, the mechanical properties of lipid bilayers deserve special attention due their unique features. Bilayers are extremely soft with respect to bending but essentially incompressible under lateral tension. This particular combination of elastic properties of the lipid bilayer ensures high deformability as it is necessary to allow for cell migration and at the same time it guarantees integrity without loss of material.

The elastic properties of vesicles are generally determined by all classical deformation modes such as extensible deformation, shearing, and bending. In the fluid state shearing is negligible since the molecules can move freely

in two dimensions. Two parameters, the bending modulus κ and the area compressibility K_a determine the mechanical behavior of the bilayer. The elastic properties are mainly governed by the lipid composition. For instance, it was found that addition of cholesterol to fluid bilayers such as DMPC increases K_a and κ drastically up to a factor of 6 due to the condensing effect of the chain packing.[1] Since the pioneering work of Helfrich and Evans the outstanding role of bending elasticity for the structure and function of biological membranes has become increasingly evident.[1] Bilayer elasticity is essential for the lipid/protein interaction, the behavior of lipid-mixtures, for lyotropic phase transitions, fusion, exo-and endocytosis just to name a few relevant examples. Hence, precise measurements of elastic properties of lipid bilayers are an important challenge in biological physics.

The elastic properties can be quantified by a variety of different techniques such as scanning force microscopy,[2] micropipette aspiration techniques,[3] extrusion[4] or optical measurements,[5] generating deformation by mechanical forces. Deforming vesicle membranes can also be provoked by electric fields. Kummrow and Helfrich[6] were the first to employ an alternating electric field to stretch vesicles membranes of giant unilamellar vesicles that could easily be observed by optical microscopy.

Here, we describe a novel means to quantify nanoscopically small deformations of liposomes using thickness shear mode resonators in conjunction with an external electrical field applied simultaneously. We found that small deformations of giant liposomes attached to the working electrode of the quartz resonator via electrostatic interactions or molecular linkers (avidin-biotinylated lipids) in the nanometer range can be monitored while applying an alternating voltage in the millivolts regime. We found that adding of cholesterol to the lipid mixture considerably decreases the deformability of the vesicles rendering our new approach a sensitive tool to study the bending rigidity of liposomes employing ultrasmall deformations with little physical or chemical constraints.

4.2 Material and Methods

4.2.1 Experimental Setup

Deformations of giant vesicles are induced by an external alternating electric field and read out by the response of a thickness shear mode resonator. In figure 4.1 the experimental setup is schematically depicted. 5 MHz AT-cut quartz crystals (KVG, Neckarbischofsheim, Germany) coated on both sides with circular gold electrodes ($\varnothing$ = 5 mm)[7] were mounted as the bot-

tom plate into a home-made crystal holder (Teflon). The setup basically consists of the quartz resonator and a phase-lock oscillator (QCM100, SRS Inc., Sunnyvale, CA, USA) that allows monitoring the resonance frequency and applying an alternating voltage across the upper electrode on top of the quartz surface simultaneously.

Vesicle adsorption was achieved using a thermostatted flow system as depicted in figure 4.1. A pump ensures a constant flow of buffer solution through the tubes, the QCM cell, and the reaction chamber. Liposomes are first injected into the reaction chamber and then directed to the quartz surface in the QCM cell by convection.

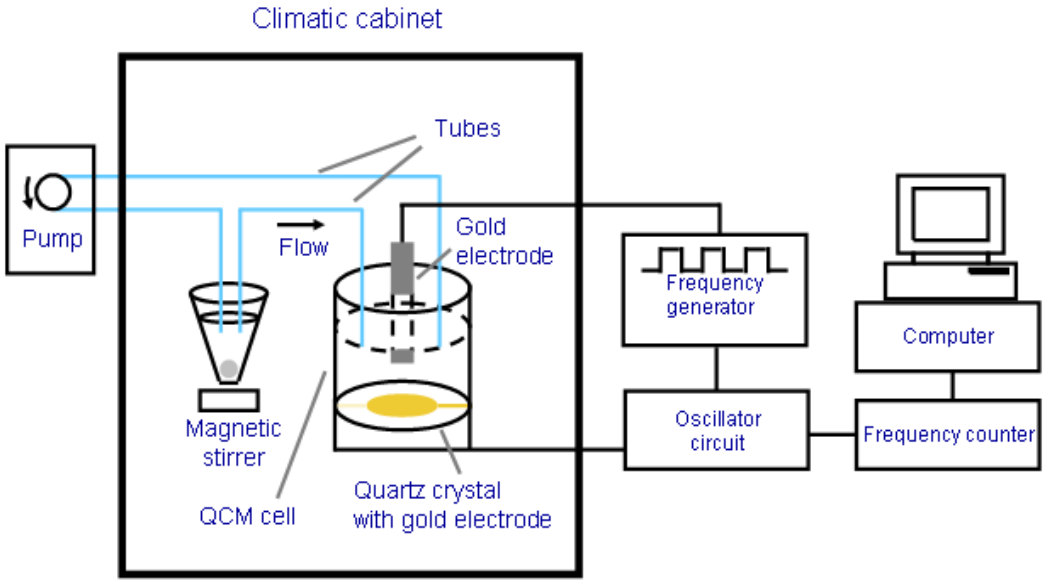

Figure 4.1: Experimental setup used for the observation of electrical induced deformation of giant liposomes, equipped with an electrode in the top. Between this gold electrode and the electrode on the top of the quartz crystal, referred to as the working electrode a square wave voltage is applied using a frequency generator.

All experiments were carried out at 37 °C. The resonance frequency of the oscillating crystal was recorded by a frequency counter (Agilent 53181A, Agilent Technologies, Palo Alto, Calif., USA) and subsequently transferred via GPIB to a computer. An alternating voltage around zero volts with an amplitude of 20 - 100 mV was applied across the working electrode on top of the quartz crystal and a large counter electrode (gold) immersed in solution.

The space between the two electrodes was about 3.2 mm.

4.2.2 Preparation of Giant Liposomes and Surface Functionalization

Asolectin (Sigma), 1-palmitoyl-2-oleoyl-sn-glycero-3-[phospho-rac-(1-glycerol)] (POPG) (Avanti), 1,2-dipalmitoyl-sn-glycero-3-phosphoethanolamine-N-(CapBiotinyl) (N-biotinyl Cap-PE) (Avanti) and cholesterol (Sigma) were used as purchased and dissolved in chloroform/methanol (1:2, v/v) to prepare films of asolectin/POPG/cholesterol (70:25:5 (w/w)) with variable biotin-content (N-biotinyl Cap-PE) (0 and 15 % (w/w) at the cost of asolectin) and with variable cholesterol-content (5 and 20 % (w/w) at the cost of asolectin) exhibiting a total weight of 0.2 mg. The lipids were placed at the desired weight ratio in a small glass vial and first dried at 55 °C under a gentle stream of nitrogen and second under vacuum for 3 hours at the same temperature. The films were hydrated in 2 ml of an aqueous solution containing 150 mM sucrose. After an overnight incubation giant unilamellar vesicles (GUVs) were formed spontaneously. The suspension was shaken gently and diluted with 2 ml buffer solution (150 mM NaCl, 1 mM TRIS-HCl, pH 8). Unilamellarity of the vesicles was verified by confocal laser-scanning microscopy (Leica) using 1 mole % -Bodipy FL C12-HPC (Molecular Probes) as a label (figure 4.2).

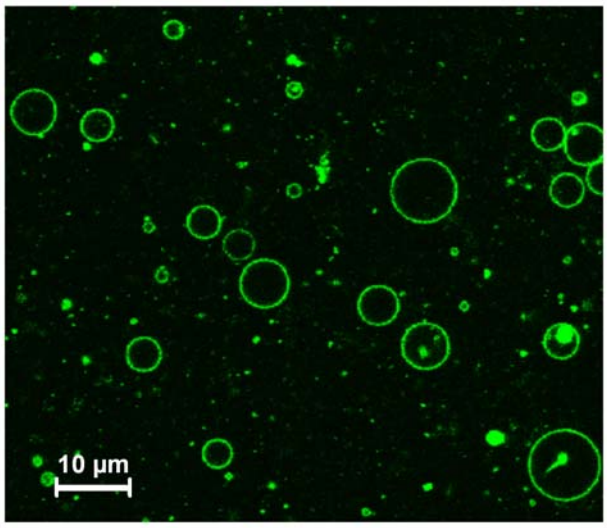

Figure 4.2: Fluorescence light microscopy of giant unilamellar vesicles.

Surface functionalization the quartz crystals was carried out using an argon plasma for 30 s, which ensures an intense cleaning of the electrodes. Directly after plasma cleaning, the crystals were assembled in the QCM cell and then immersed in an aqueous solution of either (i) 2-mercapto-ethylamine (Sigma) or (ii) 1 mM 3-mercaptopropionic acid (Sigma), which self-assembles on the gold surface forming a charged monomolecular layer providing a charged surface. After 30 min, the electrodes were thoroughly washed with ultrapure water. On the electrode functionalized with 3-mercaptopropionic acid a total of 200 μl of a 1 mM avidin (Sigma) solution (buffer: 150 mM NaCl and 1 mM TRIS-HCl at pH 8) was added and incubated for 60 min. The positively charged avidin attaches to the carboxylate group of 3-mercaptopropionic acid via electrostatic interactions.[8, 9] Giant liposomes were adsorbed either electrostatically on the positively charged self-assembly MEA layer deposited on the gold electrode or via quasi-covalent linkages of biotin-avidin contacts in the case of biotinylated GUVs.

4.2.3 General Measurement Procedure

After functionalization of the gold surface as described above at first GUVs were injected into the reaction chamber (figure 4.1) and the time course of the resonance frequency was monitored. After completion of the adsorption process the pump was switched of and the alternating voltage was applied across the deposited liposomes (1 Hz, 20-100 mV amplitude) while changes in the resonance frequency were monitored.

4.2.4 TSM Resonators under Viscoelastic Load

The vibration behavior of TSM resonators in fluids is influenced by the physical properties of the surrounded medium, namely density and viscosity.[10, 11, 12] Recent studies[13, 14] provide a model for the oscillation of quartz resonators in contact with a fluid under viscoelastic load. In most cases when biological systems are studied with the QCM, it is safe to assume that a viscoelastic solid is in contact with the quartz resonator immersed in water. Using the complex shear modulus $G^* \equiv G' + iG''$ of the viscoelastic film the change in resonance frequency from its unperturbed value can approximately be expressed as:[13, 14]

$$\Delta f = -\frac{2h\rho}{h_q\rho_q} f_0 \left[1 - 2\frac{\pi\rho_{fl}\eta_{fl}}{\rho}\frac{G''}{G'^2 + G''^2}\right], \tag{4.1}$$

with f_0 the fundamental resonance frequency of the quartz resonator, $h_q = 3.3 \cdot 10^{-2}\ cm$ is its thickness and $\rho_q = 2.65\ \frac{g}{cm^3}$ the density of the quartz crys-

tal. ρ is the density of the viscoelastic layer, h its thickness, η_{fl} and ρ_{fl} the viscosity and the density of the surrounding liquid. The liquid is represented by the buffer solution, so the viscosity η_{fl} is approximately $\eta_{H_2O} = 1.002 \cdot 10^{-2}$ $\frac{g}{cm \cdot s}$ with a density of $\rho_{H_2O} = 0.99823$ $\frac{g}{cm^3}$. The adsorbed vesicles can be described as a thin viscoelastic layer on the quartz resonator. Thus ρ in equation 4.1 becomes $\rho_v = 1.047$ $\frac{g}{cm^3}$,[15] while $h = h_v$ represents the mean thickness of the vesicle layer. Equation 4.1 reveals that the thickness of the vesicle layer h_v is direct proportional to the corresponding change in resonance frequency Δf. Hence, as the complex shear modulus of the vesicles is unavailable at this frequency, the change in height of the viscoelastic layer can be roughly estimated from the observed frequency shift of 140 Hz corresponding to the adsorption of giant liposomes with an average diameter about 5 μm:

$$\Delta h_v \approx 36 \Delta f \frac{nm}{Hz} \tag{4.2}$$

with $\Delta f = \Delta f(h_v) - \Delta f(h'_v)$ the frequency change due to vesicle deformation.

4.2.5 Fourier Analysis

Expecting a signal $\xi(t)$ which repeats after a period T, means $\xi(t+T) = \xi(t)$, Fourier showed that this periodic signal can be built by the sum of harmonic oscillations. The first, the fundamental oscillation owns the frequency $\nu = 1/T$. The other oscillations, the overtones are given by whole numbers of ν: $\nu_2 = 2\nu$, $\nu_3 = 3\nu$ and so on. So $\xi(t)$ can be expressed by the following equation:

$$\xi(t) = \sum_{-\infty}^{+\infty} \xi_n e^{i(n 2\pi \nu t + \varphi_n)}, \tag{4.3}$$

where φ_n is the phase and ξ_n is the amplitude of the fourier-component.

In practise, an empirical signal $c(t)$ has to be analyzed. Those functions are not longer exactly calculable. So, to approximate the Fourier Transformation the discrete Fourier Transformation (DFT) is used to calculate the power spectral density spectrum $S(f)$:

$$
\begin{aligned}
C_k &= \sum_{j=0}^{N-1} c_j e^{\frac{2\pi i j k}{N}} = DFT(c(t)) \qquad k = 1, 2, ..., (N-1) \qquad (4.4)\\
\Phi(0) &= \Phi(f_0) = \frac{1}{N^2} |C_0|^2 \\
\Phi(f_k) &= \frac{1}{N^2} \left(|C_k|^2 + |C_{N-k}|^2 \right) \qquad k = 1, 2, ..., (N/2-1) \\
\Phi(f_c) &= \Phi(f_{N/2}) = \frac{1}{N^2} \left| C_{N/2} \right|^2
\end{aligned}
$$

where $f_k = \frac{k}{N\Delta t} = 2 f_c \frac{K}{N}$ $(k = 0, 1, ..., N/2)$ and N is an even number, the number of sampling points. f_k is defined for zero and positive frequencies, Δt is the sampling interval and $f_c = \frac{1}{2\Delta t}$ is the maximum frequency within the Nyquist interval. Finally, $\Phi(f)$ is divided by the sampling frequency Δf and multiplied by N to obtain the *power spectral density function* $S(f)$ in accordance with Parseval's theorem. Data with equidistant time scale is recorded, subdivided into sets containing multiples of 2^n data points. Each subset of the original data is subjected to a Fast Fourier transformation and the mean of the power spectrum from all data subsets is calculated.

4.3 Results and Discussion

Figure 4.3 displays the frequency response and the change of the dissipation factor of a 5 MHz TSM resonator upon vesicle adsorption. Here, giant unilamellar liposomes composed of asolectin/POPG/cholesterol (70:25:5 (w/w)) were exposed to a charged surface, functionalized with 2-mercaptoethylamine, using the setup as described above. Typically a frequency decrease of approximately 140 Hz (black curve) and an increase of the dissipation factor of $45 \cdot 10^{-6}$ (grey curve) can be observed.

Deformation experiments of giant liposomes are performed after adsorption of the vesicles is complete. An alternating voltage with an amplitude of 20 – 100 mV was applied across the vesicle layer with a frequency of 1 Hz. The resonance frequency was recorded with a sampling rate of 13 Hz, i.e. one data point every 75 ms. A linear trend attributed to a non specific drift in the signal was subtracted from each individual dataset so that the presented data show changes in the resonance frequency around zero Hz. Figure 4.3B shows a scheme illustrating the deformation of vesicles as a function of the applied potential, reflecting essentially a modulation of adhesion energy by changes of the surface potential. Exerting attractive forces results in a flattening of

the attached liposomes due to an increase in adhesion, while the opposite behavior is induced when the voltage creates repulsive forces. In fact, we found that the resonance frequency decreases if the forces are repulsive, i.e. the height increases while at the same time the contact area decreases. This is in good accordance to previous findings of Faiss et al.,[16] where we could show that the shift in resonance frequency decreases with larger adhesion force due to stronger binding of vesicles to the surface accompanied by flattening. The frequency response of negatively charged giant liposomes containing different amounts of cholesterol to a square wave voltage is shown in figure 4.4.

The objective was to investigate whether a stiffening of the membrane by addition of cholesterol can be assessed by measuring the deformation of the liposomes as a result of a given external voltage. Liposomes containing 5 % (w/w) cholesterol, adsorbed on an electrode functionalized with MEA (2-mercapto-ethylamine), respond to the applied alternating voltage of 100 mV with a average overall frequency shift of 0.8 Hz (figure 4.4A). Connecting an oscilloscope to the setup, we observed that an increase of the resonance frequency is correlated to a positive voltage as depicted in figure 4.3B. Conversely, a negative voltage provokes a decrease of the resonance frequency.

Due to the given relationship between the resonance frequency and the thickness of the vesicle layer (equation 4.1), the observed frequency shift can be attributed to a deformation of the liposomes, i.e. a reduction in height if an attractive contact potential is applied.[17] It has been shown experimentally and theoretically that vesicles adopt a flat shape if the adhesion energy increases.[9, 17] According to equation 4.2 a change in height of nm is induced by the applied voltage of 100 mV. A decrease in height of the GUVs is observed if the voltage imposes attractive forces thus resulting in an increase in resonance frequency, while reduction of adhesion results in an increase in vesicles height. Neither detachment nor rupture was observed in the voltage regime up to 100 mV.

Liposomes with a higher concentration of cholesterol, i.e. 20 % (w/w), exhibit a significantly reduced frequency response (figure 4.4B). Only a frequency shift of 0.2 Hz could be observed employing a voltage of 100 mV. This reduction of the frequency response due to a higher concentration of cholesterol is attributed to the increased bending rigidity of the GUVs withstanding deformation by an external field more efficiently. Using equation 4.2 we found a change in the height of the liposomes $\Delta h_v \approx (28.8 \pm 4.3)\ nm$ for vesicles containing 5 % (w/w) cholesterol but merely $\Delta h_v \approx (7.2 \pm 1.1)$ $nm$for those containing 20 % (w/w) cholesterol. The average diameter of the used giant unilamellar liposomes is about 5 μm. Thus the calculated changes in height leads to a relative deformation $\frac{\Delta h_v(5\%chol)}{h_v} \approx 0.6\%$ and

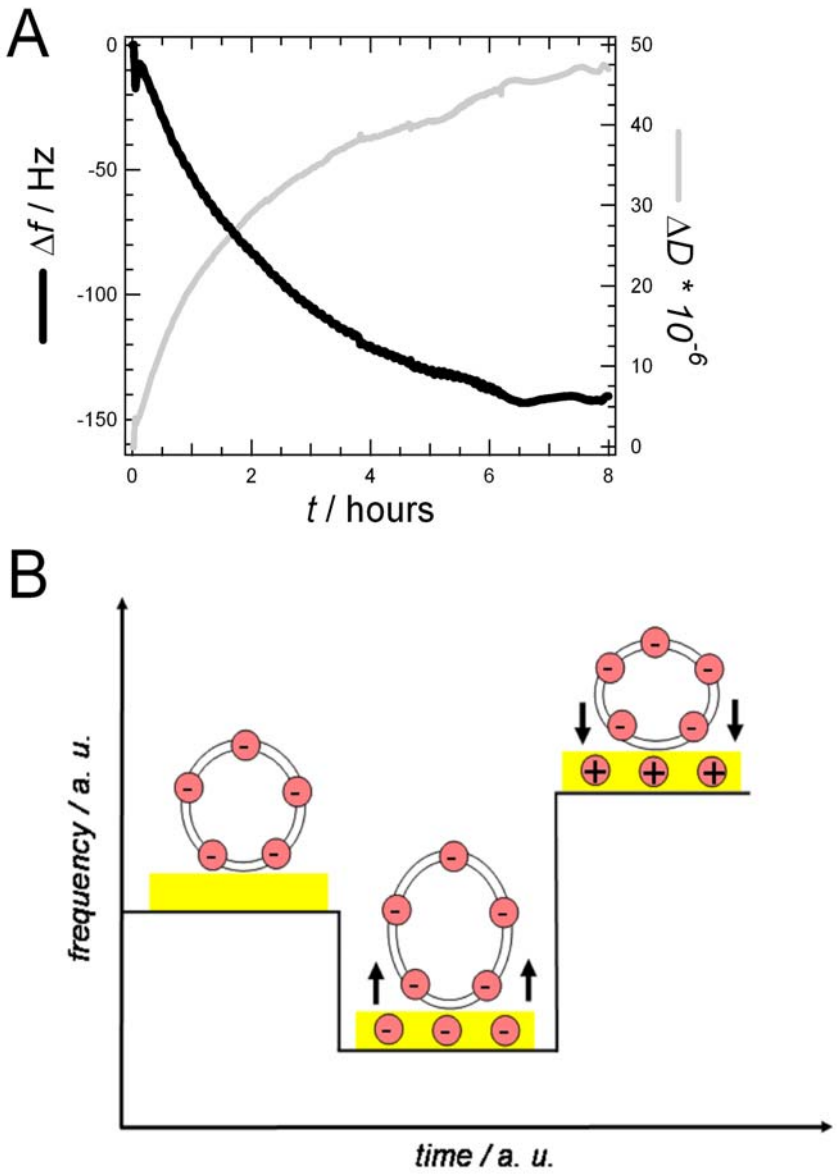

Figure 4.3: (A) Shift of the resonance frequency Δf and the dissipation factor ΔD due to adsorption of giant vesicles on the electrode of the quartz crystal. (B) Schematic diagram of vesicle deformation due to the applied alternating electrical voltage and the corresponding change of the resonance frequency.

$\frac{\Delta h_v(20\%chol)}{h_v} \approx 0.1\%$. In fact, using large unilamellar vesicles (LUVs) made from gel phase lipids (DPPC/DPPG) do not respond to an external voltage at all.

Washing the electrode with the detergent triton-X (Sigma) essentially destroys the liposomes almost entirely abolishing the frequency response of the quartz resonator to the external voltage. In fact, in the absence of liposomes we found only negligible changes in frequency when a voltage of about 100 mV was applied. Therefore, we can clearly say that the observed changes in the normalized frequency shown in figure 4.4A and 4.4B are due to the deformation of giant unilamellar liposomes as a response to an alternating electric square wave voltage. Control experiments in the absence of vesicles show no detectable changes in the resonance frequency upon changes in the surface potential.

If our hypothesis was right that the liposomes respond to the external voltage with shape changes we should be able to suppress this response by attaching the liposomes more firmly to the substrate. We used liposomes doped with varying amounts of biotinylated lipids adhering to avidin-covered surfaces in order to modulate the adhesion force. Figure 4.5 displays the behavior of charged giant liposomes containing different concentrations of biotinylated lipids.

While we found a frequency shift of 0.15 Hz for giant unilamellar vesicles with 0% Biotin-X-DPPE applying a voltage of 100 mV, the frequency response to the square voltage is significantly reduced to merely 0.04 Hz when doping the vesicles with 15% biotinylated lipids (figure 4.5B). Using equation 4.2, we estimate a change in height of $\Delta h_v \approx (5.4 \pm 0.8)\ nm$ for liposomes without biotin and $\Delta h_v \approx (1.4 \pm 0.2)\ nm$ for liposomes containing 15 % (w/w) biotinylated lipid. This leads to a relative deformation $\frac{\Delta h_v(0\%biotin)}{h_v} \approx 0.11\%$ and $\frac{\Delta h_v(15\%biotin)}{h_v} \approx 0.03\%$. The reduced frequency response of the liposomes with high amount of biotinylated lipid can be attributed to the strong interaction of biotin and avidin. In preceding studies using scanning force microscopy[8] and electrochemical impedance measurements[18] we observed that liposomes show a stronger flattening on avidin-coated surfaces with an increasing biotin content. At a threshold of approximately 30 mol% biotinylated lipid the vesicles start rupturing. Therefore deformation of vesicles containing 15 % (w/w) biotinylated lipid is reduced, due to the strong adhesion and resulting flattening on the surface. Notably, we have chosen the highest possible biotin content, which does not yet produce planar bilayers as shown previously.[9]

Interestingly, we observed that the frequency shift found for liposomes attached to avidin is typically less than 20 % as compared to liposomes of

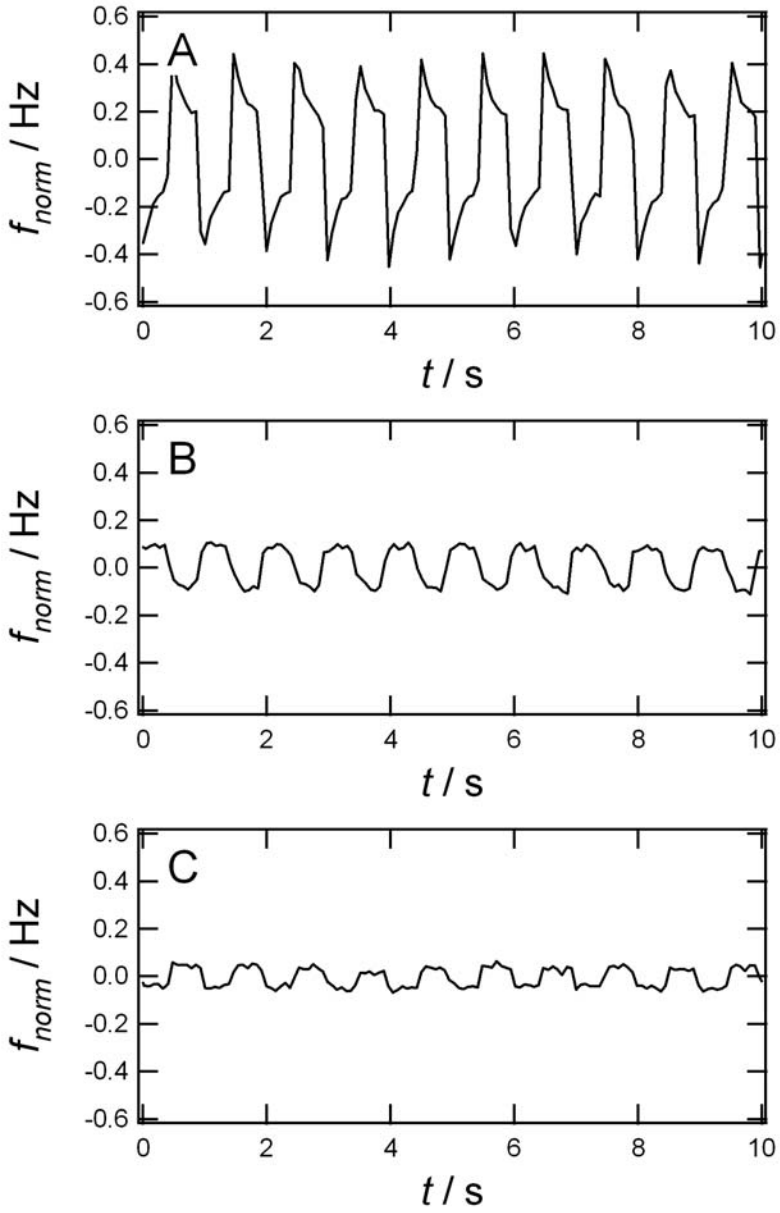

Figure 4.4: Time course of the resonance frequency while a square wave voltage of 100 mV is applied. The negatively charged vesicles contain different concentration of cholesterol, (A) 5 % (w/w) and (B) 20 % (w/w). (C) shows the response of the quartz crystal after removal of adsorbed vesicles with detergent triton-X. The surface of the quartz crystal functionalized with MEA self assembled on the gold electrode.

the same composition adsorbed on a MEA-functionalized electrode (figure 4.4/4.5). This can be explained by the differences in voltage drop across the two different self-assembly layers. The layer consisting of MPA (3-mercaptopropionic acid) and avidin produces a larger voltage loss than the MEA covered gold electrode. This way the liposomes experience smaller external deformation forces in the case of avidin covering the surface. The change in resonance frequency scales roughly linear with the applied voltage. We kept the voltage below 100 mV in order to avoid interference with typical membrane potential. Below 20 mV a frequency shift could not be detected.

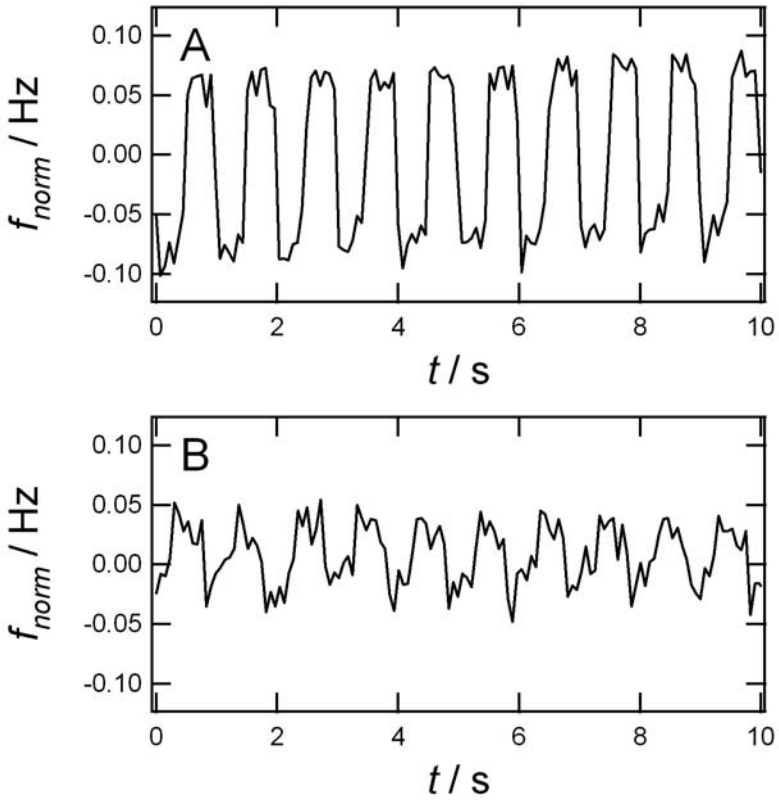

Figure 4.5: Time course of the resonance frequency while a square wave voltage of 100 mV is applied. The negatively charged giant vesicles contain different concentrations of biotinylated lipid, (A) 0 % (w/w) and (B) 15 % (w/w).

Deformation of giant liposomes was induces by a periodic signal. As explained above every periodic signal can be described as the sum of its fundamental frequency and the corresponding overtones. Here the fundamental

frequency is given by the frequency of the applied square wave voltage. To visualize the overtones of the observed periodic deformation we calculated the power spectrum $S(f)$ of the normalized frequency as described above. This analysis of the recorded data provides a frequency-resolved view on the measurement. The used sampling rate of 13 Hz is correlated to a frequency range of the power spectrum up to 6.5 Hz permitting observation of overtones of the mechanical response of the excited liposomes.

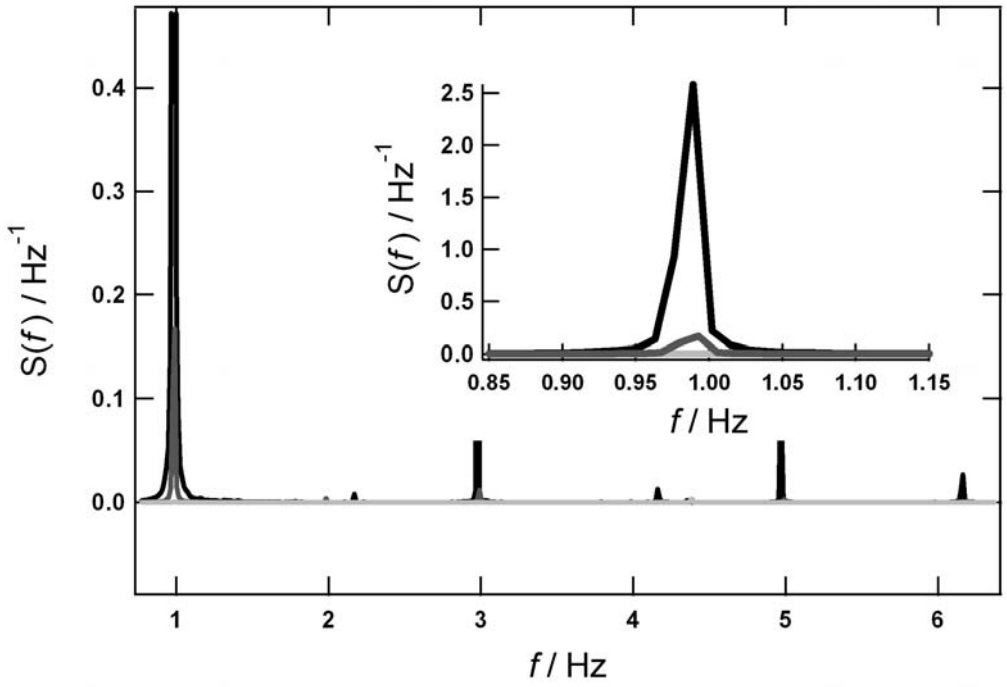

Figure 4.6: Power spectrum *S(f)* of the normalized raw data shown in figure 4.4. The FFT algorithm was applied to subsets of the datasets comprising 1024 points. The resulting power spectra of the individual subsets were averaged to yield the spectrum. The insert shows the power spectrum of negatively charged liposomes containing different amount of cholesterol, (black) 5 % (w/w) and (dark grey) 20 % (w/w) between 0.85 and 1.15 Hz. (light grey) represents the control experiment after washing the electrode with triton-X.

Figure 4.6 displays the power spectrum corresponding to the electrically induced deformation shown in figure 4.4. The black curve represents liposomes composed of asolectin/POPG/cholesterol (70:25:5 (w/w)), the dark grey curve corresponds to liposomes containing 20 % cholesterol and the light grey line reflects the electrode after washing with the detergent triton-X. The

black curve in figure 3 shows odd overtones of the fundamental frequency (1 Hz) at 3 and 5 Hz with high amplitude. Also overtones at even numbers occur, but their magnitude is much smaller. The occurrence of overtones is related to the observed inertia-effect in figure 4.4A. In figure 4.4A a sharp change of the resonance frequency due to switching of the voltage, i.e. the immediately deformation of the liposomes, can be observed, which is replaced by a slight change of the resonance frequency due to inertia of the vesicles. Thus the observed signal in figure 4.4A is a overlapping of a square wave function and a triangular function which leads to the occurrence of the observed overtones.

Additional to the information about overtones the magnitude of the power spectrum is a measure of the strength of the oscillation. Comparing the power spectrum found for vesicles containing 5 and 20 % cholesterol (insert figure 4.6) the magnitude of the power density at the fundamental frequency $S(1\text{Hz})$ decreases with increasing cholesterol concentration. While $S(1\text{Hz})$ is about 2.6 Hz^{-1} for giant liposomes containing 5 % cholesterol, $S(1\text{Hz})$ is about 0.2 Hz^{-1} found for the higher concentration of cholesterol. By washing the electrode with the detergent triton-X, liposomes are destroyed and no further signal is observed in the power spectrum (figure 4.6, light grey line).

Taken together, the present study demonstrates that thickness shear mode resonators, in the way they have been applied here are a powerful and very sensitive tool to study small mechanical deformations of giant liposomes. We could show that it is possible to quantitatively assess the bending rigidity of membranes as a function of cholesterol content. So far no integral technique is available that measures deformation of whole liposomes in the nanometer regime rendering our approach an interesting alternative to common micropipette based techniques used to measure deformability of biological shells.

Bibliography

[1] Lipowsky, R.; Sackmann, E. *Structure and Dynamics of Membranes* Elsevier Sience, Vol. 1, Chaper 5, 1995.

[2] Steltenkamp, S.; Müller, M. M.; Deserno, M.; Hennesthal, C.; Steinem, C.; Janshoff, A. *Biophys. J. BioFAST* 2006, in press.

[3] Evans, E.; Rawicz, W. *Phys. Rev. E* 1990, 64, 2094.

[4] Frisken, B.; Asman, C.; Patty, P. *Langmuir* 2000, 16, 928-933.

[5] Lee, C.-W.; Lin, W.-C.; Wang, *J. Phys. Rev. E* 2001, 64, 1-4.

[6] Kummrow, M.; Helfrich, W. *Phys. Rev. A* 1991, 44, (12), 8356-8360.

[7] Steinem, C.; Janshoff, A.; Ulrich, W. P.; Sieber, M.; Galla, H. *J. Biochim. Biophys. Acta* 1996, 1279, (2), 169-180.

[8] Pignataro, B.; Steinem, C.; Galla, H. J.; Fuchs, H.; A., J. *Biophys. J.* 2000, 78, 487-498.

[9] Reiss, B.; Janshoff, A.; Steinem, C.; Seebach, J.; Wegener, J. *Langmuir* 2003, 19, 1816-1823.

[10] Kanazawa, K. K.; Gordon, J. G. *Anal. Chem.* 1985, 57, 1770-1771.

[11] Kanazawa, K. K.; Gordon, J. G. *Anal. Chim. Acta* 1985, 175, 99-105.

[12] Martin, S. J.; Granstaff, V. E.; Frye, G. C. *Anal. Chem.* 1991, 63, 2272-2281.

[13] Voinova, M. V.; Jonson, M.; Kasemo, B. *Biosensors and Bioelectronics* 2002, 17, 835-841.

[14] Lucklum, R.; Hauptmann, P. *Meas. Sci. Technol.* 2003, 14, 1854-1864.

[15] Goormaghtigh, E.; Scarborough, G. A. *Anal. Biochem.* 1986, 159, 122-131.

[16] Faiss, S.; Lüthgens, E.; Janshoff, A. Eur. *Biophys. J. 2*004, 33, 555–561.

[17] Seifert, U.; Lipowsky, R. *Phys. Rev. A* 1990, 42, (8), 4768-4771.

[18] Sapper, A.; Reiss, B.; Janshoff, A.; Wegener, J. *Langmuir* 2006, 22, (2), 676-680.

Chapter 5

Cell Motility Probed by Noise Analysis of Thickness Shear Mode Resonators

5.1 Introduction

Invasive and metastatic behavior of malignant cells is the major cause of mortality in all cancer patients. Migration of cancer cells, as opposed to normal ones, is critically regulated by (i) physical adhesion of cells to each other and to their non-cellular surroundings, i.e. the extracellular matrix and (ii) by transmission and interpretation of signals from the extracellular environment into various intracellular signaling cascades. The ability of cells to move - often considered as a direct measure for malignancy - can be inferred from their vertical motility, i.e. the dynamics of forming and breaking focal contacts without net lateral movement. This 'stepping on the spot' is associated with the continuous formation and breakage of non-covalent bonds between extracellular matrix proteins and corresponding receptors embedded in the cellular plasma membrane.[1] Integrins are the major family of cell surface adhesion receptors than bind to ligands in the extracellular matrix. They are responsible for the formation of so-called focal contacts and serve as mediators between the intra- and extracellular compartment. Moreover, vitality of cells in general is also manifested in their ability to perform shape fluctuations most often induced by dynamics of the cytoskeleton as it is impressively demonstrated by the collective contraction of cardiomyocytes in vitro.[2, 3, 4] Among other contributors to cell motility the dynamics of actin polymerization and filament turnover play important roles.[5] Many aspects of animal cell motility are directly correlated with dynamic changes in cell volume, vis-

coelasticity, cell-cell- and cell-matrix contacts. Thus, it was our objective to establish a new and powerful experimental technique to sense these cellular shape fluctuations in real time and to derive a direct measure of cell motility from fluctuation measurements.

Fluctuations in biological systems have recently been investigated with regard to the enzymatic function of proteins,[6] molecular machines,[7] gene expression,[8] individual cells,[2] and ion channels.[9] The stochastic nature of ion transport through transmembrane channels has been used as a sensor to detect individual molecules (stochastic sensor). Recently, we characterized the dynamics of protein-membrane interactions by recording and analyzing the noise created by the adsorption and desorption of proteins on a biomimetic surface.[10]

A cell, however, is a nonequilibrium soft material whose fluctuations are actively driven. Highly regulated biochemical signalling pathways control the energy-dependent dynamics of living cells which are a sensitive indicator for their metabolic activity. In fact, fluctuations in living cells are a measure of the cells´ adaptability to changes of the environment.[11] Typically, mechanical noise originating from living cells is orders of magnitude higher than fluctuations produced by thermal motion and it shows a different frequency dependence. A soft or plastic system is characterized by a large variability of its viscoelastic properties, thus, it can be tuned in to meet the cells´ requirements. Hence, measuring the stochastic micro-mechanical properties of living cells may serve as an extremely sensitive indicator to monitor the response of cells to external challenges and may form the basis for a new type of whole-cell biosensor.

So far, only electric cell-substrate impedance sensing (ECIS) has demonstrated sufficient sensitivity to detect fluctuations in cell shape - so called micromotion - when the cells are grown on electrically conductive substrates.[12, 13, 14] In ECIS the electrical impedance of a cell-covered, substrate-integrated micro-electrode is recorded with a time resolution of 1 second. Since the electrode impedance is modulated by the shape of the cells that are attached to it, the ECIS readout can be applied to monitor fluctuations in cell shape. A single study based on TIRAF microcopy has picked up micromotion-like fluctuations in the area of cell-to-substrate adhesion.[15]

Recently, we showed that the quartz crystal microbalance (QCM) is an excellent tool to monitor the de novo formation and modulation of cell-matrix interactions with high time resolution. It additionally provides quantitative information about the micro-mechanical properties of the cell-matrix contact sites.[16, 17, 18] This sensitivity for cell-matrix adhesion together with its superior time resolution renders the QCM approach a promising transducer to monitor shape fluctuations of living cells. Thus, we report on a new approach

to assess the dynamics of adherent cells by measuring the fluctuations that are imposed on the resonance frequency of a thickness shear mode (TSM) resonator that is covered by a monolayer of cells and serves as a cell culture substratum. Compared to ECIS or TIRAF the QCM-approach is neither limited to transparent nor conductive surfaces, and provides a fast readout in the millisecond regime.

5.2 Material and Methods

5.2.1 QCM-Based Fluctuation Experiments

AT-cut quartz crystals (5 MHz fundamental resonance; KVG, Neckarbischofsheim, Germany) coated on both sides with circular gold electrodes (Ø = 5 mm) were mounted as the bottom plate of a cell culture dish into a home-made crystal holder (Teflon). To study frequency fluctuations of the quartz resonator we used a phase-lock oscillator (QCM100; SRS, Inc., Sunnyvale, CA, USA). The frequency was recorded by a frequency counter (Agilent 53181A; Agilent Technologies, Palo Alto, CA, USA) and then transferred via GPIB to a computer (time resolution 70 ms). QCM- and ECIS-based (next paragraph) fluctuation measurements were carried out in incubators with 5 (v/v)% CO_2 atmosphere at 37 °C.

To characterize the mechanical load of the quartz resonator under the various experimental conditions we also measured the Q-factor of the shear oscillation by impedance analysis using a continuous-wave impedance analyzer (SI-1260; Solartron Instruments, Farnborough, UK) in the frequency regime close to the quartz fundamental resonance (5 MHz). Impedance data was analyzed by adjusting the parameters of the Butterworth-van-Dyke (BVD) equivalent circuit as described elsewhere,[16] providing energy storage (inductance) and energy dissipation (resistance) as fitting parameters, thus, the Q-factor.

5.2.2 ECIS-Based Fluctuation Experiments

ECIS measurements were performed using eight-well cell culture dishes with circular gold-film electrodes ($d = 250\ \mu$m) deposited upon the bottom of each well (Applied Biophysics, Inc., Troy, NY; www.biophysics.com), a lock-in amplifier (SR830, SRS, Inc., Sunnyvale, CA, USA) with an internal oscillator, and a personal computer that controls the measurement and stores data.[14, 19, 20]

5.2.3 Noise Analysis

To analyze resistance (ECIS) and frequency (QCM) fluctuations we applied Fast Fourier Transformation (FFT) and variance analysis (i.e. computing the variance of the normalized and de-trended raw data along the entire dataset as a direct measure for the fluctuation amplitude). Whereas computation of the variance along the dataset provides an easy to interpret measure for the overall amplitude of the observed fluctuations, FFT is particularly useful to look either for periodicities or to demonstrate aperiodicity. Applying FFT to a fluctuating time series - or noise - provides the corresponding power spectral density function or short power spectrum of the measured time series. The power spectrum plots the relative contribution of an individual harmonic function of a specified frequency (sinus or cosinus) to the overall time series as a function of frequency. Thus, any periodicity within the experimental data can be easily spotted as a peak in the power spectrum at its characteristic frequency. The absence of peaks is indicative for a time series without any periodicity. But even without well-defined peaks the power spectrum of a fluctuating or noisy time series provides a useful tool to characterize the frequency-dependent fluctuations in the data. In fact, different types of noise are typically classified by the character of their power spectrum. So-called white noise is characterized by a power spectrum independent of frequency (horizontal line), while pink noise is represented by a $1/f$ behavior, and Brownian noise displays a $1/f^2$ power law. Taken together, Fourier transformation of the recorded data provides a frequency-resolved view on the composition of the measured time series.

Mathematically speaking, the power spectrum of a given time series is the square of the magnitude of the continuous Fourier transform of the signal. Particular attention has to be paid to normalization. Assuming that we record an N-point sample of our signal $c(t)$ at equal intervals and use the Fast Fourier Transformation to compute its discrete Fourier Transform (DFT):

$$C_k = \sum_{j=0}^{N-1} c_j e^{\frac{2\pi i j k}{N}} = DFT(c(t)) \qquad k = 0, ..., N-1 \tag{5.1}$$

The power spectrum $S(f)$ is then calculated according the following equations:

$$\Phi(0) = \Phi(f_0) = \frac{1}{N^2}\left|C_0\right|^2 \tag{5.2}$$

$$\Phi(f_k) = \frac{1}{N^2}\left(\left|C_k\right|^2 + \left|C_{N-k}\right|^2\right) \qquad k = 1, 2, ..., (\frac{N}{2} - 1) \tag{5.3}$$

$$\Phi(f_c) = \Phi(f_{N/2}) = \frac{1}{N^2}\left|C_{N/2}\right|^2 \tag{5.4}$$

where $f_k = \frac{k}{N\Delta t} = 2f_c\frac{k}{N}$ $(k = 0, 1, ..., \frac{N}{2})$ and N is an even number. f_k is defined for zero and positive frequencies, Δt is the sampling interval and $f_c = \frac{1}{2\Delta t}$ is the maximum frequency within the Nyquist interval. Finally, $\Phi(f)$ is divided by the sampling frequency Δf and multiplied by N to obtain the *power spectral density function* $S(f)$ in accordance with Parseval's theorem. Data with equidistant time scale is recorded, subdivided into sets containing multiples of 2^n data points. Each subset of the original data is subjected to a Fast Fourier transformation and the mean of the power spectrum from all data subsets is calculated.

The data of this study has been checked for stationarity and ergodicity as described elsewhere.[21] We found that neither the mean resonance frequency value nor its variance changed with time within one measurement hence fulfilling the requirements for "weak stationarity". Power spectra recorded at different times of one experiment did not show any noticeable differences as required for ergodic systems.

5.2.4 Cell Culture

MDCK-II cells were cultured in Earle's minimum essential medium supplemented with 4 mM glutamine, 100 μg/ml of both, penicillin and streptomycin (all purchased by Biochrom, Berlin, Germany), and 10 % (v/v) fetal calf serum (PAA Laboratories GmbH, Cölbe, Germany). Stocks of these cells were grown in incubators with a 5 % CO_2 atmosphere. Since the fluctuation amplitude might depend on the passage number (age of the cell line) we performed each series of experiments with cells originating from the same passage number to provide absolute comparability of the power spectra.

5.3 Results and Discussion

Figure 5.1A traces the shift of the frequency response of a 5 MHz TSM resonator upon seeding 1.6×10^5 MDCK-II cells on the gold electrode of the quartz resonator. A typical frequency decrease of approximately 600

Hz due to the attachment and spreading of the cells on the surface can be observed.[17] It is important to note, that the mass-sensitivity of the quartz resonator is a function of position on its surface. Cells attached to the centre of the electrode contribute more than cells in the periphery. The radial sensitivity behaves like a Gaussian function. However, with a homogenous load situation - i.e. a homogenous distribution of cells on the gold electrode - all further considerations can be reliably based on an average integral sensitivity.

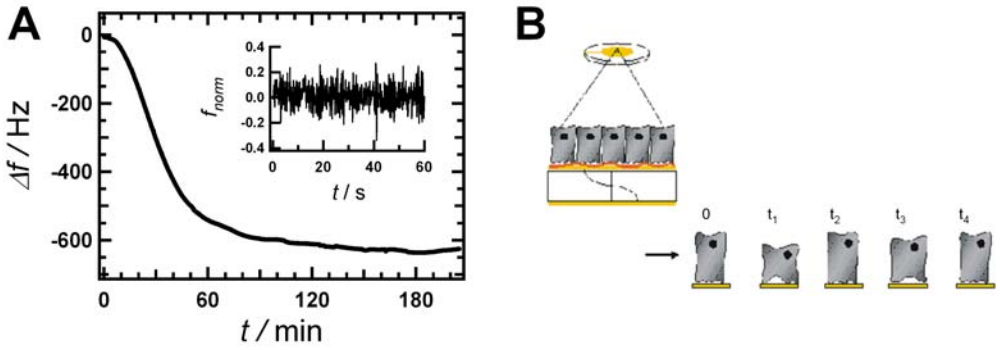

Figure 5.1: (A) Shift of the resonance frequency Δf when a suspension of MDCK-II cells is allowed to settle on a 5 MHz- shear wave resonator. The insert shows fluctuations of the resonance frequency that originate from the dynamic activities of the cells on the surface. T = 37 °C. (B) Schematic diagram of a confluent cell monolayer, cultured on the gold electrode of a thickness shear mode resonator, and a sketch illustrating shape fluctuations.

Fluctuation analysis is performed after attachment and spreading of the cells is completed and a confluent cell monolayer is established on the surface. Accordingly, adhesion of cells does not interfere with motility recordings. The schematic in figure 5.1B illustrates shape fluctuations as envisioned for confluent cell monolayers grown on a quartz resonator. The formation and breakup of focal contacts produce a fluctuating contact area and as a consequence a transient change in free volume between the cell monolayer and the substrate. Moreover, the cells themselves might exhibit transient changes in volume and their micro-mechanical properties. Therefore the signal of the thickness shear mode (TSM) resonator shows a fluctuating resonance frequency (compare insert in figure 5.1A) arising from the fluctuating load situation on the crystal surface.

The impact of different load situations on the resonance frequency fluctuations of the quartz crystal is shown in figure 5.2, in which the resonance frequencies (the average is set to zero) are plotted as a function of time in

the left panel, while the corresponding power density spectra are shown on the right. The resonance frequency was recorded with a sampling rate of 14 Hz, i.e. one data point every 70 ms.

Figure 5.2A (left) shows a typical time course of the fluctuating resonance frequency for a quartz crystal covered with a complete monolayer of living MDCK-II cells in culture medium, while figure 5.2B (left) shows the frequency noise of the same cell layer exposed to hypertonic medium (200 mM sucrose added to the isotonic culture medium). The amplitude of the fluctuations is reduced significantly when the cells are forced to shrink and condense in a hyperosmotic environment. A further reduction in noise is achieved by cross-linking all cell protein via paraformaldehyde (4 % (v/v) in PBS^{++}), a common fixative to stabilize biological samples (figure 5.2C). Finally the cell layer was removed from the quartz surface mechanically (figure 5.2D) but the cell debris was allowed to settle back on the surface. Even without any quantitative analysis it is already apparent from the raw data that the amplitude of the resonance frequency fluctuations observed for living MDCK-II cells (figure 5.2A) is considerably higher than the noise level found for the cell-free electrode (figure 5.2D). A more detailed characterization is provided by the power density spectra of the fluctuation data. The power density spectra of the cell-free quartz resonator (figure 5.2D, right) is essentially similar to white noise with almost no frequency dependence and no significant peaks. Living MDCK-II cells, however, show a typical peak around 1 to 3 Hz (arrow) indicative of an intrinsic resonance. Moreover we find a higher overall noise level together with a slightly negative slope of the spectrum. The peak has to be considered as an indication for synchronized and periodic fluctuations in viscoelasticity or shape of the cell bodies. The origin of this collective and periodic behavior remains to be elucidated. However, AFM studies, in which the cantilever tip was allowed to settle on the bodies of adherent cells and follow their shape fluctuations, show a similar power spectrum with resonance features at around 5 Hz using 3T3 fibroblast cells.[2] Exposing the cells to hypertonic conditions (figure 5.2B) reduces the peak substantially as well as the overall noise. The noise level decreases further when the cell's proteins were cross-linked by PFA.

The cell shape, cell-substrate anchorage and cell-movement are mainly determined by the static and dynamic properties of the actin network. Controlled polymerization of actin is a prerequisite for any movement of the cell. Therefore, we experimentally hindered f-actin formation by cytochalasin D, a fungal alkaloid, which specifically inhibits actin polymerization. We found that adding cytochalasin D (Sigma; 0.2 mM stock solution in DMSO) in a final concentration of 1 μM to vital cells leads to a substantial reduction of the resonance peak at 1-2 Hz in the power spectrum. The cellular noise level

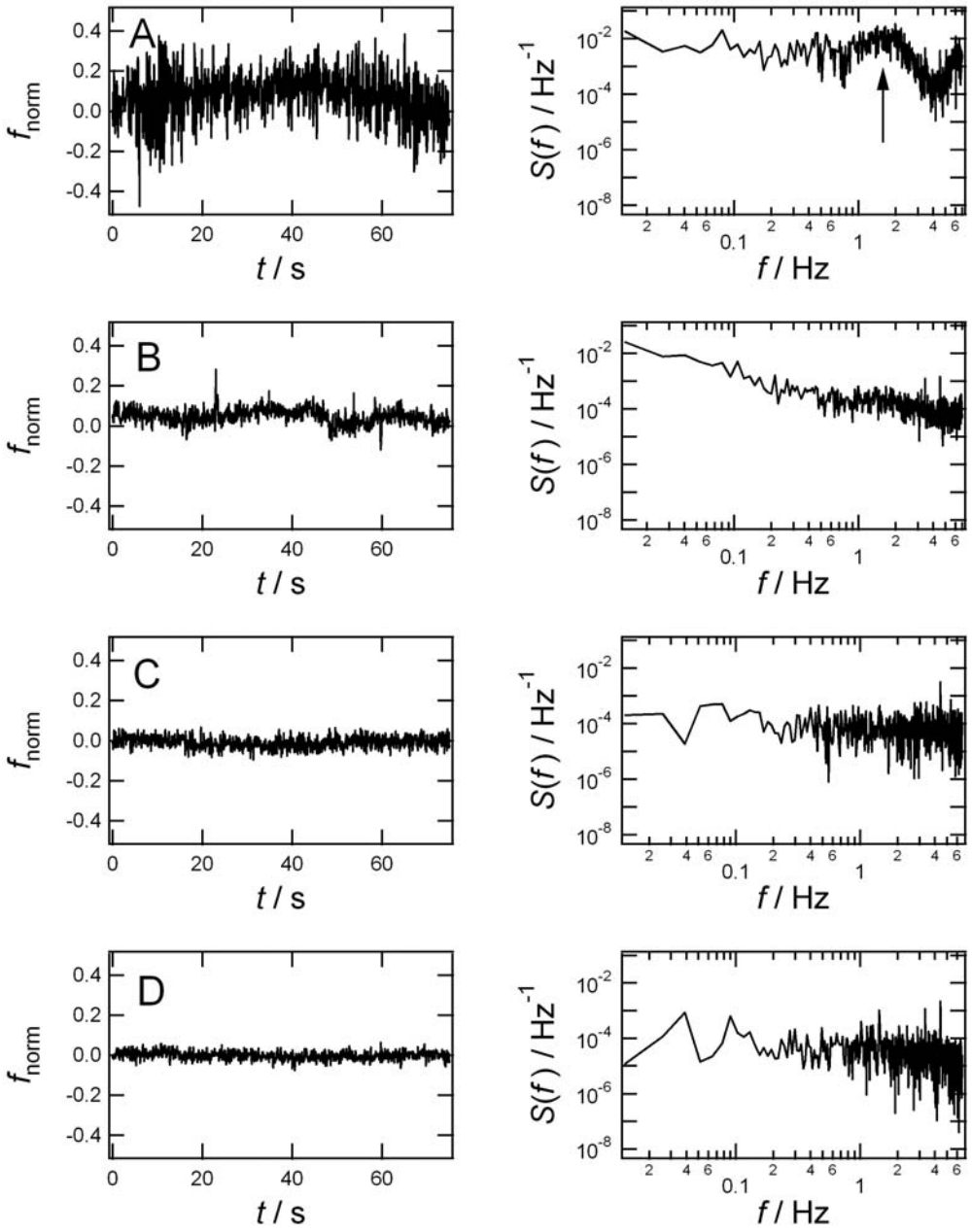

Figure 5.2: Frequency fluctuations of TSM resonators under various load situations. Power density spectra were obtained after subtraction of a linear trend from the raw data and applying an FFT algorithm to subsets of the dataset comprising 1024 points. The resulting power density spectra of the individual subsets were averaged to yield the spectrum shown in the figure on the right side. The graphs on the left show the time course of the fluctuating frequency after normalization. For normalization the average has been set to zero. (A) MDCK-II cells in isotonic culture fluid. (B) MDCK-II cells in hypertonic (200 mM sucrose added to isotonic medium) culture fluid. (C) MDCK-II cells fixed with PFA. (D) Resonator after removal of cells (immersed in buffer).

is then similar to the situation observed for fixed cells (figure 5.2D).

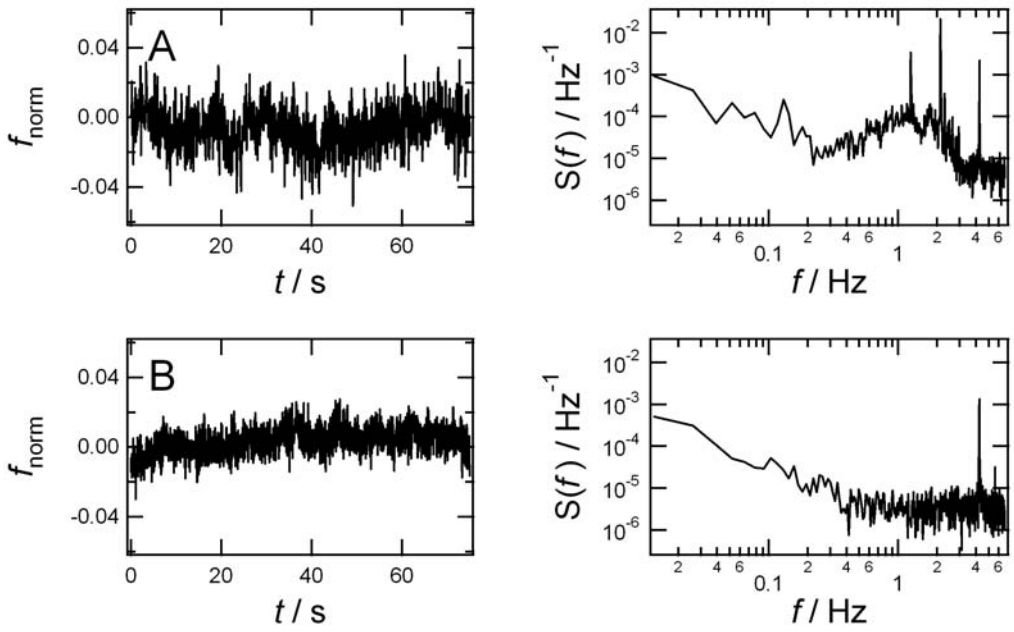

Figure 5.3: Impact of cytochalasin D (1 μM) on resonance frequency fluctuations of MDCK-II cells. The graphs on the left hand side show the time course of the fluctuating frequency after normalization. For normalization the average has been set to zero. The corresponding power density spectra are grouped right hand side. (A) MDCK-II cells under vehicle control conditions. (B) MDCK-II cells exposed to cytochalasin D.

Vehicle control experiments revealed that adding the solvent DMSO alone in the same concentrations does not have any impact on the appearance of the peak. The impact of cytochalasin D on the dynamic properties of the cells is by far more pronounced than the associated changes in overall energy dissipation of the shear oscillation as demonstrated by impedance analysis. Here, cytochalasin D reduces the motional resistance by 25 %. Since the fluctuation pattern of living cells, as reported here, is highly susceptible to drugs acting on the cytoskeleton, it is straightforward to conclude that the dynamics of actin polymerization are a likely source for the 1–2 Hz peak observed in the power spectra of unchallenged cells. In the AFM work mentioned above the resonance peak was also assigned to the dynamics of the actin cytoskeleton.[2] These experiments also demonstrate that QCM-based fluctuation analysis is a sensitive new bioanalytical means to study subtle

changes within the physiological state of adherent cells when they are mediated by the cellular cytoskeleton.

We compared the frequency fluctuations observed for cells with those obtained for chemically defined model systems. Deposition of giant liposomes (data not shown) shows essentially the same frequency fluctuation magnitude than cell-free resonators. Thus, those fluctuations observed for living cells can be attributed to their biological activity and energy-dependent motility rather than thermal membrane undulations or a decrease in the quality factor of the oscillation due to increased damping. Moreover, application of hypertonic conditions, which results in a dehydration and compression of the cell bodies, provides a significant but reversible decrease of the fluctuation amplitude and a concomitant decrease of the quality factor. Thus, the observed fluctuations are not a simple consequence of a reduced quality factor of the oscillation in the presence of cells but indeed biological in nature.

It is instructive to compare the frequency fluctuations in a QCM experiment with resistance fluctuations obtained from ECIS analysis. ECIS is a highly sensitive electrochemical technique to investigate morphological changes of adherent cells without using an optical microscope.[22] The technique reports on changes in cell-cell and cell-matrix contacts when the cells are adherently grown on gold-film electrodes. The electrical impedance of the electrodes increases when the cells attach and spread on the surface as the current has to bypass the cellular bodies instead of leaving the electrode directly into the bulk. With the cells behaving like insulating particles the impedance is a function of cell shape and can be used to monitor shape fluctuations as described above. Fluctuations in electrode resistance when MDCK-II cells completely cover the electrode surface (diameter of 250 μm) are shown in figure 5.4A.The sampling rate for the impedance measurements performed at 4 kHz was 1 Hz. The power density spectra (right) of the living cells display a slope in the range of (-2.1 to -2.7) s^{-2} indicative for biologically active cells.[23] Exposing the cells to hyperosmolar solution (figure 5.4B) does not induce any significant change in the power density spectrum, while fixation with PFA (figure 5.4C) substantially decreases the noise (slope: -0.8 s^{-2}) as consistently observed in QCM measurements as well. Removal of the cells (figure 5.4D) reduces the slope of the power spectrum to its lowest value (slope: -0.3 s^{-2}). In more recent studies we learned that thermal membrane fluctuations of giant liposomes are easily detected in an ECIS setup with the liposomes attached to the same ECIS-electrodes that was used in cell experiments here. The power spectrum of liposome fluctuations is typically characterized by a slope close to -2 s^{-2} indicative of Brownian noise.[23, 24, 25]

Looking for reasons to explain the observed differences between QCM-

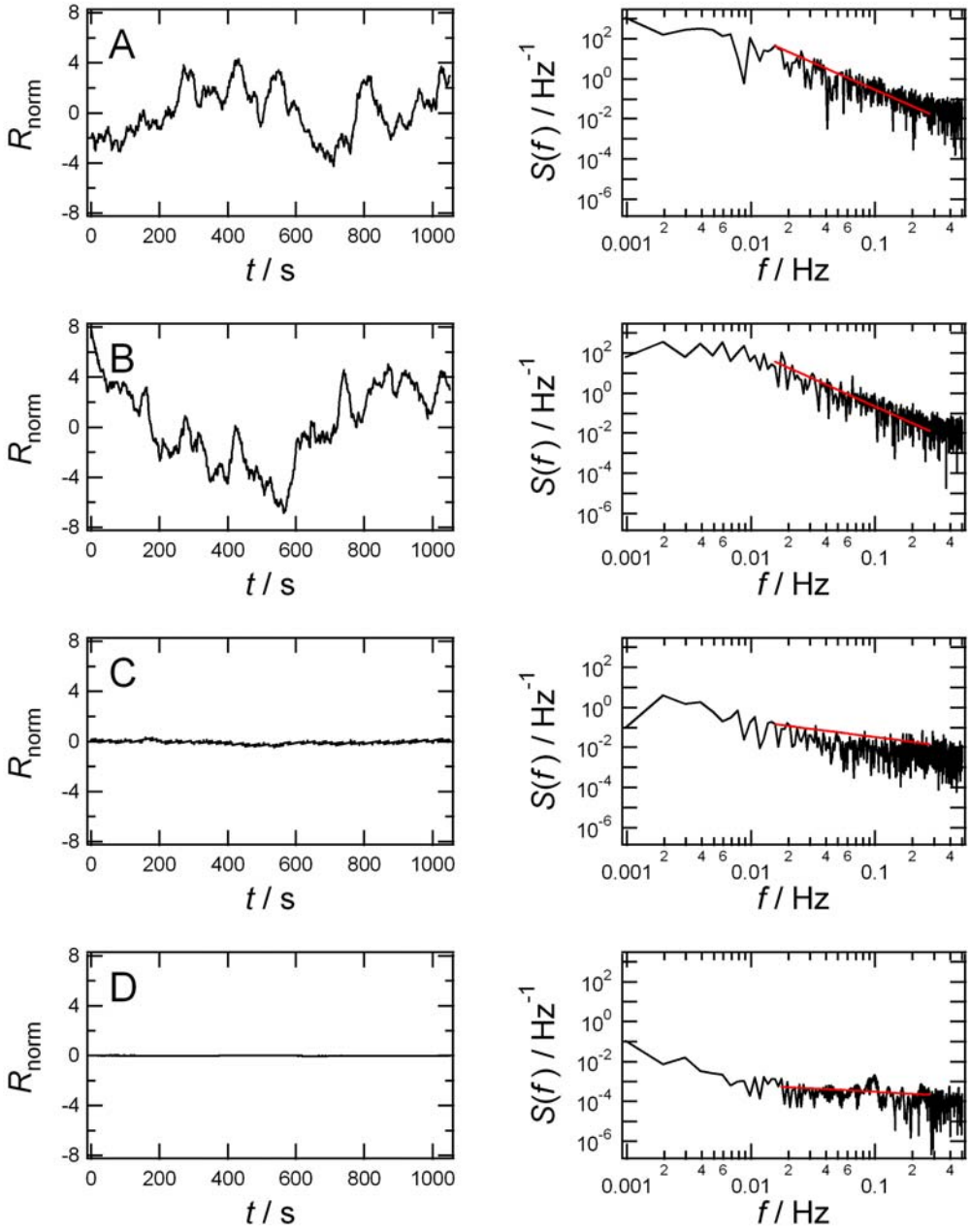

Figure 5.4: Analysis of ECIS-based resistance fluctuations under various experimental conditions. Prior to FFT a linear trend was subtracted from the raw data. The power density spectra of data subsets comprising 1024 points were averaged to yield the spectra shown in the right panel. The graphs on the left show the time course of the normalized resistance. For normalization the first data point has been set to zero. (A) MDCK-II cells in isotonic culture fluid. (B) MDCK-II cells in hypertonic (200 mM sucrose) culture fluid. (C) MDCK-II cells fixed with PFA. (D) Bare electrode just immersed in buffer.

based and ECIS-based fluctuation experiments one has to recognize two technical details. While the sensing area in ECIS experiments is only 0.0005 cm^2 the active area of the quartz resonator amounts to 0.33 cm^2. Since the surface area of the measuring electrode determines the number of cells that contribute to the signal, and thus signal averaging, it is not surprising to find individual readouts for both techniques. Moreover, the bandwidth of the ECIS technique is different from the QCM approach. While ECIS is limited at the high frequency end of the power spectrum to 0.5 Hz, the QCM approach provides data up to 7 Hz. Thus, it remains to be elucidated whether ECIS readings with a better time resolution would also show a resonance peak at 1-2 Hz in the power spectrum. Also the origin of both signals has to be considered: the real part of the complex impedance measured by the ECIS technique mirrors the width of the electrolyte filled spaces between adjacent cells and between cell and electrode surface.[23] The QCM, however, reads the overall viscoelastic load on the resonator, which is governed by the space between ventral cell membrane and gold electrode but also by changes in cell volume and viscoelasticity. These individual signal sources might account for the different frequency dependences in the ECIS- or QCM-based power density spectra.

Taken together, QCM measurements provide a novel means to monitor the dynamics of living adherent cells by detecting their transient shape fluctuations. However, data holds different information than in ECIS recordings. This conclusion is supported by the different cell reactions observed in fluctuation analysis upon exposure to osmotic stress. Figure 5.5A and B summarize the variance σ^2 of the resonance frequency (A, QCM) and resistance (B, ECIS) fluctuations, respectively, for cells under different osmotic conditions. Here the variance along the entire dataset is used as an easy to grasp and intuitive parameter that directly mirrors the fluctuation amplitude. A hypertonic environment results in a substantial decrease in frequency fluctuations (10 %) that recovers to 60 % of the initial value after switching the solution back to isotonic conditions. Compared to fixed cells, the fluctuations of cells in hypertonic medium are only slightly higher, while the bare quartz provides the smallest variance. Interestingly, we found that ECIS measurements under the same conditions give a different answer (figure 5.5B). Cells in hypertonic fluid still impose the same fluctuation amplitude on the measured resistance. Chemical fixation of the cells however results in substantial decrease of resistance fluctuations, which are even further reduced by removal of the cells from the electrode surface.

In addition, QCM- and ECIS-based fluctuation analysis report differently on the cells´ motility after addition of the drug cytochalasin D. Using QCM, cells exposed to cytochalasin D show a complete loss of the cell resonance,

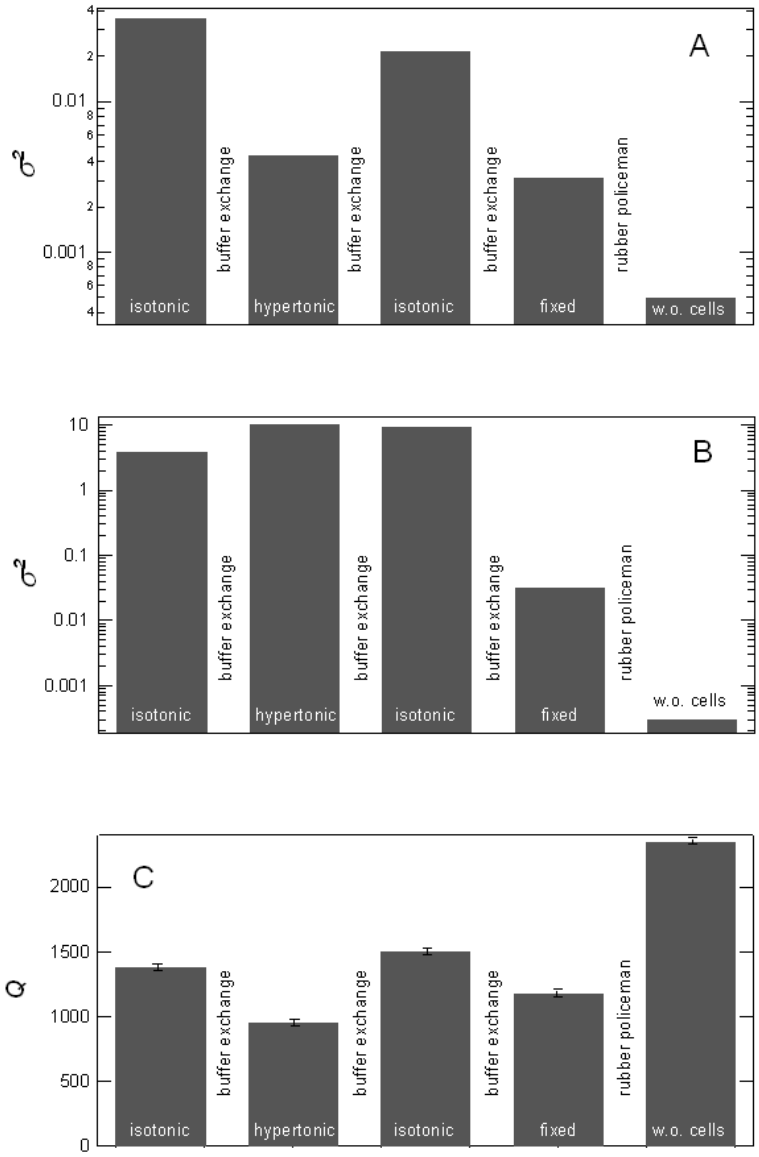

Figure 5.5: Variance σ^2 of the normalized resonance frequency (A) or resistance (B) fluctuations under various experimental conditions. After subtraction of a linear trend from the raw data σ^2–values were calculated for 2048 data points (A) and 1000 data points (B). (C) Q-factor of the quartz resonator under different conditions as extracted from impedance analysis and subsequent equivalent circuit modelling using the BVD network.

while Lo et al. report that the ECIS-fluctuations do not decrease significantly after addition of cytochalasin D.[12] These findings support our claim that fluctuations measured by ECIS and QCM contain different information about the dynamics of the cells that may complement each other.

Figure 5.5C summarizes the changes in Q-factor (Q = energy stored per cycle / energy dissipated per cycle) for the cell-covered quartz resonators under different experimental conditions. Energy dissipation of the cell-covered quartz resonator is significantly increased (Q-factor reduced) when the cells are exposed to hypertonic medium. The cells slowly recover from the osmotic stress within 2 hours even under constant hypertonic conditions (data not shown). The initial Q-value is, however, quickly recovered after switching back to isotonic buffer. Protein cross-linking also increases the energy dissipation of the resonator, while cell removal yields a Q-value almost twice as high as recorded for the cell-covered resonator. Although the load on the quartz resonator is increased considerably by applying hyperosmotic stress, the fluctuations decrease indicating its biological origin. We interpret this finding as follows: the osmotically driven water efflux from the cells results in a compression of the cells and as a consequence, they adopt a flat shape with the membrane closely attached to the cytoskeleton. Hence, the viscoelasticity of the cells increases considerably and shape fluctuations are damped down. It is important to note, that hyperosmotic medium has virtually no effect on the oscillation of the bare quartz. Moreover, in hyperosmotic media the cells show essentially the same mechanical properties compared to cells exposed to a cross-linking reagent. QCM readings indicate that paraformaldehyde not only increases the stiffness of the cells but significantly freezes their motility as shown in figure 5.5A by the dramatically decreased variance. In contrast to the impact of fixation, the response of the cells to hyperosmotic stress is more or less reversible after buffer exchange.

Comparing ECIS- and QCM-based micromotion readings we found that both methods show a clear difference between living cells and those killed by paraformaldehyde. On the other hand both techniques provide different answers when the cells are challenged by hypertonic conditions. Whereas ECIS does not indicate any difference in shape fluctuations, QCM-based readings exhibit reduced cell dynamics. These differences suggest that signal fluctuations originate from different parts of the cell body and that they reflect different subcellular activities. A precise assignment of the individual contributions awaits further studies in particular those that combine both techniques.

We show for the first time how the quartz crystal microbalance can be applied to monitor the dynamics of living adherent cells in real time which may serve as the basis for a new type of whole-cell biosensor. QCM-based

fluctuation analysis provides a quantitative means to monitor periodic micromechanical alterations of living cells with a time resolution that can be easily improved when quartz resonators with higher fundamental resonance frequency will be used. Future applications of this new technology comprise cytotoxicity screening, drug screening or - more ambitious – a direct method to quantify the motility of tumor cells derived from biopsy material. One may envision that it might become possible to characterize the metastatic potential of tumor cells from a detailed analysis of their dynamics.

Bibliography

[1] Lambrechts, A.; Van Troys, M.; Ampe, C. *Int. J. Biochem. Cell Biol.* 2004, 36, 1890-1909.

[2] Szabó, B.; Selmeczi, D.; Környei, Z.; Madarász, E.; Rozlosnik, N. *Phys. Rev. E* 2002, 65, 1-6.

[3] Luong, J. H. T. *Anal. Lett.* 2003, 36, 3147-3164.

[4] Pax, M.; Rieger, J.; Eibl, R. H.; Thielemann, C.; Johannsmann, D. *Analyst* 2005, 130, 1474-1477.

[5] Carlier, M.-F.; Pantaloni, D. *J. Mol. Biol.* 1997, 459-467.

[6] Tang, K. E. S.; Dill, K. A. J. *Biomol. Struct. Dyn.* 1998, 16, 397-411.

[7] Ishijima, A.; Kojima, H.; Funatsu, T.; Tokunaga, M.; Hijuchi, H.; Tanaka, H.; Yanagida, T. *Cell* 1998, 92, 161-171.

[8] Simpson, M. L.; Cox, C. D.; Sayler, G. S. *Proc. Natl. Acad. Sci. USA* 2003, 100, 4551-4556.

[9] Bayley, H.; Cremer, P. S. *Nature* 2001, 413, 226-230.

[10] Lüthgens, E.; Janshoff, A. *ChemPhysChem* 2005, 6, 444-448.

[11] Sato, K.; Ito, Y.; Yomo, T.; Kaneko, K. *Proc. Natl. Acad. Sci. USA* 2003, 100, 14086-14090.

[12] Lo, C.-M.; Keese, C. R.; Giaever, I. *Exp. Cell Res.* 1993, 204.

[13] Pei, Z.; Keese, C. R.; Giaever, I.; Kurzawa, H.; Wilson, D. E. *Exp. Cell Res.* 1994, 212, 225-229.

[14] Giaever, I.; Keese, C. R. *Proc. Natl. Acad. Sci. USA* 1991, 88, 7896-7900.

[15] Geggier, P.; Fuhr, G. *Appl. Phys. A* 1999, 68, 505.

[16] Wegener, J.; Seebach, J.; Janshoff, A.; Galla, H.-J. *Biophys. J.* 2000, 78, 2821-2833.

[17] Wegener, J.; Janshoff, A.; Galla, H.-J. *Eur. Biophys. J.* 1998, 28, 26-37.

[18] Reiss, B.; Janshoff, A.; Steinem, C.; Seebach, J.; Wegener, J. *Langmuir* 2003, 19, 1816-1823.

[19] Wegener, J.; Keese, C. R.; Giaever, I. *Exp. Cell Res.* 2000, 259, 158-166.

[20] Giaever, I.; Keese, C. R. *Nature* 1993, 366, 591-592.

[21] Bezegh, A.; Janata, *J. Anal. Chem.* 1987, 59, 494A-506A.

[22] Lo, C.-M.; Keese, C. R.; Giaever, I. *Biophys. J.* 1995, 69, 2800-2807.

[23] Giaever, I.; Keese, C. *IEEE Trans. Biomed. Eng.* 1986, 33, 242-247.

[24] Sapper, A.; Reiss, B.; Janshoff, A.; Wegener, J. *Langmuir* 2006, 22, 676-680.

[25] Marinari, E.; Parisi, G.; Ruelle, D.; Windey, P. *Phys. Rev. Lett.* 1983, 50, 1223-1225.

Chapter 6

Impact of Taxol and Nocodazole on the Vertical Motility of Cells

6.1 Introduction

Motility is a fundamental property of cells and has been widely observed in tissue culture, as most mammalian cells have the ability to crawl upon surfaces. This in vitro phenomenon of cell migration plays a pivotal role in embryonic development and also in wound healing, tissue maintenance, and immune system function in the adult animal.[1] Several recent studies have reported a link between the metastatic behavior of cancer cells and their motility in culture.[2, 3, 4] The highly complex integrated process of cell movement is a prime example of such complex coordinated cytoskeletal action. Besides protrusion at the leading edge of the cell and the traction, in which the bulk of the trailing cytoplasm is drawn forward, the attachment plays an important role. Cell attachment, in which the cytoskeleton connects across the plasma membrane to the substratum, attributes to the so called focal adhesion complexes and is mediated by integrins, the major family of cell surface adhesion receptors.

Another important prerequisite for cell crawling is the development and maintenance of an overall structural polarity as observed in epithelial cells whose plasma membrane is divided into two domains, the apical membrane, which in vivo faces the external milieu and the basolateral membrane pointing the internal milieu of the organism. The two parts of the plasma membrane exhibit different protein composition, reflecting the ability of these cells to transport newly synthesized membrane and secretory proteins vec-

torially to each cell surface. Several studies have shown that microtubules are involved in orientation of intracellular transport.[5, 6, 7, 8] Together with microtubule-organizing centers (MTOCs) they are thought to determine the axis of polarity in many cells. Microtubules are polymers in a dynamic equilibrium with a pool of soluble subunits of tubulin, α-tubulin and β-tubulin. An optimal organization of the cytoplasm by microtubules needs both tight control and flexibility towards changes in the cellular environment. Changing the dynamic properties of microtubules influences this organization of the cytoplasm, i.e. the polarity. Polymerization of microtubules can be altered by drugs, such as nocodazole and taxol. The effects of the taxol and nocodazole are quite different, even opposite. While nocodazole depolymerizes microtubules,[9] taxol facilitates polymerization of microtubules and stabilizes polymerized microtubules.[10] Exposing polarized Madin-Darby canine kidney (MDCK) epithelial cells to nocodazole effects disrupters of microtubules leading in depolarization.[5, 6, 7, 8] In taxol-treated MDCK-II cells a hyperpolymerization of microtubules in the periphery of the cells occurs.[6] By altering the polymerization of microtubules by drugs the polarization vanishes and by this the motility of the cells might decrease.

The conversion of cellular shape mediated by actin filaments, intermediate filaments and microtubules, can be easily observed using fluorescence microscopy. Using this technique cells have to be stained with fluorescence labelled molecules, which is mostly invasive or extremely time-consuming. In addition to these drawbacks no studies had been reported using fluorescence microscopy to visualize cell motility.

In this paper, we quantified the impact of nocodazole and taxol on cell motility assessed by means of the fluctuating response of thickness shear mode (TSM) resonators. TSM resonators, the major constituent of the well-known quartz crystal microbalance (QCM), are excellent tools to monitor cell adhesion[11, 12, 13, 14] and as recently shown a highly sensitive device to study cell motility in vitro.[15] Complementary information about micromotion of cells were provided by electric cell-substrate impedance sensing (ECIS) measurements.[16, 17, 18]

6.2 Material and Methods

6.2.1 QCM-Based Fluctuation Experiments

AT-cut quartz crystals (5 MHz fundamental resonance; KVG, Neckarbischofsheim, Germany) coated on both sides with circular gold electrodes ($\varnothing = 5$ mm) were mounted as the bottom plate of a cell culture dish into a home-

made crystal holder (Teflon). Frequency fluctuations of the quartz resonator were recorded using a phase-lock oscillator (QCM100; SRS, Inc., Sunnyvale, CA, USA), connected with a frequency counter (Agilent 53181A; Agilent Technologies, Palo Alto, CA, USA). Data was transferred via GPIB to a computer achieving a time resolution of 75 ms. QCM- and ECIS-based (next paragraph) fluctuation measurements were carried out in incubators with 5 (v/v) % CO_2 atmosphere at 37 °C.

The Q-factor, a measure of energy dissipation, which is a consequence of the mechanical load of the quartz resonator under the various experimental conditions, is measured by impedance analysis using a continuous-wave impedance analyzer (SI-1260; Solartron Instruments, Farnborough, UK) in the frequency regime close to the quartz fundamental resonance (5 MHz). Impedance data were analyzed by adjusting the parameters of the Butterworth-van-Dyke (BVD) equivalent circuit as described elsewhere.[11]

6.2.2 ECIS-Based Fluctuation Experiments

ECIS measurements were performed with a lock-in amplifier (SR830, SRS, Inc., Sunnyvale, CA, USA) using eight-well cell culture dishes with circular gold-film electrodes ($d = 250$ μm) deposited upon the bottom of each well (Applied Biophysics, Inc., Troy, NY; www.biophysics.com).[18, 19, 20]

6.2.3 Noise Analysis

Resistance (ECIS) and frequency (QCM) fluctuations were analyzed by Fast Fourier Transformation (FFT), which is particularly useful to check either for periodicity or to demonstrate aperiodicity, as described elsewhere in more detail.[15] In short, FFT were applied to normalized and detrended raw data providing the corresponding power density function of the measured time series as described recently.

6.2.4 Cell Culture

MDCK-II cells were cultured in Earle's minimum essential medium supplemented with 4 mM glutamine, 100 μg/ml of both, penicillin and streptomycin (all purchased by Biochrom, Berlin, Germany), and 10 % (v/v) fetal calf serum (PAA Laboratories GmbH, Cölbe, Germany). Stocks of these cells were grown in incubators with a 5 % CO_2 atmosphere. Each series of experiments were carried out with cells originating from the same passage number to provide absolute comparability of the power spectra.

6.3 Results and Discussion

MDCK-II cells added to the TSM resonator sediment though the media and serum onto the gold surface on the upper side of the quartz crystal. Settled MDCK-II cells adhere to the surface and induce a considerable decrease in resonance frequency. Typically a frequency shift of approximately 600 Hz due to the attachment and spreading of the MDCK-II cells (cell-number: $1.6 \cdot 10^5$) on the gold electrode of a 5 MHz TSM resonator is found. After several hours, when attachment and spreading is completed and a confluent cell monolayer is established on the surface, no further frequency decrease can be observed. In this regime, frequency fluctuations can be monitored as illustrated in figure 6.1B. These fluctuations lead back to shape and viscoelasticity fluctuations of the cell monolayer grown on the quartz crystal. The formation and breakup of focal contacts produce a fluctuating contact area and as a consequence a transient change in free volume between cell monolayer and substrate. Moreover, the cells themselves exhibit transient changes in volume and their micromechanical properties. As a consequence, the resonance frequency of the TSM resonator is fluctuating due to the inherent noise of the load situation on the quartz surface.

Cell shape fluctuations, cell-substrate-interactions, dynamics of the cell-cell anchorage as well as cell movements are mainly determined by the dynamic properties of the cytoskeleton, comprising intermediate filaments, actin filaments and microtubules. From a previous study we know that interfering with actin polymerization by adding cytochalasin D effectively abolishes cell motility.[15] Here, we investigate the impact of drugs interacting with microtubules on the motility of adherent MDCK-II cells. Microtubules are known to be affected in their dynamic properties by molecules interacting with the major microtubule structural protein subunit called tubulin. The drug nocodazole binds these subunits and prevents their polymerization. In contrast, the drug taxol, extracted from the bark of a rare species of yew tree, binds to and stabilizes microtubules, causing a net increase in tubulin polymerization. Figure 6.1B shows the typical time course of the fluctuating resonance frequency of a quartz crystal covered with a monolayer of vital MDCK-II cells. The time courses of the fluctuating resonance frequency found for MDCK-II cell exposed to nocodazole (Sigma; 10 mM stock solution in DMSO, final concentration 10 μM) and taxol (Sigma; 6 mM stock solution in DMSO, final concentration 6 μM) are shown in figure 6.1C and 1D. The amplitude of the noise level is reduced significantly upon addition of the corresponding drug. To quantify the observed frequency fluctuations the power density spectra of the fluctuating data were computated (figure 6.2). Vital MDCK-II cells display a typical peak at around 1-2 Hz indicative of an intrinsic resonance,

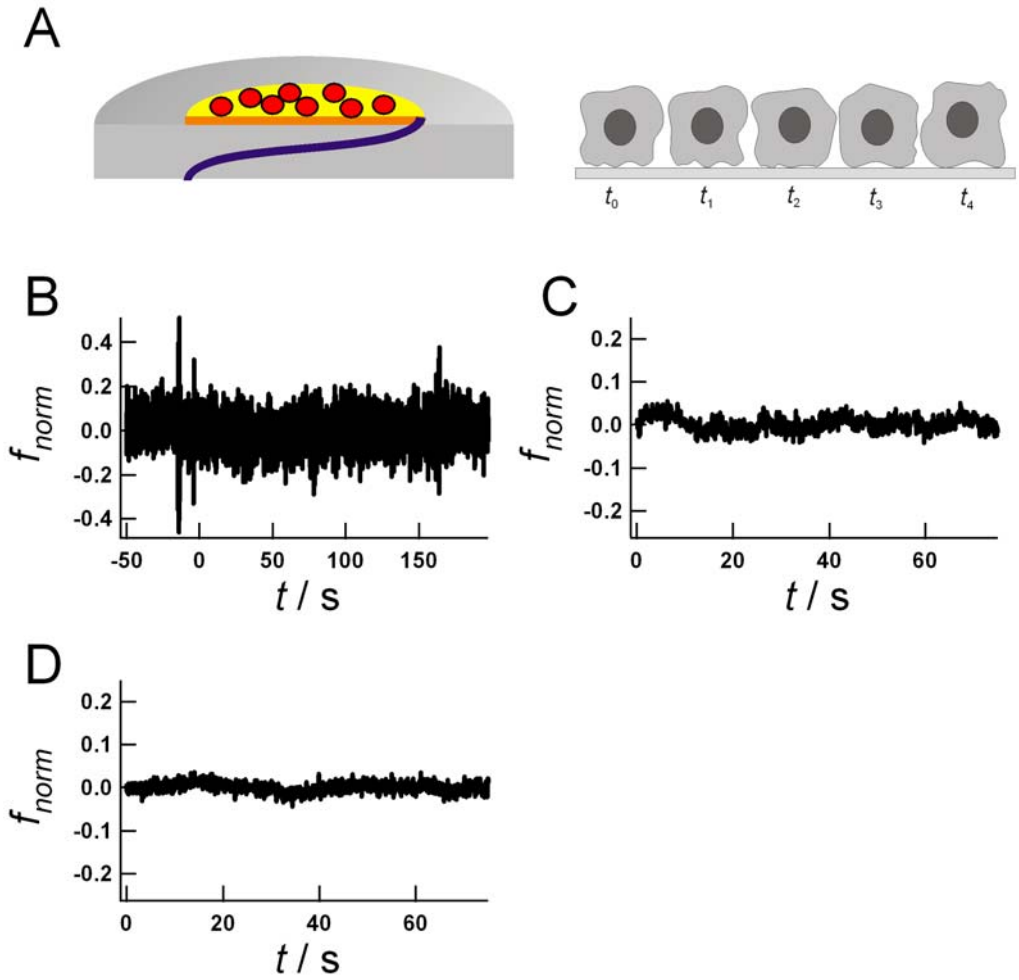

Figure 6.1: (A) Schematic diagram of a cell monolayer on the gold electrode of a TSM resonator, and a sketch illustrating shape fluctuations. The size of the electrode is not drawn to scale with respect to the cells. (B-D) Fluctuations of the normalized resonance frequency of the quartz crystal under various load situations. (B) Vital MDCK-II cell in culture fluid. (C) MDCK-II cell exposed to nocodazole. (D) MDCK-II cells treated with taxol

that originates from collective motion of the cells. Since our analysis is bandwidth limited to 13 Hz the collective motion might be faster than 1-2 Hz due to aliasing effects. Since no information is inferred from the frequency, aliasing does not impact our findings. Exposing the cells to microtubule-specific drugs nocodazole (figure 6.2B) and taxol (figure 6.2C) leads to a significant reduction of the noise level and the resonance peak. Cross-linking all proteins via paraformaldehyde (4 % (v/v) in PBS^{++}), a common fixation to stabilize biological samples, and finally removal of the cells from the quartz surface mechanically leads to a further decrease of the noise level and obliteration of the peak in the power density spectra at 2 Hz (figure 6.2D and E). Therefore we conclude that the peak at 2 Hz is indicative of synchronized periodic fluctuation in viscoelasticity or shape of the living cell bodies. Several recent studies reported that disrupture of microtubules leads to an increasing number of focal contacts, which anchorage cells to the substratum.[21, 22] Ballestrem et al.[23] showed that this effect leads to a decreasing velocity of the protruding lamellipodium and a lower ruffle retraction rate. As the motility of living cells is highly susceptible to drugs acting on the polymerization of microtubules it is straightforward to conclude that the dynamics of the cytoskeleton are a probable source of the peak observed in the power density spectra of vital cells. Recently we examined the influence of cytochalasin D on actin polymerization.[15] We found that the fungal alkaloid cytochalasin D also provokes a substantial reduction of the resonance peak at 2 Hz, comparable to the results found for microtubule-specific drugs.

To prove that the observed decrease of the fluctuations in figure 6.2 is not an effect of detachment of the cells due to the addition of the drugs and the noise of the bare electrode is detected, we measured the Q-factor (Q = energy stored per cycle /energy dissipated per cycle) under various conditions (figure 6.3). To calculate the Q-factor the transfer function of the BVD equivalent circuit was fitted to the recorded phase data ϕ(f). Figure 6.3A shows data for a resonator covered with a confluent cell layer of vital MDCK-II cells (■) compared with a confluent cell layer exposed to taxol (◯) and a bare quartz after removal of the cell layer (△). Exposing MDCK-II cells to taxol results in a decrease of the phase maximum ϕ_{max}, while removal of the cell layer leads to an increase of ϕ_{max}. Figure 6.3B shows the corresponding Q-factor, calculated from the parameters of the transfer function of the BVD network after fitting the impedance spectra. We found that the Q-factor of the cell-covered quartz resonator decreases when cells are exposed to 10 μM nocodazole, i.e. the energy dissipation increases. This observation is in agreement with studies of Marx et al.[13] showing that treatment of endothelial cells with nocodazole leads to a decreasing resonance frequency and an increasing resistance, i.e. increasing energy dissipation. Treating

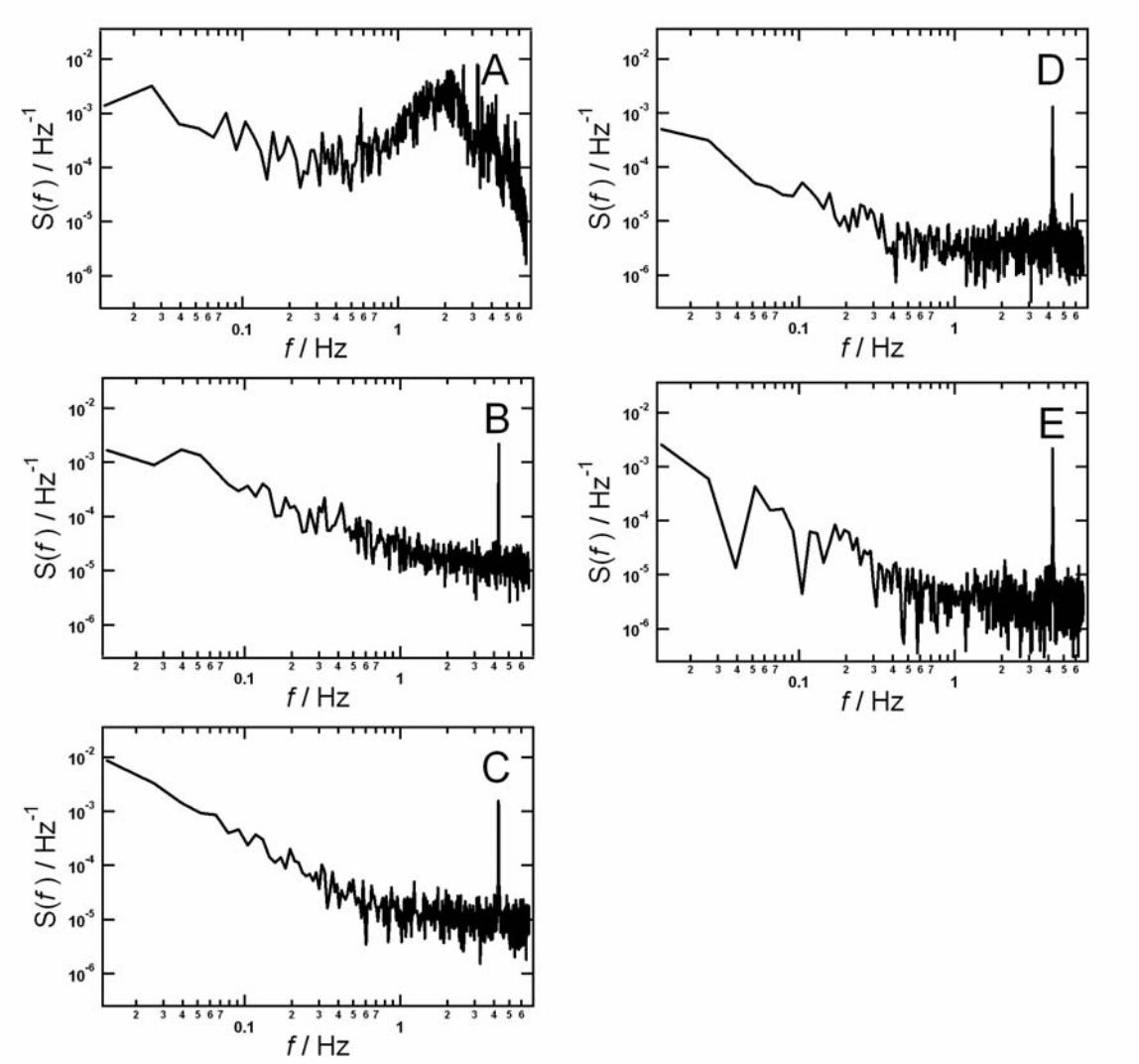

Figure 6.2: Power density spectra of frequency fluctuations under various load situations. Power density spectra were obtained after subtraction of a linear trend from the raw data and applying an FFT algorithm to subsets of the dataset comprising 1024 points. The resulting power density spectra of the individual subsets were averaged to yield the spectrum. (A) Vital MDCK-II cell in culture fluid. (B) MDCK-II cell exposed to nocodazole. (C) MDCK-II cells exposed to taxol. (D) MDCK-II cells fixed with PFA. (E) Resonator after removal of cells (immersed in culture fluid).

MDCK-II cell with 6 μM taxol leads to an even stronger increase of the energy dissipation (decreasing Q-factor). For comparison protein cross-linking with paraformaldehyde also increases the energy dissipation, while mechanical removal of the cells yields a Q-factor almost twice as high as recorded for the cell covered quartz resonator. The increase of energy dissipation upon exposure of cells to nocodazole and taxol indicates that the decrease of the fluctuations is a result of changes in the shape or viscoelasticity and not due to partial detachment of the cells from the crystal surface.

The dynamic shape of an isolated cell results from an interplay between protrusion, adhesion and contraction activities. These are most closely associated with the actin cytoskeleton. In many cell types, microtubules have been shown to be involved in the development of morphological polarity required for directional migration. This suggests a role for the microtubule system in regulating both actin cytoskeleton and the formation of cell-substrate adhesions. The most prominent role of microtubules in the cell is in transport of vesicles and organelles. Experiments of Ballestrem et al.[23] suggest that drugs stabilizing microtubules as well as disrupting microtubules lead to a considerable reduction of cell motility mouse melanoma cells. Thus microtubule-dynamics play a crucial role for the speed of cell locomotion explaining our findings that both taxol and nocodazole reduce vertical motility of adherent cells.

Interestingly, we observed a decrease in Q, which is indicative of an increase in viscoelasticity associated with the addition of nocodazole and taxol. Conversely, addition of cytochalasin D results in an increase in Q, which suggests the disruption of actin filaments accompanied with partial detachment of the cells. Disruption of microtubules leads to contraction of the cell thus increasing the viscoelastic load of quartz crystal due to cell-shrinkage. However, adding taxol stiffens the cells thus increasing the resistance R, which is correlated to the complex shear modulus G of the cell, resulting in a decrease in $Q = 1/R$. Cytochalasin D, conversely, makes the cell more flexible and as a consequence increases Q.

Comparing the frequency fluctuations in a QCM experiment with resistance fluctuations obtained from ECIS measurements yields additional information about the observed noise. ECIS is a highly sensitive electrochemical technique to investigate morphological changes of adherent cells.[24] The technique is based on the measurement of the frequency-dependent impedance between two gold electrodes immersed in tissue culture medium.[16, 18] The electrical impedance increases when cells attach and spread on the surface of the gold electrode as the current has to bypass the cells behaving like an insulating particle. So, the impedance is a function of the cell shape and the space formed between the ventral surface and the substratum and

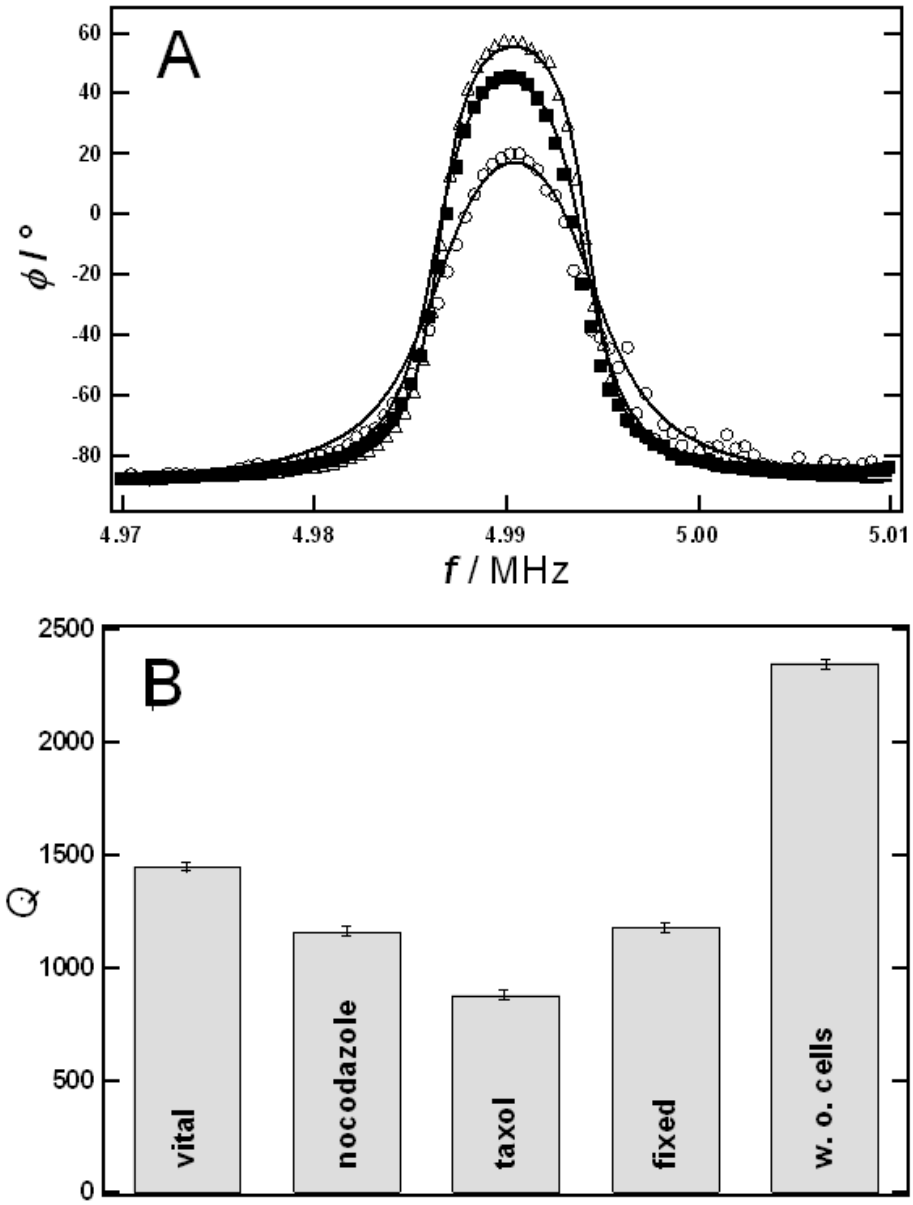

Figure 6.3: (A) Phase shift ϕ as a function of frequency for a 5 MHz quartz resonator near its fundamental resonance. (■) Vital MDCK-II cell in culture fluid. (◯) MDCK-II cells exposed to taxol. (△) Resonator after removal of cells (immersed in culture fluid). Solid lines represent the transfer functions of the BVD network after parameter fitting. (B) Q-factor of the quartz resonator under different conditions as extracted from impedance analysis and subsequent equivalent circuit modelling using the BVD network.

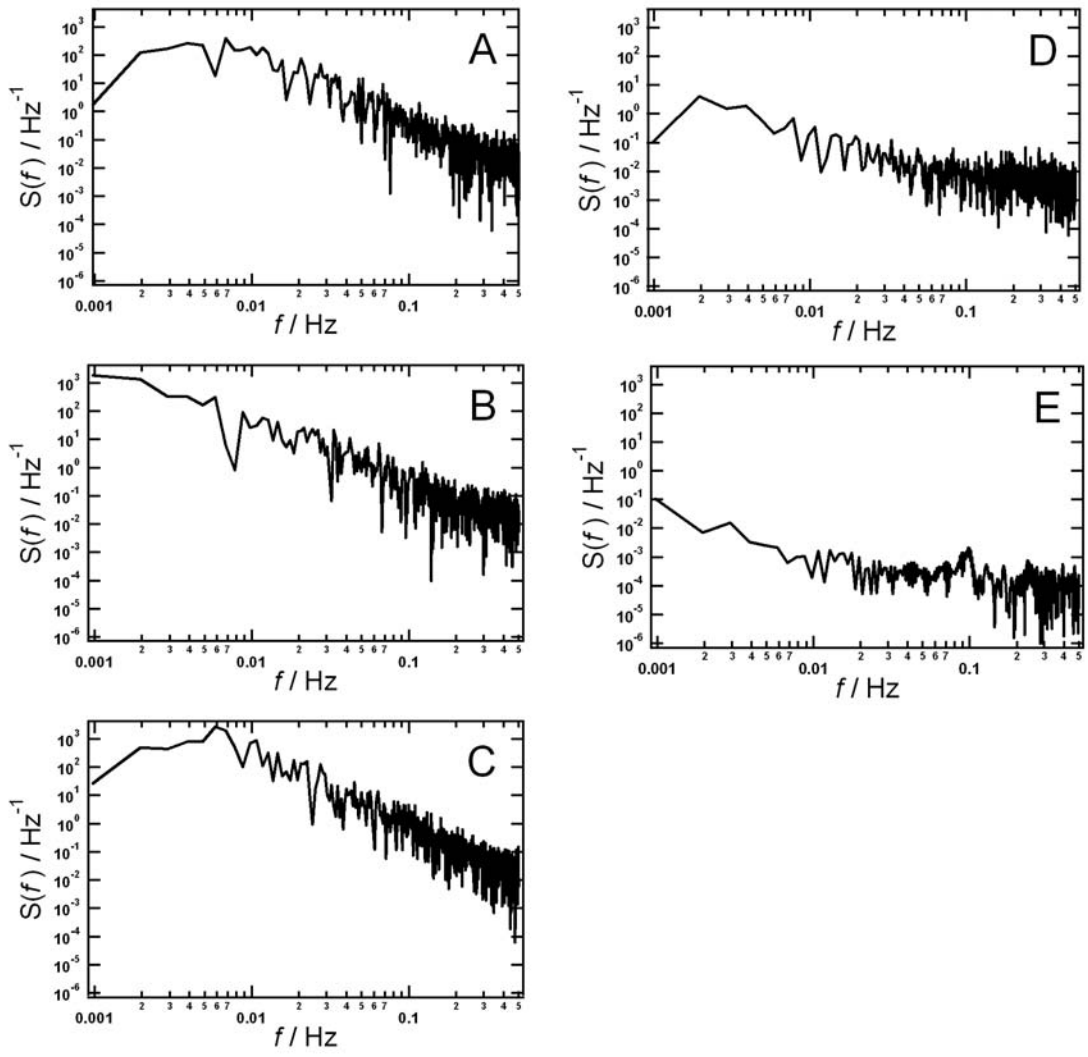

Figure 6.4: Analysis of ECIS-based resistance fluctuations under various load conditions. Prior to FFT a linear trend was subtracted from the raw data. The power density spectra of data subsets comprising 1024 points were averaged to yield the spectra shown. (A) Vital MDCK-II cell in culture fluid. (B) MDCK-II cell exposed to nocodazole. (C) MDCK-II cells exposed to taxol. (D) MDCK-II cells fixed with PFA. (E) Bare electrode just immersed in culture fluid.

ECIS technique can be used to monitor shape fluctuations. Fluctuations in electrode resistance when the electrode surface (area of $5 \cdot 10^{-4}$ cm^2) is completely covered with MDCK-II cells are shown in figure 6.4. The sampling rate for the impedance measurements performed at 4 kHz was 1 Hz. The power density spectra of vital cells (figure 6.4A) displays a slope in the range of (-2.1 to -2.7) s^{-2} indicative for biological active cells.[25] Exposing cells to nocodazole or taxol (figure 6.4B and 6.4C) does not induce any significant change in the power density spectrum. For comparison, the cells were treated with paraformaldehyde (figure 6.4D) leading to a significant decrease of the noise (slope: -0.8 s^{-2}) as consistently observed in QCM measurements. Mechanical removal of the cells (figure 6.4E) as a control experiment yields the lowest value found for the slope (slope:-0.3 s^{-2}).

The resistance, i.e. the real part of the complex impedance observed with ECIS is a measure for the space formed between the ventral surface and the substratum.[24] In contrast, the QCM reads out the overall viscoelastic load on the resonator, which is governed by the space between ventral cell membrane and gold electrode but also by changes in cell volume and viscoelasticity. Therefore we conclude that fluctuations in viscoelasticity due to actin and microtubule-dynamics are observed in the resonance frequency fluctuations rather than pure shape fluctuations as monitored by ECIS. Generally spoken, QCM measurements hold different information than ECIS recordings. This conclusion is supported by variance analysis of the resonance frequency (figure 6.5A, QCM) and resistance (figure 6.5B, ECIS) fluctuations. The variance σ^2 of the entire dataset is an intuitive parameter, that directly mirrors the fluctuation amplitude. Exposing MDCK-II cells to nocodazole or taxol yields in a substantial decrease in frequency fluctuations (nocodazole: 4 %, taxol: 2 %). Fluctuations observed after fixation of cells are of the same magnitude than fluctuations of taxol-treated cells. A further reduction of the frequency fluctuations is obtained after removal of the cells. Interestingly, we observed different effects in ECIS measurements under the same conditions (figure 6.5B). MDCK-II cells, exposed to nocodazole or taxol still show high resistance fluctuations. Fixation of the cells, results in a decrease of resistance fluctuations, while the bare electrode provides the smallest variance.

Taken together, fluctuation analysis of TSM resonators provides a sensitive means to study changes in viscoelasticity as dictated by dynamics of the cytoskeleton (actin, microtubules). In addition measurements of the quality factor renders the method highly suitable to judge how a particular treatment changes viscoelasticity of living cells.

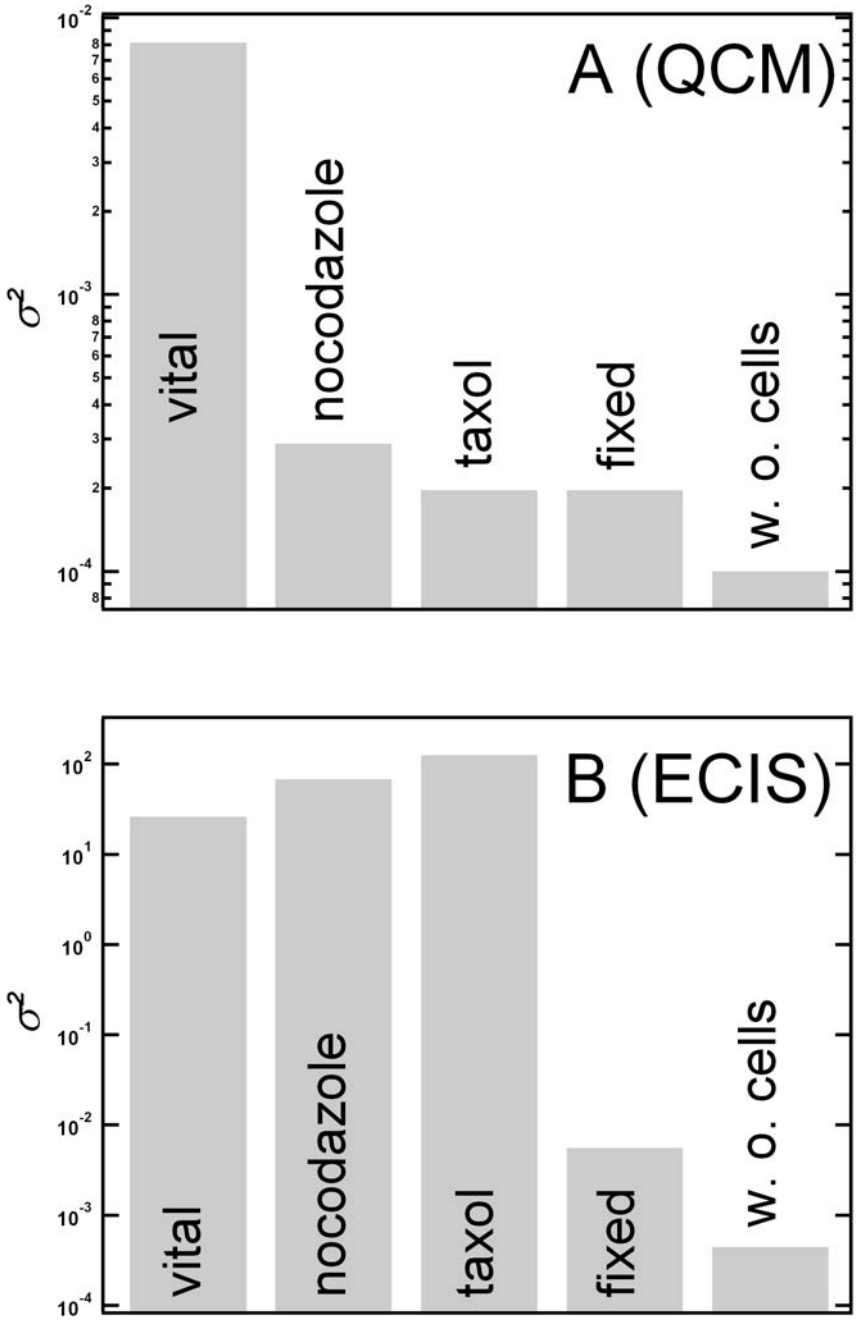

Figure 6.5: Variance σ^2 of the normalized resonance frequency (A) or resistance (B) fluctuations under various experimental conditions. σ^2-values were calculated for 1100 data points.

Bibliography

[1] Alberts, B.; Johnson, A.; Lewis, J.; Raff, M.; Roberts, K.; Walter, P. *Molecular Biology of the Cell* Garland Science, 2002.

[2] Brady-Kalnay, S. M.; Soll, D. R.; Brackenbury, R. *Int. J. Cancer* 1991, 47, 560-568.

[3] Partin, A. W.; Isaac, J. T.; Treiger, B.; Coffey, D. S. *Cancer Res.* 1988, 48, 6050-6053.

[4] Partin, A. W.; Schoeniger, J. S.; Mohler, J. L.; Coffey, D. S. *Proc. Natl. Acad. Sci. USA* 1989, 86, 1254-1258.

[5] Parczyk, K.; Haase, W.; Kondor-Koch, C. *J. Biol. Chem.* 1989, 264, 28, 16837-16846.

[6] van Zeijl, M. J. A. H.; Matlin, K. S. *Cell Regulation* 1990, 1, 921-936.

[7] Tajika, Y.; Matsuzaki, T.; Suzuki, T.; Ablimit, A.; Aoki, T.; Hagiwara, H.; Kuwahara, M.; Sasaki, S.; Takata, K. *Histochem. Cell Biol.* 2005, 124, 1-12.

[8] Breitfeld, P. P.; McKinnon, W. C.; E., M. K. *J. Cell Biol.* 1990, 111, 2365-2373.

[9] De Brabander, M. J.; Van de Veire, R. M. L.; Aerts, F. E. M.; Borgers, M.; Janssen, P. A. J. *Cancer Res.* 1976, 36, 905-916.

[10] De Brabander, M. J.; Geuens, G.; Nuydens, R.; Willebrords, R.; De Mey, J. *Proc. Nat. Acad. Sci. USA* 1981, 78, 5608-5612.

[11] Wegener, J.; Seebach, J.; Janshoff, A.; Galla, H.-J. *Biophys. J.* 2000, 78, 2821-2833.

[12] Wegener, J.; Janshoff, A.; Galla, H.-J. *Eur. Biophys. J.* 1998, 28, 26-37.

[13] Marx, K. A.; Zhou, T.; Montrone, A.; Schulze, H.; Braunhut, S. *Biosensors and Bioelectronics* 2001, 16, 773-782.

[14] Rodahl, M.; Höök, F.; Fredriksson, C.; Keller, C. A.; Krozer, A.; Brzezinski, P.; Voinova, M.; Kasemo, B. *Faraday Discuss.* 1997, 107, 229-246.

[15] Sapper, A.; Wegener, J.; Janshoff, A. *Anal. Chem.* 2006, in press.

[16] Lo, C.-M.; Keese, C. R.; Giaever, I. *Exp. Cell Res.* 1993, 204, (102-109).

[17] Pei, Z.; Keese, C. R.; Giaever, I.; Kurzawa, H.; Wilson, D. E. *Exp. Cell Res.* 1994, 212, 225-229.

[18] Giaever, I.; Keese, C. R. *Proc. Natl. Acad. Sci. USA* 1991, 88, 7896-7900.

[19] Wegener, J.; Keese, C. R.; Giaever, I. *Exp. Cell Res.* 2000, 259, 158-166.

[20] Giaever, I.; Keese, C. R. *Nature* 1993, 366, 591-592.

[21] Bershadsky, A.; Chausovsky, A.; Becker, E.; Lyubimova, A.; Geiger, B. *Curr. Biol.* 1996, 6, 1279-1289.

[22] Kaverina, I.; Krylyshkina, O.; Small, J. V. *J. Cell Biol.* 1999, 146, 1033-1043.

[23] Ballestrem, C.; Wehrle-Haller, B.; Hinz, B.; Imhof, B. A. *Mol. Biol. Cell* 2000, (11), 2999-3012.

[24] Lo, C.-M.; Keese, C. R.; Giaever, I. *Biophys. J.* 1995, 69, 2800-2807.

[25] Giaever, I.; Keese, C. *IEEE Trans. Biomed. Eng.* 1986, 33, (2), 242-247.

Chapter 7

Physical and Physiological Stimuli

7.1 Introduction

The fundamental property of cells to move is one of the most intriguing programs in cell biology. Cell motility is centrally involved in a wealth of biological processes such as embryonic development, tissue maintenance, wound healing and immune system function. But it is also the root of many diseases, including metastatic cancer, arthritis, and neurological birth defect. The complexity of cell migration is still poorly understood as there are many interacting pathways and processes like metabolism or cell adhesion. To get a more precise picture about cell migration it's wise to study the influence of distinct, single processes on cell motility.

Cell activity and vitality is maintained by a highly integrated network of chemical reactions called metabolism. As most enzymes are very sensitive to temperature, the metabolic rate, i.e. the metabolism per unit time, is influenced by the ambient temperature. The relation between temperature and metabolism rate is given by the Q_{10} rule: Decreasing the temperature about 10 degrees reduces the metabolic rate about 50 %. Inversely, increasing the temperature in the same range yields rise in the metabolic rate. However, since enzymes being proteins are subject to thermal denaturation the rate of an enzymatically catalyzed reaction falls with increasing temperature once the denaturation temperature has been surpassed. The influence of the metabolism on cell motility has been reported by Lo et al..[2] In this study, a substantial reduction of cell locomotion as observed as the ambient temperature decreases.

Besides the metabolism, integrins, a family of heterodimeric transmem-

brane proteins, play a pivotal role in cell motility. It is well known that integrins mediate cell attachment to extracellular matrix (ECM) components including collagen, fibronectin, and laminin. Thus most integrins are exposed on the basal cell surface whereas only a few of these proteins are found on the basal surface of the cell.[11] In addition, integrin-dependent cell binding to ECM components has been shown to initiate a number of cellular responses as changes in intracellular ion concentration[9, 10] and the activation of traditional second messengers such as tyrosine kinase, phospholipase C, and protein kinase. Leavesley at al. reported a linkage between integrin-induced transmembrane signals and cell movement.[12] In this study, binding of collagen and vitronectin to their respective integrins promotes distinct intracellular signaling events which facilitate cellular migration.

In this chapter the influence of the metabolic rate on cell motility were studied by thickness shear mode resonators and electrochemical impedance measurements. Furthermore the linkage between integrin-induced transmembrane signals and cell motility had been proven.

7.2 Material and Methods

7.2.1 QCM-Based Fluctuation Experiments

AT-cut quartz crystals (5 MHz fundamental resonance; KVG, Neckarbischofsheim, Germany) were equipped on both sides with circular gold electrodes (diameter 5 mm). The quartz slides were mounted as the bottom of a cell culture dish into homemade crystal holders (Teflon). A phase-lock oscillator (QCM100; SRS, Inc., Sunnyvale, CA, USA) connected to the crystal supports the resonance frequency. The signal was read out by a frequency counter (Agilent 53181A; Agilent Technologies, Palo Alto, CA, USA) and transferred via GPIB to a computer achieving a time resolution of 75 ms. QCM- and ECIS-based (next paragraph) fluctuation measurements were carried out in incubators with 5 (v/v) % CO_2 at 37 °C.

Mechanical load of the quartz resonator under various experimental conditions were characterized by the Q-factor (Q, energy stored per cycle/energy dissipated per cycle). It is measured by impedance analysis using a continuous-wave impedance analyzer (SI-1260; Solartron Instruments, Farnborough, UK) in the frequency regime close to the fundamental resonance frequency (5 MHz). To determine the Q-factor, impedance data were analyzed by adjusting the parameters of the Butterworth-van-Dyke equivalent circuit as described elsewhere.[13]

7.2.2 ECIS-Based Fluctuation Experiments

The measurement system consists of a lock-in amplifier (SR830, SRS, Inc., Sunnyvale, CA, USA) and an eight-well cell culture dish with circular gold-film electrodes (diameter 250 μm) deposited upon the bottom of each well (Applied Biophysics, Inc., Troy; www.biophysics.com).[14, 15, 16]

7.2.3 Noise Analysis

In order to check either periodicity or aperiodicity Fast Fourier Transformation (FFT) were used to analyze frequency (QCM) and resistance (ECIS) fluctuations. After subtraction of a linear trend from the raw data FFT algorithm were applied providing the corresponding power density function of the measured time series as described in chapter 5 and chapter 6.

7.2.4 Cell Culture

MDCK-II cells were cultured in Earle's minimum essential medium supplemented with 4 mM glutamine, 100 μg/ml of both, penicillin and streptomycin (all purchased by Biochrom, Berlin, Germany), and 10 % (v/v) fetal calf serum (PAA Laboratories GmbH, Cölbe, Germany). Stocks of these cells were grown in incubators with a 5 % CO_2 atmosphere.

7.3 Effect of Temperature - Physical Stimuli

As the metabolic activity of the cell depends on temperature, cell motility was monitored at 37 °C and 27 °C. MDCK-II cells were added to the TSM resonator as described in chapter 5 and 6. After attachment and spreading were completed, i.e. steady state were reached (figure 5.1) time course of the fluctuating resonance frequency of a quartz crystal covered with a monolayer of vital MDCK-II cells were taken at 37 °C. Then MDCK-II cells were cooled down to 27 °C and frequency fluctuations were recorded subsequently. Finally, cells were warmed up again to 37 °C. Figure 7.1 shows the power density spectra obtained by FFT of the fluctuating resonance frequency at different temperatures.

At 37 °C MDCK-II cells display a typical peak around 1-3 Hz indicative of an intrinsic resonance, that originates from collective motion of the cells (figure 7.1A). Decreasing temperature leads to a significant reduction of the noise level and the resonance peak (figure 7.1B). As the temperature is set back to 37 °C, MDCK-II cells recover as shown in figure 7.1C. Removal of the cells from the quartz surface mechanically leads to a further decrease in

the noise level and the peak in the power density spectra vanishes substantially (figure 7.1D). Therefore, it is straightforward to conclude that the peak around 1-3 Hz is indicative of synchronized periodic fluctuation in viscoelasticity or shape of living cell bodies. The observed reduction of the noise level and the resonance peak at 27 °C gives credence to the hypothesis that the observed cell motility is related to the metabolic activity of the cell.

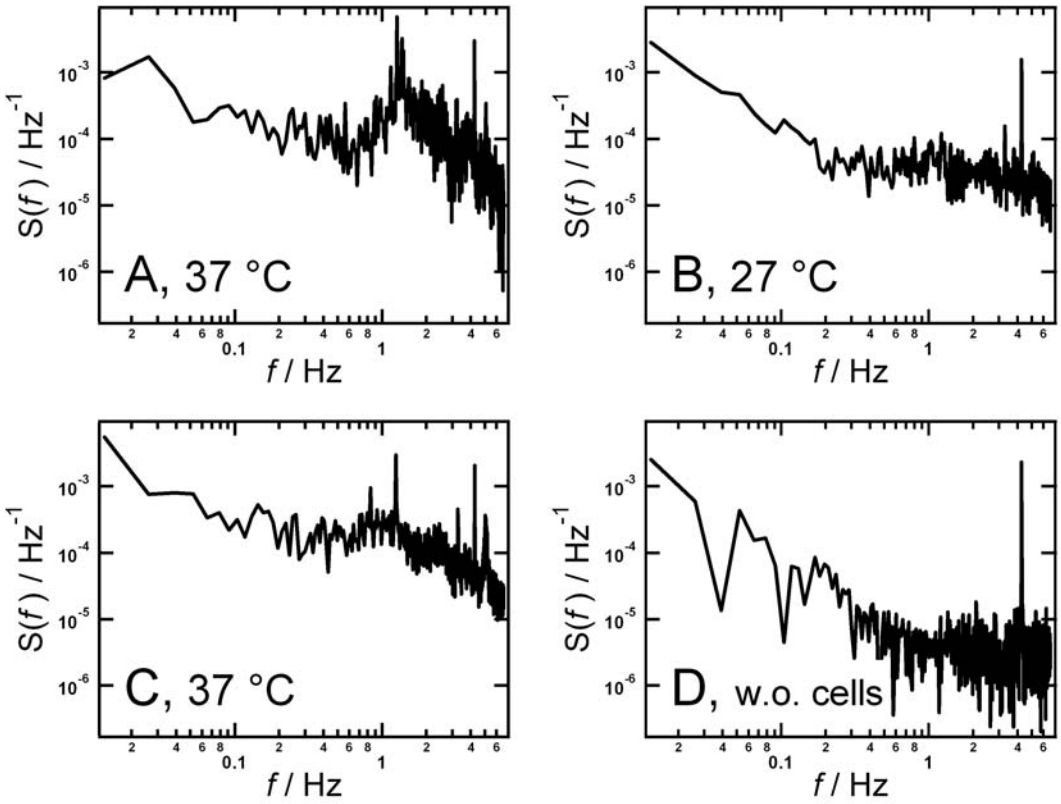

Figure 7.1: Cellular frequency fluctuations as a function of temperature. The power density spectra were obtained after subtraction of a linear trend from the raw data and applying an FFT algorithm to subsets of the dataset comprising 1024 points. The resulting power density spectra of the individual dataset were averaged to yield the spectrum. (A) Vital MDCK-II cells at 37 °C. (B) MDCK-II cells at 27 °C. (C) MDCK-II cells when temperature is set back to 37 °C. (D) Resonator after removal of cells (immersed in culture fluid).

Frequency fluctuations of adherent cells in a QCM experiment were compared with resistance fluctuations obtained from ECIS measurements to yield

additional information about the observed noise. Moreover, these experiments have first been reported by Lo et al..[2] Fluctuations in electrode resistance when the electrode surface (area of $5 \cdot 10^{-4}$ cm^2) is completely covered with a monolayer of MDCK-II cells are shown in figure 7.2. The sampling rate for the impedance measurements performed at 4 kHz was 1 Hz.

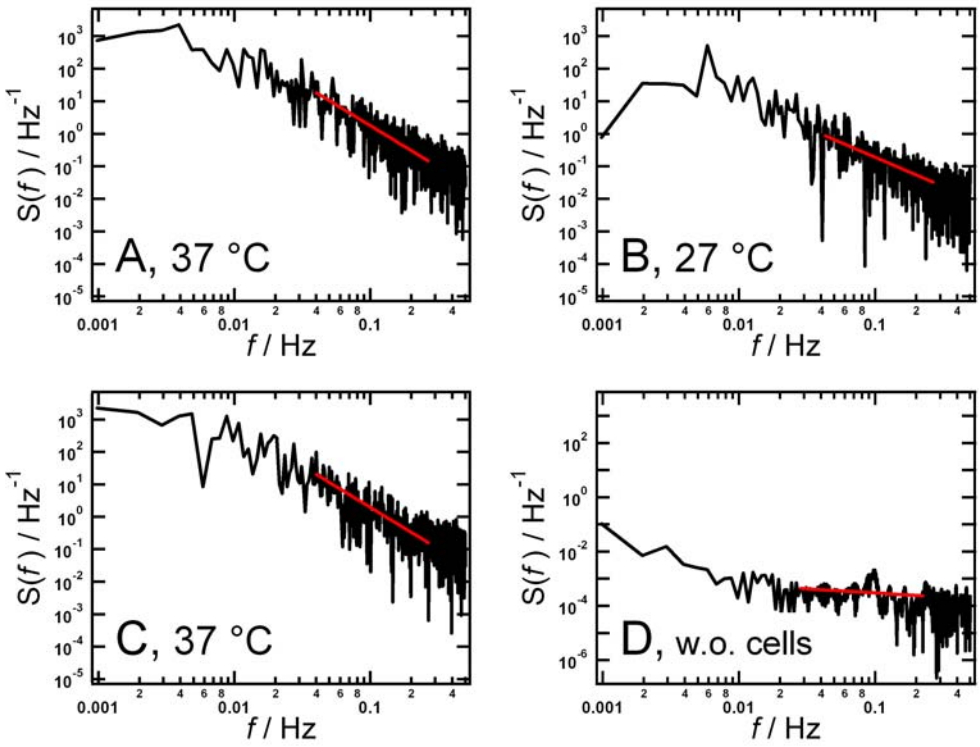

Figure 7.2: Power density spectra of resistance fluctuations obtained by ECIS measurements as a function of temperature. After subtraction of a linear trend from the raw data an FFT algorithm was applied. The power density spectra of data subsets comprising 1024 points are averaged to yield the spectra. (A) Vital MDCK-II cells at 37 °C. (B) MDCK-II cells at 27 °C. (C) MDCK-II cells when temperature is set back to 37 °C. (D) Resonator after removal of cells (immersed in culture fluid).

Figure 7.2A shows a typical power density spectra of vital MDCK-II cells at 37 °C, while figure 7.2B displays the effect of low temperature. MDCK-II cells recover after decreasing the temperature to 37 °C again (figure 7.2C). Mechanical removal of the cells as a control experiment yields the lowest noise level (figure 7.2D). To get more quantitative comparison between the diverse spectra, the slopes of the power density spectra in the regime between

0.25 and 0.025 were calculated. For the four different systems we obtained: (A) (-2.6 ± 0.1) s^2, (B) (-1.8 ± 0.1) s^2, (C) (-2.5 ± 0.1) s^2 and (D) (-0.3 ± 0.1) s^2. The slope found for vital cells at 37 °C is in the typical range of (-2.1 to -2.7) s^2 indicative of biological active cells.[8] Decreasing of the slope in 7.2B is in agreement with the hypothesis that the observed cell motion is associated to metabolic activity. This finding is supported by experiments of Lo et al..[2] They reported that cell motion monitored with ECIS is related to biochemical reaction within the cell.

A further intuitive parameter that directly mirrors the average fluctuation amplitude is the variance σ^2 of the data set. Figure 7.3 shows the variance of the fluctuating resonance frequency (A, QCM) and resistance (B, ECIS). Decreasing temperature leads to a reduction of frequency (A) and resistance (B) fluctuations. As temperature is set back to 37 °C frequency and resonance fluctuations recover to the initial value. Removal of the cells results the smallest variance found for frequency and resonance fluctuations.

Results from QCM-measurements and ECIS-experiments provide corresponding information about biological activity in a sense that all motility is significantly reduced within decrease of temperature. However, the origin of both signals are different: the resistance, i.e. the real part of the complex impedance observed with ECIS is governed by the width of the electrolyte filled space formed between the ventral cell membrane and the substrate.[1] In contrast, the QCM monitors overall viscoelastic load on the resonator, which mirrors the space between ventral cell surface and gold electrode but also changes in viscoelasticity and cell volume. The individual origin of the signals might explain the different frequency dependences in the ECIS- and QCM-based power density spectra.

Taken together, this section underlines that QCM measurements in the way they have been applied here, are a sensitive tool to study changes in metabolic activity of the cell. It might be of interest to observe the effect of depriving cells of glucose as it is known that cell motion is driven by metabolism of glucose.[2]. Furthermore it is motivating to elucidate whether changes of cell motility are detectable as oxygen is withdrawn from cells, forcing them into an anaerobic metabolism.

7.4 RGD-Peptides as Physiological Stimuli

The correlation between integrin-mediated signal transduction and cell motility was studied by frequency fluctuation measurements. MDCK-II cells were grown on the gold surface on the upper side of the quartz crystal. When formation of the cell monolayer on the gold surface is completed frequency

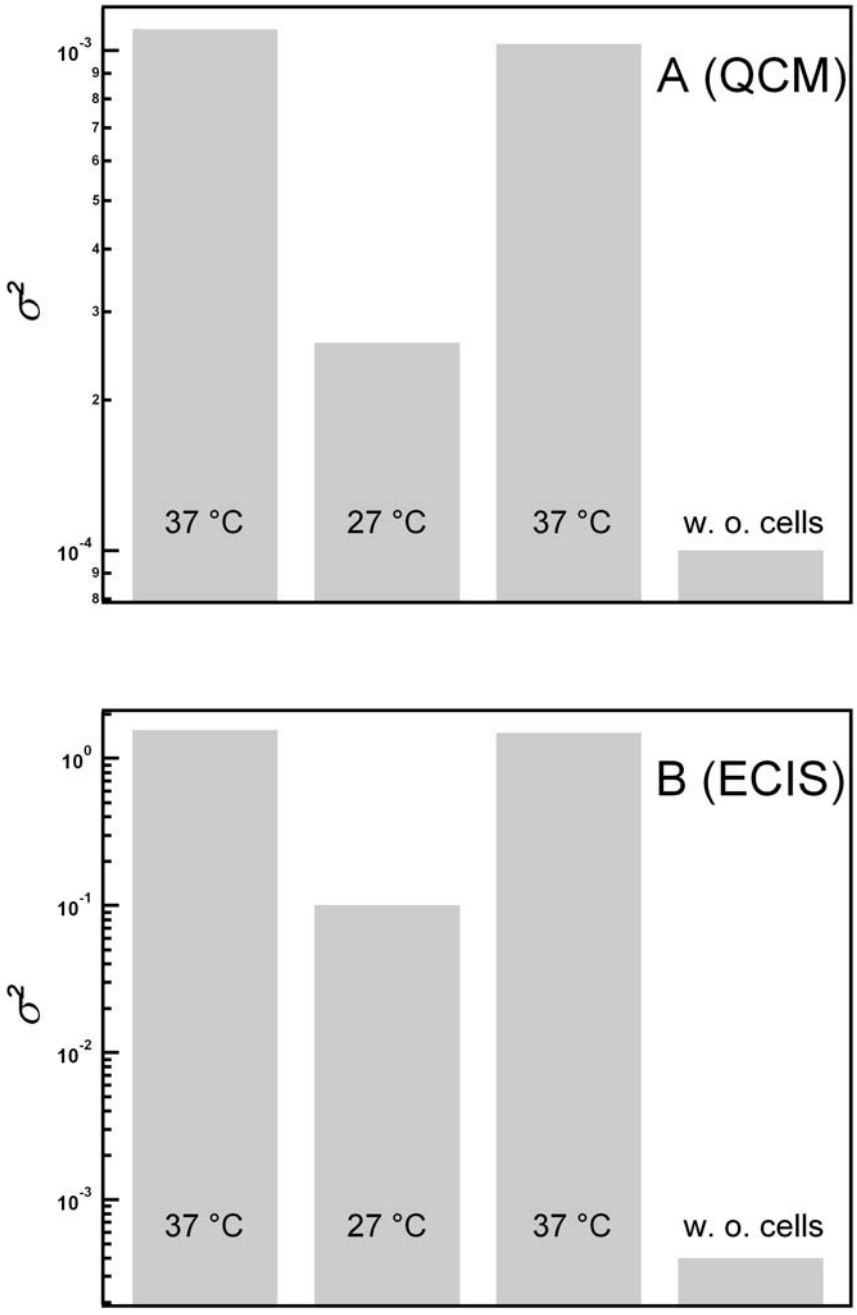

Figure 7.3: Variance σ^2 of the normalized resonance frequency (A) or resistance (B) fluctuations under various experimental conditions. σ^2-values for each experiment were calculated for 1100 data points.

fluctuations were monitored. These fluctuations lead back to shape and viscoelasticity fluctuations of the cell monolayer as described in more detail in chapters 5 and 6.

Figure 7.4A shows a typical power density spectrum of vital MDCK-II cells grown on the gold surface on the upper side of a quartz crystal. Again, a typical peak around 1-3 Hz is observed, indicative of an intrinsic resonance that originates from collective motion of the cells. Exposing MDCK-II cells to 1 mM of the tripeptide RGD (Arg-Gly-Asp) leads to a significant amplification of the resonance peak (figure 7.4B). The same even more pronounced effect is observed when 1 mM of the pentapeptide GRGDS (Gly-Arg-Gly-Asp-Ser) is supplemented (figure7.4C) Mechanical removal of the cells from the gold surface leads to obliteration of the peak around 1-3 Hz.

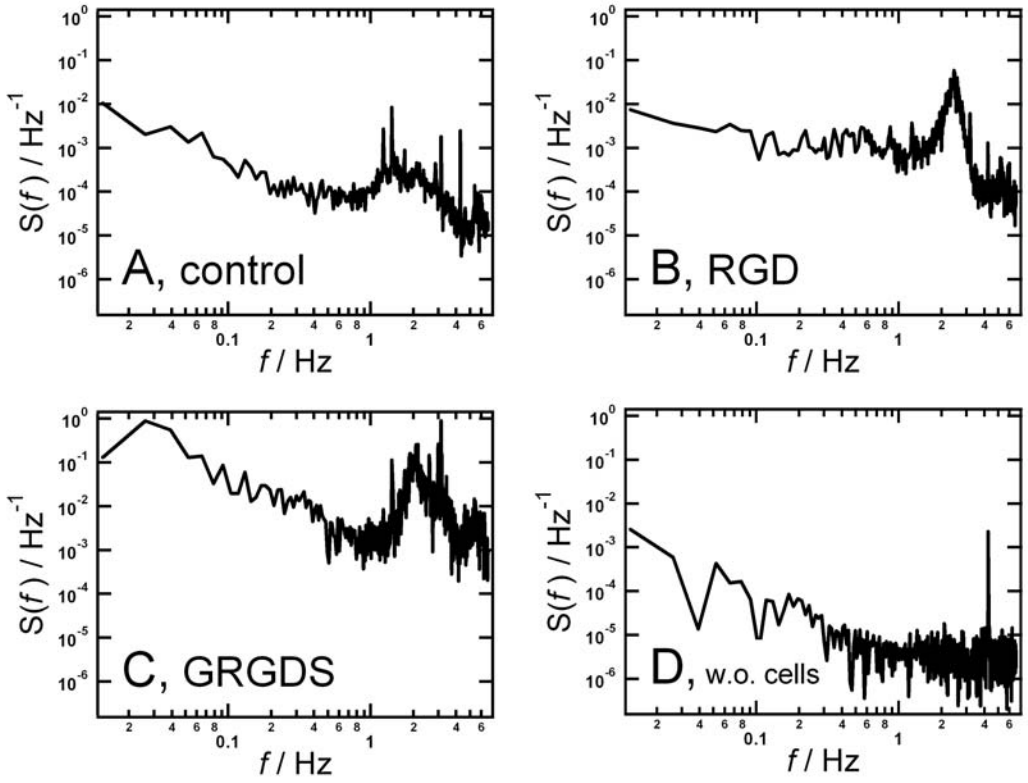

Figure 7.4: Power density spectra of frequency fluctuations as a function of peptide stimuli. The power density spectra were obtained as described above. (A) MDCK-II cells in culture fluid. (B) MDCK-II cells exposed to 1 mM RGD. (C) MDCK-II cells exposed to 1 mM GRGDS. (D) Resonator after removal of cells (immersed in culture fluid).

The changes of the noise level shown in the power density spectra (figure 7.4) is reflected in the changes of the variance σ^2 of the entire dataset (figure 7.5). MDCK-II cells exposed to RGD related peptides provide higher variance than cells in tissue culture fluid (control). Supplementation of the pentapeptide GRGDS to MDCK-II cells results the highest variance. Here the variance is more than five orders of magnitude higher than the σ^2 of untreated cells in tissue culture fluid. Removal of the cells yields a clear reduction of the frequency fluctuation to the smallest variance.

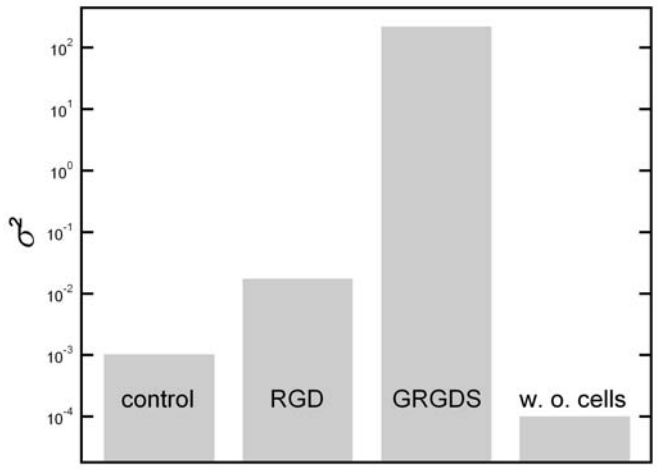

Figure 7.5: Variance σ^2 of the normalized resonance frequency fluctuations under various experimental conditions. σ^2-values were calculated for 1100 data points.

RGD is known to be an integrin recognition motif found in many ECM proteins. So it is straightforward to conclude that peptides containing the RGD sequence binds to cellular integrins. Integrins are mostly found on the basal surface of the cell, serving as an anchorage of cells to the ECM. However, Zanetti et al. showed that integrins are also exposed on the apical cell surface.[11] As, tight junctions serve as a selective permeability barriers in all epithelial cells, they hamper diffusion of peptides to the basolateral surface of the cell. Therefore, RGD peptides also bind to integrins of the apical cell surface. Several studies have reported that integrins initiate changes in Ca^{2+}-concentrations.[9, 10] The cytosolic free calcium plays a potential role in cell migration.[12, 17] Leavesley et al. showed that vitronectin recognition by the $\alpha_V\beta_3$-integrin promotes cellular migration in a calcium-dependent

manner.[12] This observations are in accordance with the present frequency fluctuation measurements. The observed increase of noise due to exposure to the two peptides RGD and GRGDS is indicative of a higher cell motility. It is fair to assume that the RGD peptides bind to apical integrins and in this way promote cell motility. Comparing the power density spectra and the variance for 1 mM RGD on the one hand and 1 mM GRGDS on the other hand, it is obvious that GRGDS is a more potential promoter of cell motility. This observation can be explained by different binding constants of the ligand-receptor-couple, i.e. the binding constant is lower for the RGD tripeptide than for the GRGDS pentapeptide.[18]

Taken together, the integrin-induced transmembrane signals leading to a locomotory response can be observed and quantified by QCM-based frequency fluctuation measurements. A prospective application might be to distinguish between different integrin activations to get detailed information about the complex mechanism of cell motility governed by integrin receptors.

Bibliography

[1] Lo, C.-M.; Keese, C. R.; Giaever, I. *Biophys. J.* 1995, 69, 2800-2807.

[2] Lo, C.-M.; Keese, C. R.; Giaever, I. *Exp. Cell Res.* 1993, 204.

[3] Isaacs, J. T.; Isaacs, W.B.; Feitz, W.F.; Scheres, J. *Prostate* 1986, 9, 271-281.

[4] Hauck, C. R.; Hsia, D.A.; Puente, X.S.; Cheresh, D.A.; Schlaepfer, D.D. *The EMBO Journal* 2002, 21, 6289-6302.

[5] Albrecht-Buehler, G. *Cell* 1977, 11, 395-404.

[6] Albrecht-Buehler, G. *J. Cell Biol.* 1979, 80, 53-60.

[7] Obeso, J. L.; Auerbach, R. *J. Immunol. Methods* 1984, 70, 141-152.

[8] Giaever, I.; Keese, C. *IEEE Trans. Biomed. Eng.* 1986, 33, 242-247.

[9] Schwartz, M. A. *J. Cell Biol.* 1993, 120, 1003-1010.

[10] Sjaastad M. D.; Angres, B.; Lewis, R. S:; Nelson, W. J. *Proc. Natl. Acad. Sci. USA* 1994, 91, 8214-8218.

[11] Zanetti, A.; Conforti, G.; Hess, S.; Martìn-Padura, I.; Ghibaudi, E.; Preissner, K. T.; Dejana, E. *Blood* 1994, 84, 1116-1123.

[12] Leavesley, D. I.; Schwartz, M. A.; Rosenfeld, M.; Cheresh, D. A. *J. Cell Biol.* 1993, 121, 163-170.

[13] Wegener, J.; Seebach, J.; Janshoff, A.; Galla, H.-J. *Biophys. J.* 2000, 78, 2821-2833.

[14] Giaever, I.; Keese, C. R. *Proc. Natl. Acad. Sci. USA* 1991, 88, 7896-7900.

[15] Wegener, J.; Keese, C. R.; Giaever, I. *Exp. Cell Res.* 2000, 259, 158-166.

[16] Giaever, I.; Keese, C. R. *Nature* 1993, 366, 591-592.

[17] Marks, P. W.; Maxfield, F. R. *J. Cell Biol.* 1990, 110, 43-52.

[18] Pierschbacher, M. D.; Rouslahti, E. *Nature* 1984, 309, 30-33.

Chapter 8

Motility of Various Cell Types

8.1 Introduction

Although most mammalian cells have the ability to move, there are differences in the locomotive behavior of various cell types. Several recent studies have reported a link between the metastatic behavior of cancer cells and their motility in culture.[1, 2] Thus, determination of the metastatic behavior of tumor cells is important in clinical research to give a statement about the benignancy or malignancy of tumor tissue cells. Common tools to study the metastatic potential of tumor tissue cells are *in vivo assays* and *in vitro assays*[3, 4] like *wounding-assays*[4] or *phagokinetic track assays.*[5, 6, 7] A drawback of these time-consuming techniques is that each of them possesses a poor time resolution. Thus, a new powerful experimental technique to sense cell motility in real time is required.

The present study shows that QCM-based frequency fluctuation measurements provide a sensitive tool to monitor the dynamics of living adherent cells in real time. Changes in viscoelasticity as dictated by dynamics of the cytoskeleton as well as changes in motility mediated by integrin-induced transmembrane signals can be easily observed. Thus, the QCM-technique may serve as the basis of a new type of whole cell biosensor. Such a biosensor might enable the characterization of the metastatic potential of tumor cells from a detailed analysis of cellular dynamics.

As frequency fluctuation measurements provide a sensitive means to monitor cell motility and the impact of various stimuli, it was straightforward to study two pancreatic carcinoma cell lines, derived from the same original tumor, but known to hold different metastatic potential.

8.2 Material and Methods

8.2.1 QCM-based Fluctuation Experiments

AT-cut quartz crystals (5 MHz fundamental resonance; KVG, Neckarbischofsheim, Germany) coated on both sides with circular gold electrodes (Ø = 5 mm) were mounted as the bottom plate of a cell culture dish into a homemade crystal holder (Teflon). Frequency fluctuations of the quartz resonator were studied using a phase-lock oscillator (QCM100; SRS, Inc., Sunnyvale, CA, USA). The frequency was recorded by a frequency counter (Agilent 53181A; Agilent Technologies, Palo Alto, CA, USA) and then transferred via GPIB to a computer (time resolution 75 ms). All measurements were carried out in incubators with 5 (v/v)% CO_2 atmosphere at 37 °C.

Mechanical load of the quartz resonator under the various experimental conditions we characterized by the Q-factor of the shear oscillation. It is measured by impedance analysis using a continuous-wave impedance analyzer (SI-1260; Solartron Instruments, Farnborough, UK) in the frequency regime close to the quartz fundamental resonance (5 MHz). To determine Q-factor, impedance data were analyzed by adjusting the parameters of the Butterworth-van-Dyke equivalent circuit as described elsewhere.[8]

8.2.2 Noise Analysis

Frequency fluctuations were analyzed by Fast Fourier Transformation (FFT), which is particularly useful to check either for periodicity or to demonstrate aperiodicity, as described in chapter 5 in more detail. After raw data were normalized and detrended FFT were applied providing the corresponding power density function of the measured time series as described recently.

8.2.3 Cell Culture

MDCK-II Cells

MDCK-II cells were cultured in Earle's minimum essential medium supplemented with 4 mM glutamine, 100 μg/ml of both, penicillin and streptomycin (all purchased by Biochrom, Berlin, Germany), and 10 % (v/v) fetal calf serum (PAA Laboratories GmbH, Cölbe, Germany). Stocks of these cells were grown in incubators with a 5 % CO_2 atmosphere.

PaTu8988S and PaTu8988T Cells

We used Dulbecco's minimum essential medium supplemented with 2 mM glutamine, 100 μg/ml of both, penicillin and streptomycin (all purchased by Biochrom, Berlin, Germany), 5 % (v/v) fetal bovine serum and 5 % (v/v) fetal horse serum (PAA Laboratories GmbH, Cölbe, Germany). Stocks of these cells were grown in incubators with a 5 % CO_2 atmosphere.

8.3 Results and Discussion

The dynamics of human pancreatic carcinoma cell lines PaTu8988S and PaTu8988T were studied by means of resonance fluctuation imposed on quartz resonators. Both cell lines were derived from the same original tumor and exhibit identical genetic fingerprints.[3] PaTu8988S cells exhibit an epithelial like organization and grow in tight clusters. By way of contrast PaTu8988T cells grow loosely to the substrate and show no cell-cell contacts. Elsässer et al. reported that PaTu8988S and PaTu8988T cells represent two different forms of differentiation of the same tumor, in which PaTu8988T cells are most differentiated.[3] To monitor cell motility by QCM each cell-line was grown on the gold surface on the upper side of the quartz crystal to provide formation of a cell monolayer. After attachment and spreading were completed time course of the fluctuation resonance frequency of the cell-covered quartz crystal were recorded. Figure 8.1A shows the power density spectra obtained by FFT of the fluctuating resonance frequency for PaTu8988S (left hand side) and PaTu8988T (right hand side) cells. The noise level of PaTu8988S cells is about one order of magnitude higher than the noise found for PaTu8988T cells. Cross-linking cell proteins with paraformaldehyde (4 % (v/v) in PBS^{++}) results in a substantial reduction of the noise level for both cell lines (figure 8.1B). Finally, mechanical removal of the cells as a control experiment leads to the lowest noise level shown in figure 8.1C.

In addition to analysis of frequency fluctuations by Fourier transformation, the variance σ^2 of the data set was calculated. The variance σ^2 directly mirrors the fluctuation amplitude. Figure 8.2 shows the variance σ^2 of the fluctuating resonance frequency for PaTu8988S and PaTu8988T cells under various conditions. We found that σ^2 of vital PaTu8988S cells is more than one order of magnitude higher than the variance of vital PaTu8988T cells. Fixation of each cell line results in a clear reduction of σ^2, while the bare quartz provides the smallest variance.

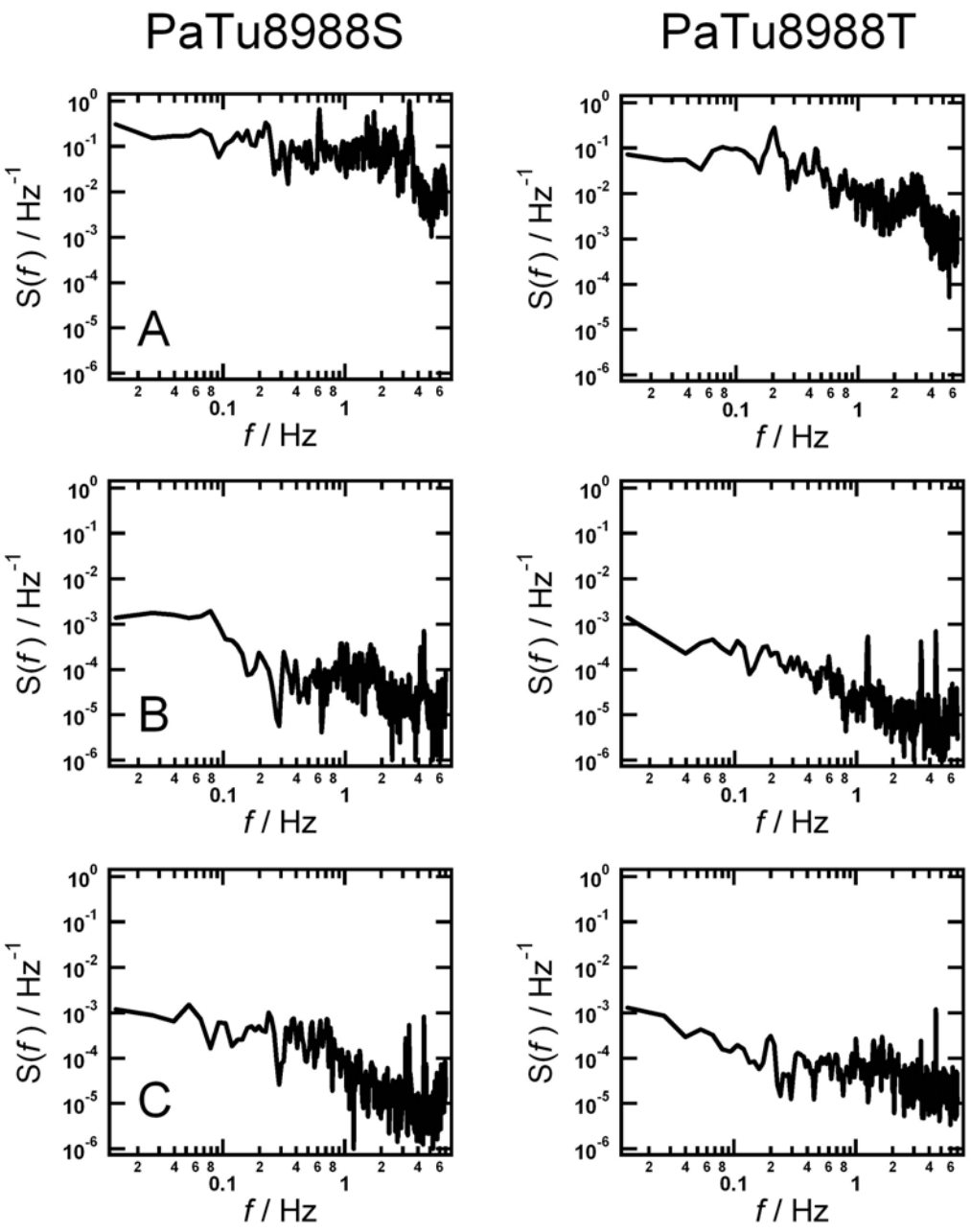

Figure 8.1: Power density spectra of frequency fluctuations found for PaTu8988S and PaTu8988T cells. The spectra were obtained after subtraction of a linear trend from the raw data and applying an FFT algorithm. (A) Vital cells. (B) Cells fixed with PFA. (C) Resonator after removal of cells (immersed in culture fluid).

Both, fourier and variance analysis of frequency fluctuation measurements show that PaTu8988S cells provide higher noise than PaTu8988T cells.

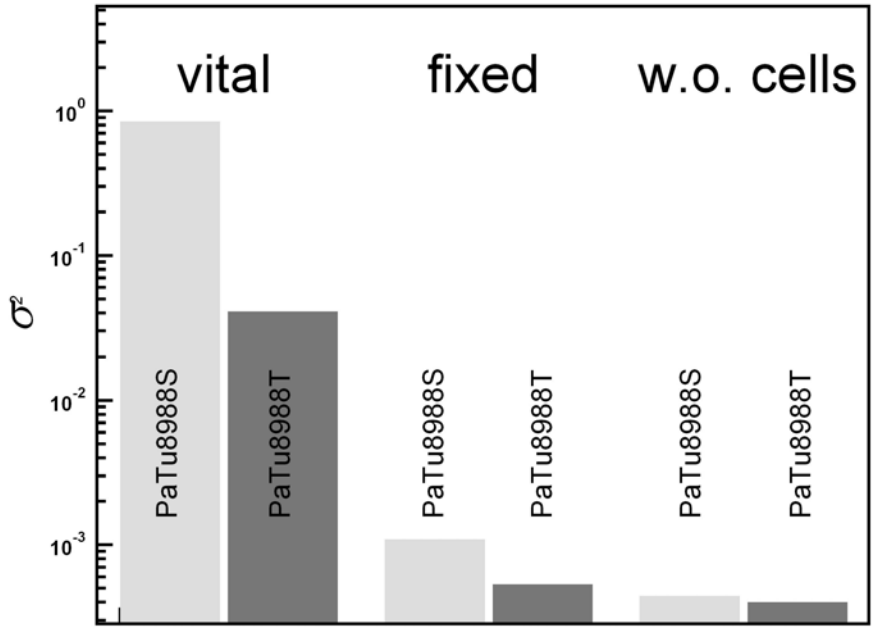

Figure 8.2: Variance σ^2 of the normalized resonance frequency fluctuations under various experimental conditions. σ^2-values for each experiment were calculated for 1100 data points.

In in-vitro-wounding-assays the motility of both pancreatic carcinoma cell lines were studied.[4] In this study PaTu8988T cells showed a higher motility than PaTu8988S cells. The higher motility leads back to a lack of the cadherin-catenin complex. Cadherins are proteins that mediate Ca^{2+}-dependent cell-cell adhesion. They are linked to the cytoskeleton via catenins. Some of these proteins like $p120^{ctn}$ and β-catenin are known to take part in signal transduction pathways.[5, 6] Due to the lack of cadherins, i.e. cell-cell contacts, PaTu8988T cells are able to leave their united cell structure and migrate through the tissue. This observation seems to be inconsistent with results of frequency fluctuation measurements. Looking for a reason to explain the differences, one has to recognize the technical details. The oscillating piezoelectric crystal excite a shear wave that propagates and is dissipated in the biofilm on the surface of the gold electrode. The decay length of the shear wave is given by $\delta = \sqrt{\eta/\pi f \rho}$, where f is the fundamental

resonance frequency of the quartz crystal, η is the viscosity and ρ is the density of the film. For a 5 MHz crystal in water this yields $\delta \sim 250\ nm$. Thus the sensitivity of the QCM is limited to the decay length δ, i.e. QCM reads the changes of the viscoelastic load on the resonator within this space. Therefore the space between the ventral cell membrane and the gold electrode plays a pivotal role in QCM-based measurements. As the cell layer is too far from the substrate, the shear wave can't reach it with a sufficient amplitude. An indication of the space between the ventral cell membrane and the gold electrode is the Q-factor. This value represents the space between the ventral cell membrane and the gold electrode and the viscosity of the cell layer. The Q-factor increases if the space gets higher and/or the viscosity is reduced.[7] As shown in figure 8.3 the Q-factor of PaTu8988T cells is higher than for PaTu8988S cells, i.e. the space between the ventral cell membrane and the gold electrode might be higher. Thus we conclude that the shear wave reaches the basal plasma membrane of PaTu8988T cells with a smaller amplitude resulting in a smaller fluctuation amplitude.

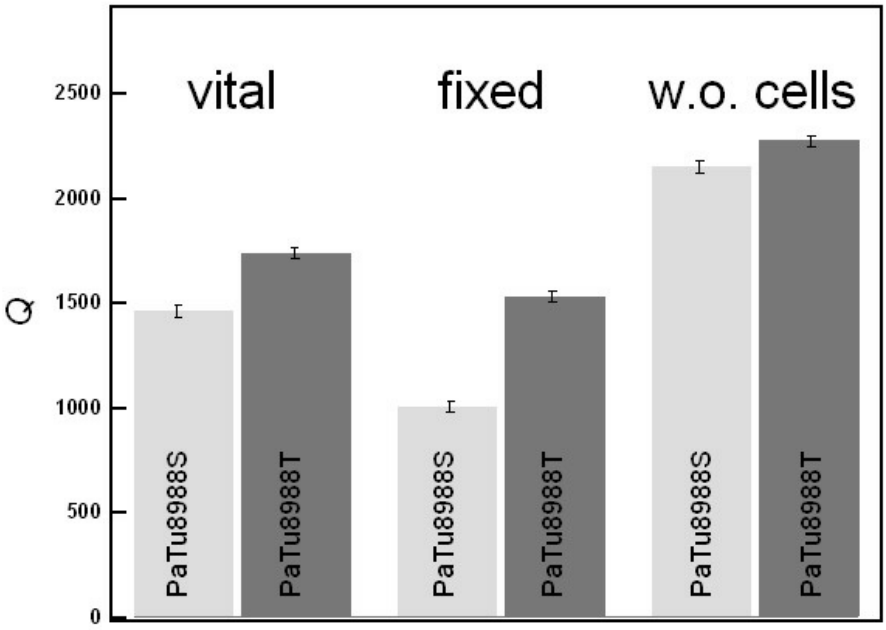

Figure 8.3: Q-factor of the quartz resonator under different conditions as extracted from impedance analysis and subsequent equivalent circuit modelling using the BVD network.

Figure 8.3 summarizes the changes in Q-factor for the quartz resonator covered with PaTu8988S and PaTu8988T cells under various experimental conditions. Energy dissipation is significantly increased when cells are fixated with paraformaldehyde, while removal of the cells yields a typical Q-factor of a bare quartz crystal.

Frequency fluctuations measurements of PaTu8988S and PaTu8988T cells were compared with experiments of MDCK-II cells. As described in chapters 5 and 6 MDCK-II cells were grown on the surface of TSM resonators. Frequency fluctuations measurements were taken after attachment and spreading were completed. Figure 8.4A shows the power density spectra of MDCK-II cells as well as PaTu8988S and PaTu8988T cells. The blue curve, representing the power density spectra of PaTu8988S cells exhibits the highest noise level while MDCK-II cells (black curve) possess especial in the low frequency regime the smallest noise. These differences are even more pronounced in the variances σ^2 of the fluctuation resonance frequency (figure 8.4B). Here, the variance σ^2 of MDCK-II cells is significantly smaller than the variances of the both pancreatic carcinoma cells.

As described above the fluctuation amplitude might depend on the space between the basal plasma membrane and the surface of the gold electrode the top of the quartz crystal. Therefore the Q-factor, which represents this space and the viscosity of the cell layer, was determined (figure 8.5). The Q-factor of MDCK-II cells is approximately the same level as that of PaTu8988S cells, i.e. the space between the ventral cell membrane and the gold electrode as well as the viscosity might be approximately the same. Thus, the differences of the fluctuation amplitude, i.e. the different variances σ^2 of MDCK-II cells and PaTu8988S cells might be due to different motion of the cells. Comparing MDCK-II cells and PaTu8988T cells different Q-factors are found. The Q-factor of PaTu8988T cells is higher than for MDCK-II cells and therefore the space between the ventral cell membrane and the substrate might be higher. Although the space might be higher and thus the amplitude of the fluctuation amplitude is reduced as described above, the variance σ^2 of PaTu8988T cells is significantly higher than for MDCK-II cells. So, we assume that the two pancreatic carcinoma cells, PaTu8988S and PaTu8988T, possess a higher motility than MDCK-II cells. An explanation of this observation might be that epithelial MDCK-II cells possess more cell-cell and cell-substrate contacts than pancreatic carcinoma cells. So, this contacts might hamper the motility of MDCK-II cells. In prospective studies the influence of cell-cell and cell-substrate contacts has to be scrutinized to elucidate the different dynamics of various cell lines.

Taken together, this observations demonstrates that QCM-based frequency fluctuation measurements provide a sensitive tool to distinguish between the

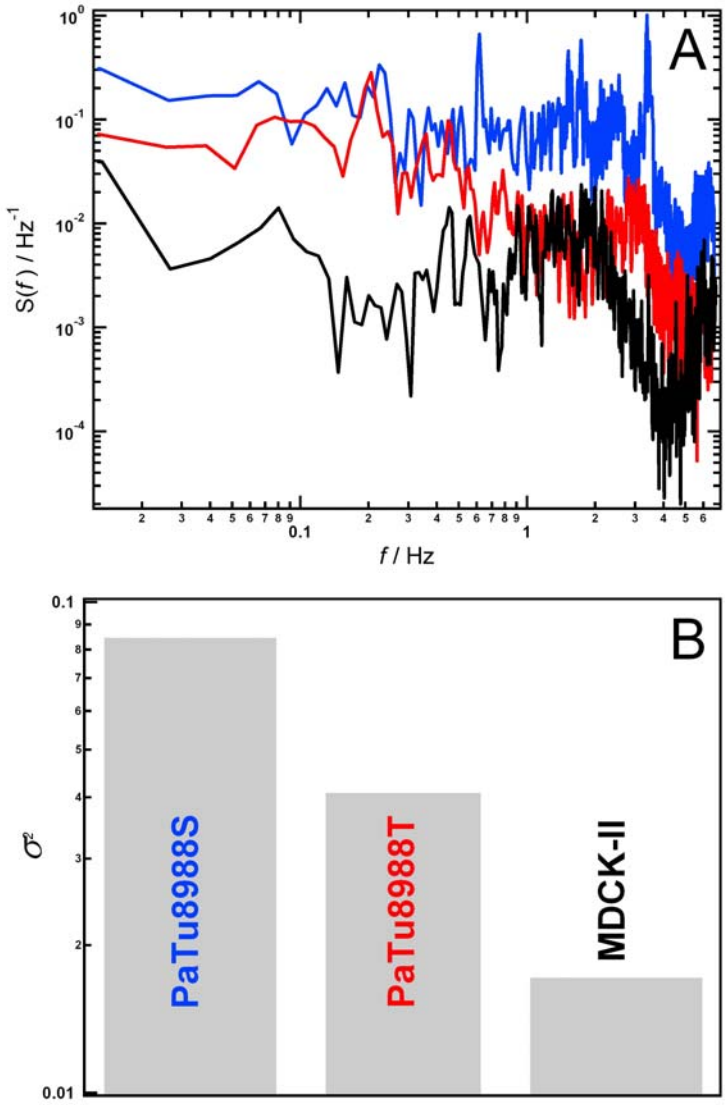

Figure 8.4: (A) Power density spectra of frequency fluctuations found for (black) MDCK-II cells (red) PaTu8988T cells and (blue) PaTu8988S cells. The spectra were obtained as described above. (B) Variance σ^2 of the normalized frequency fluctuations found for the different cell lines. σ^2-values for each experiment were calculated for 1100 data points.

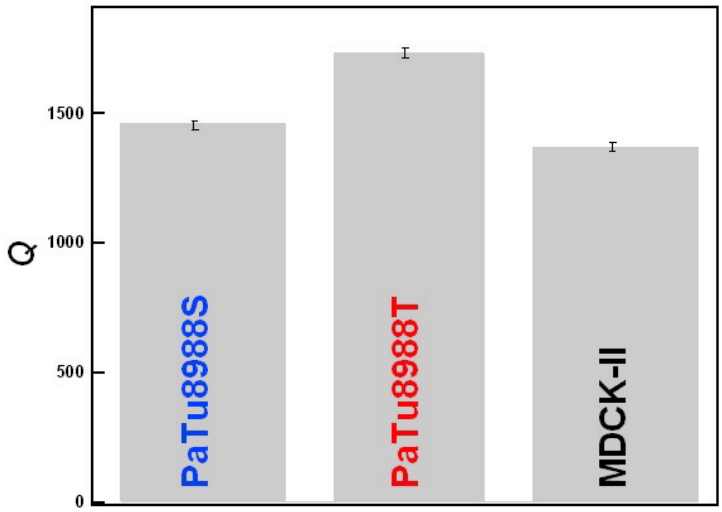

Figure 8.5: Q-factor of the quartz resonator covered with a monolayer of different cell types.

two pancreatic carcinoma cells PaTu8988S and PaTu8988T. Furthermore, different dynamics of MDCK-II cells and the two pancreatic carcinoma cells can be quantified.

Bibliography

[1] Brady-Kalnay, S. M.; Soll, D. R.; Brackenbury, R. *Int. J. Cancer* 1991, 47, 560-568.

[2] Partin, A. W.; Isaac, J. T.; Treiger, B.; Coffey, D. S. *Cancer Res.* 1988, 48, 6050-6053.

[3] Elsässer, H. P.; Lehr, U. Agricola, B.; Kern, H. F. *Virchows Arch. B Cell Pathol. Incl. mol. Pathol.* 1992, 61, 295-306

[4] Neuhaus, U. *Inaugural-Dissertation* 2004, Medizinsiche Fakultät der Westfälischen Wilhelms-Universität Münster.

[5] Dale, T. C. *Biochem. J.* 1998, 329, 209-223.

[6] Reynolds, A. B.; Daniel, J.; McCrea P. D.; Wheelock M. J.; Wu J.;, Zhang, Z. *Mol. Cell Biol.* 1994, 14, 8333-8342.

[7] Wegener, J.; Seebach, J.; Janshoff, A.; Galla, H.-J. *Biophys. J.* 2000, 78, 2821-2833.

[8] Wegener, J.; Seebach, J.; Janshoff, A.; Galla, H.-J. *Biophys. J.* 2000, 78, 2821-2833.

[9] Wegener, J.; Keese, C. R.; Giaever, I. *Exp. Cell Res.* 2000, 259, 158-166.

[10] Giaever, I.; Keese, C. R. *Nature* 1993, 366, 591-592.

Chapter 9

The Origin of the Broad Cell Resonance

9.1 Introduction

In the previous chapters 5, 6, 7, and 8 frequency fluctuation measurements were used to monitor cell motility. The power density spectra of vital MDCK-II cells shown in these chapters display a typical broad resonance around 1-3 Hz. This resonance was considered as an indication for synchronized and periodic fluctuations in viscoelasticity or shape of the cell bodies. Although the shape of this resonance was influenced by diverse stimuli such as microtubule-specific drugs or osmotic stress, it's origin remains to be elucidated. Two main questions arise. Is the observed peak in the power density spectra the result of an externally excited collective vibrations as for instance amplified building vibrations? Is the frequency of 1-3 Hz the real resonance or the result of aliasing due to the low sampling rate? The following section tries to shine light on these aspects.

9.2 Material and Methods

9.2.1 QCM-Based Fluctuation Experiments

AT-cut quartz plates with a 5 MHz fundamental resonance (KVG, Neckarbischofsheim, Germany) frequency were coated with gold electrodes ($\varnothing = 5$ mm) on both sides. The quartz crystals were mounted as the bottom plate of a cell culture dish into a homemade crystal holder. To study frequency fluctuations of the quartz resonator we used a phase-lock oscillator (QCM100; SRS, Inc., Sunnyvale, Technologies, Palo Alto, CA, USA). The signal was

read out by a frequency counter (Agilent 53132A; Agilent Technologies, Palo Alto, CA) and then transferred via GPIB to a computer achieving a time resolution of 7.5 ms. All measurements were carried out in incubators with 5 (v/v) % CO_2 atmosphere at 37 °C.

9.2.2 Noise Analysis

QCM-based frequency fluctuations were analyzed by Fast Fourier Transformation (FFT). The FFT is a useful tool to check either for periodicity or to demonstrate aperiodicity as described in chapter 5 in more detail. In short, FFT were applied to normalized and detrended raw data providing the corresponding power density function of the measured time series.

9.2.3 Cell Culture

Earl's minimum essential medium was used as the culture medium supplemented with 4 mM glutamine, 100 μg/ml of both, penicillin and streptomycin (all purchased by Biochrom, Berlin, Germany), and 10 % (v/v) fetal calf serum (PAA Laboratories GmbH, Cölbe, Germany). Stocks of these cells were grown in incubators with a 5 % CO_2 atmosphere.

Since fluctuation amplitude might depend on the age of the cells, experiments were performed 12-16 hours after seeding MDCK-II cells on the gold electrode of the quartz resonator.

9.3 Results and Discussion

9.3.1 Aliasing Effect

Sampling theory plays an important role in determining the accuracy and feasibility of any digital signal processing scheme. For this reason effects of periodic sampling like aliasing or non ideal sampling have to be considered.

Aliasing is an effect that causes different continuous signals to become indistinguishable when sampled. Figure 9.1 describes this phenomenon by means of a sinusoidal signal. If a sinusoidal signal of frequency f_{org} (figure 9.1 red curve) is sampled with a rate $f_s \leq 2f_{org}$ the resulting samples will be compatible with sinusoidal signal of lower frequency f_{alias} (figure 9.1 blue curve). In general, the frequency of the recorded signal f_{alias} depends on the sampling rate f_s as described by the following equation:[1]

$$f_{alias} = \frac{frac\left(\frac{f_{org}}{f_s}\right)}{\frac{1}{f_{org}} + \frac{1}{f_s}}, \qquad \text{for } \frac{f_{org}}{f_s} < 0.5, \tag{9.1}$$

where "$frac$" denotes the decimal fraction. Furthermore it is possible that two different peaks are mirrored to the same frequency f_{alias}, thus they are no longer distinguishable. In order to avoid aliasing the Nyquist sampling theorem has to be met. This theorem states that the sampling rate must be at least twice the frequency of the highest frequency component in the waveform being sampled.[2, 3]

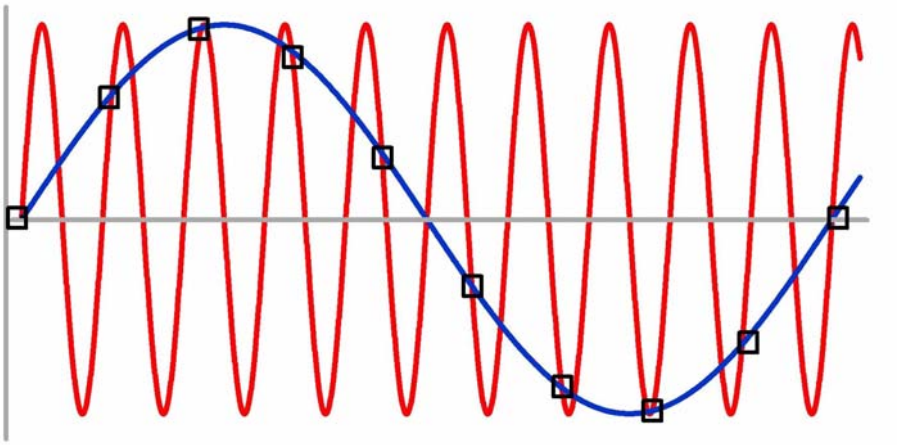

Figure 9.1: Schematic drawing of aliasing effect. A sinusoidal signal of frequency f_{org} (red curve) is sampled with $f_s \leq 2f_{org}$ (black squares). The recorded signal is a sinusoid of frequency $f_{alias} = 2f_{org} - f_s$ (blue curve).

In addition to aliasing we have to consider that the sampling is not ideal. That means that the signal $\zeta(t)$ is sampled with a rectangular sampling function $a(t)$ and not with a progression of delta functions $\delta_T(t)$ (figure 9.2).

Thus the sampled signal is given by following equation:[4]

$$\zeta'(t) = \zeta(t) \cdot a(t). \tag{9.2}$$

The sampling function $a(t)$ can be written as the folding of a rectangular function $a_0(t)$ with a progression of delta functions $\delta_T(t)$:

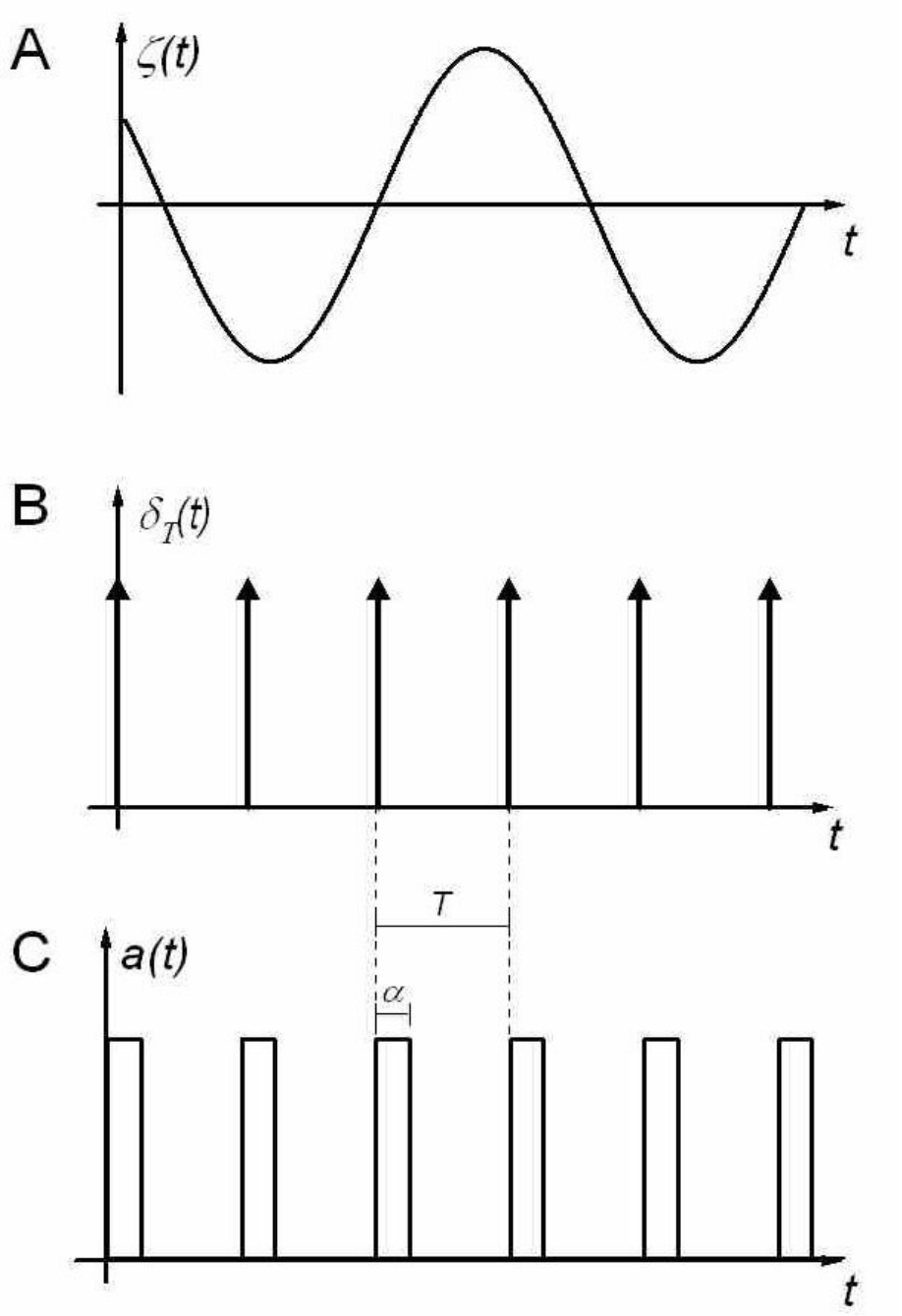

Figure 9.2: (A) Signal $\zeta(t)$. (B) Progression of delta functions $\delta_T(t)$.(C) Rectangular sampling function $a(t)$.

$$a(t) = a_0(t) \star \delta_T(t), \tag{9.3}$$

$$\text{with } a_0(t) = rect\left(\frac{t - \frac{\alpha T}{2}}{\alpha T}\right) \text{ and } \delta_T(t) = \sum_{n=-\infty}^{+\infty} \delta(t - nT), \tag{9.4}$$

where T is the period and α is the width of the rectangle.

Combining equation 9.2 and 9.3 yields equation 9.5:

$$\zeta'(t) = \zeta(t) \left[a_0(t) \star \delta_T(t)\right]. \tag{9.5}$$

The Fourier transformation (FT) $F'(\omega)$ of $\zeta'(t)$ is given by the folding of the FT $F(\omega)$ of $\zeta(t)$ and the FT $A(\omega)$ of $a(t)$:

$$F'(\omega) = \frac{1}{2\pi} \left[F(\omega) \star A(\omega)\right]. \tag{9.6}$$

As the FT of $a_0(t)$ is

$$A_0(\omega) = \alpha T \frac{\sin\left(\frac{\omega\alpha T}{2}\right)}{\frac{\omega\alpha T}{2}} e^{-i\frac{\omega\alpha T}{2}} \tag{9.7}$$

$A(\omega)$ can be written as:

$$A(\omega) = 2\pi\alpha \sum_{n=-\infty}^{+\infty} \frac{\sin(n\pi\alpha)}{n\pi\alpha} e^{-in\pi\alpha} \cdot \delta(\omega - n\omega_0), \tag{9.8}$$

where $\omega_0 = 2\pi/T$. Thus $F'(\omega)$ is given by the following equation:

$$F'(\omega) = \alpha \sum_{n=-\infty}^{+\infty} \frac{\sin(n\pi\alpha)}{n\pi\alpha} e^{-in\pi\alpha} \cdot F(\omega - n\omega_0) \tag{9.9}$$

$$\text{and } |F'(\omega)| = \alpha \sum_{n=-\infty}^{+\infty} \left|\frac{\sin(n\pi\alpha)}{n\pi\alpha}\right| \cdot |F(\omega - n\omega_0)|. \tag{9.10}$$

Equation 9.10 describes that $F(\omega)$ is weighed by a periodic function $w(n, \alpha) = \alpha\frac{\sin(n\pi\alpha)}{n\pi\alpha}$. This effect is shown in figure 9.3. Here, the sampling of a periodic signal with a rectangular sample function $a(t)$ is simulated. In this simulation, the width α of the sample function represents the gate time t_{gate} (here $t_{gate} = 10\ ms$) of the frequency counter used for QCM measurements. Figure 9.3 illustrates that the amplitude $|F'(\omega)|$ is reduced due to the weighing by $w(n, \alpha)$. If the frequency is $\omega = \frac{1}{t_{gate}}$ the amplitude $|F'(\omega)|$ even vanishes.

Equation 9.10 and figure 9.3 demonstrate that the amplitude of frequencies higher than $\omega = \frac{1}{t_{gate}}$ is less than 25 % of the of the original value. Thus we conclude that those frequencies are almost "invisible" with regard to aliasing. Furthermore, equation 9.10 shows that the amplitude of power density spectra obtained by different sampling rates are not comparable due to the relation between the amplitude $|F'(\omega)|$ and α, i.e. the gate time.

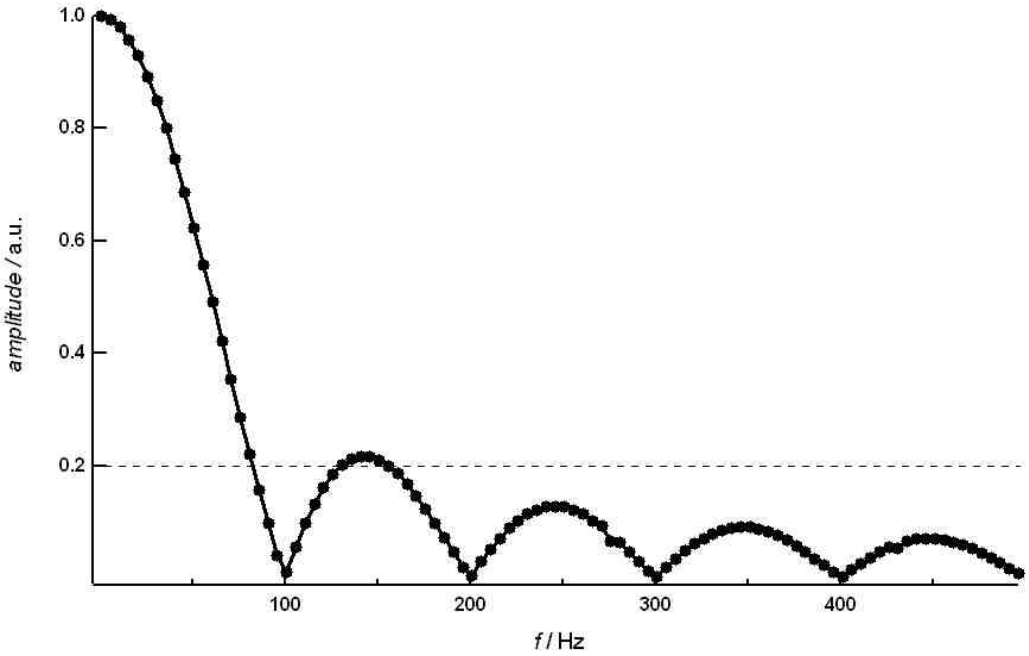

Figure 9.3: Computer simulation of a non ideal sampling of a periodic signal with a rectangular function $a(t)$. Width of the rectangular sampling function $\alpha = 10\ ms$.

The adjustable gate time of the frequency counter and a fixed time of 4.5 ms required to transfer data from the frequency counter via GPIB (General Purpose Interface Bus) to a computer determine the time resolution of QCM-based experiments. By increasing time resolution, i.e. decreasing the gate time of the frequency counter about one order of magnitude, the signal to noise ratio also decreases about one order of magnitude.[6, 5] The relation between the signal to noise ratio and the gate time depends on the frequency counter applied for QCM measurements. The frequency counter Agilent 53132A provides a frequency error which is about one order of magnitude smaller than the frequency error of the frequency counter Agilent 53181A. Thus the signal to noise ratio gets one order of magnitude better.

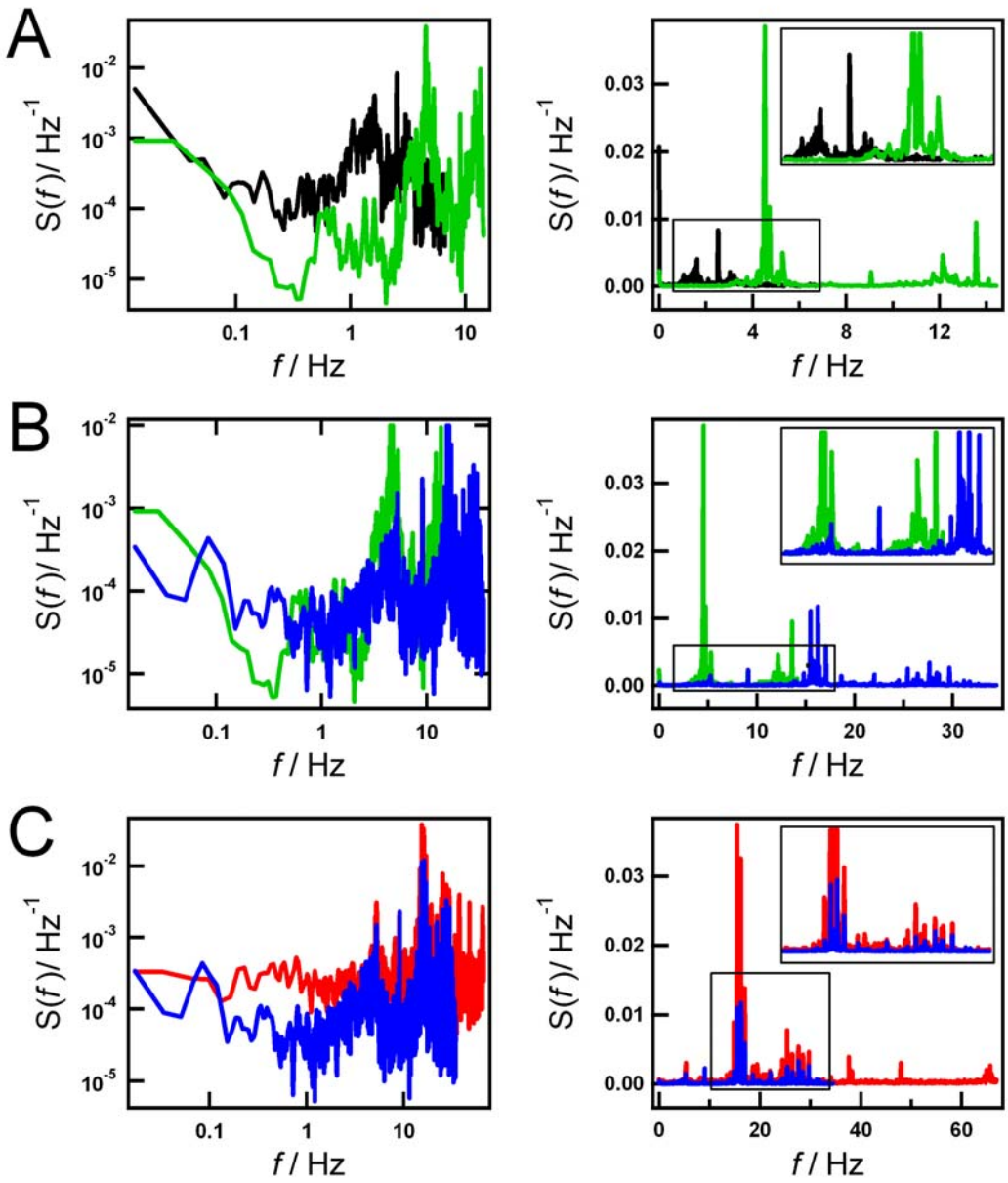

Figure 9.4: Power density spectra of frequency fluctuations recorded with different sampling rates. (A) 13 Hz (black) and 29 Hz (green). (B) 29 Hz (green) and 69 Hz (blue). (C) 69 Hz (blue) and 133 Hz (red). The spectra are plotted logarithmically (left hand side) and linearly (right hand side). The insets show enlargements of a particular part of the spectra.

Aliasing effects were scrutinized by frequency fluctuation measurements employing different sampling rates. Figure 9.4 summarizes the power density spectra of vital MDCK-II cell recorded with 13 Hz (black), 29 Hz (green), 69 Hz (blue) and 133 Hz (red). In addition to logarithmic scale (left hand side) the spectra are shown in a linear scale (right hand side) to emphasize smaller differences. The insets on the right hand side display an enlargement of a particularly interesting parts of the spectra. In figure 9.4A a sampling rate of 13 Hz is compared with sampling rate of 29 Hz. Obviously the position of the broad resonance changes, i.e. it gets shifted to a higher frequency. Furthermore, the broad resonance is split into two peaks. This behavior is characteristic for aliasing effects.

A further increase of the sampling rate to 69 Hz still provides a shift of the resonance due to aliasing effects (figure 9.4B). Moreover, the power in the frequency band increases due to aliasing. However, comparing the spectra obtained by sampling rates of 69 Hz and 133 Hz in figure9.4C no further shift of the resonance can be observed. Both spectra (red and blue curve) show broad resonances at 3-5 Hz (see figure 9.5D1), 15-17 Hz and 25-29 Hz. The power density of the whole spectra obtained by a sampling rate of 133 Hz is significantly higher than those obtained by lower sampling rates. This observations leads back to the poor signal to noise ratio which is related to short gate times as described above. As the position of the broad resonance does not change by alteration of the sampling rate from 69 to 133 Hz, it is straightforward to conclude that this resonances reflect directly the original signal. A sampling rate of 70 ms is hence the best compromise of avoiding aliasing and providing sufficient signal to noise ratio.

9.3.2 Coupling to Vibrations - Independent Movement?

The broad resonance described in chapters 5, 6 ,7 and 8 was considered as an indication for cell motility. It is, however, conceivable that the origin of the broad resonance is a coupling of the cells to vibrations of the building. Living cells might amplify these vibrations and the observed spectra reflect nothing else but these vibrations. As described in chapters 5 and 6 in more detail the resonance vanishes as cells were fixed with PFA. This observation, supported by effects of osmolarity and various drugs, was interpreted as a clear evidence for the biological origin of the signal. However, we have to consider aliasing effects. For this reason, it is imperative to scrutinize whether the resonances observed around 3-5 Hz, 15-17 Hz and 25-29 Hz also vanish due to fixation with PFA. Figure 9.5A shows the power density spectra of vital MDCK-II cells. Three broad resonances are observed: one around 3-5 Hz, another at 15-17 Hz and finally one at 25-29 Hz (red curves in figure 9.5D1-D3). Cross-

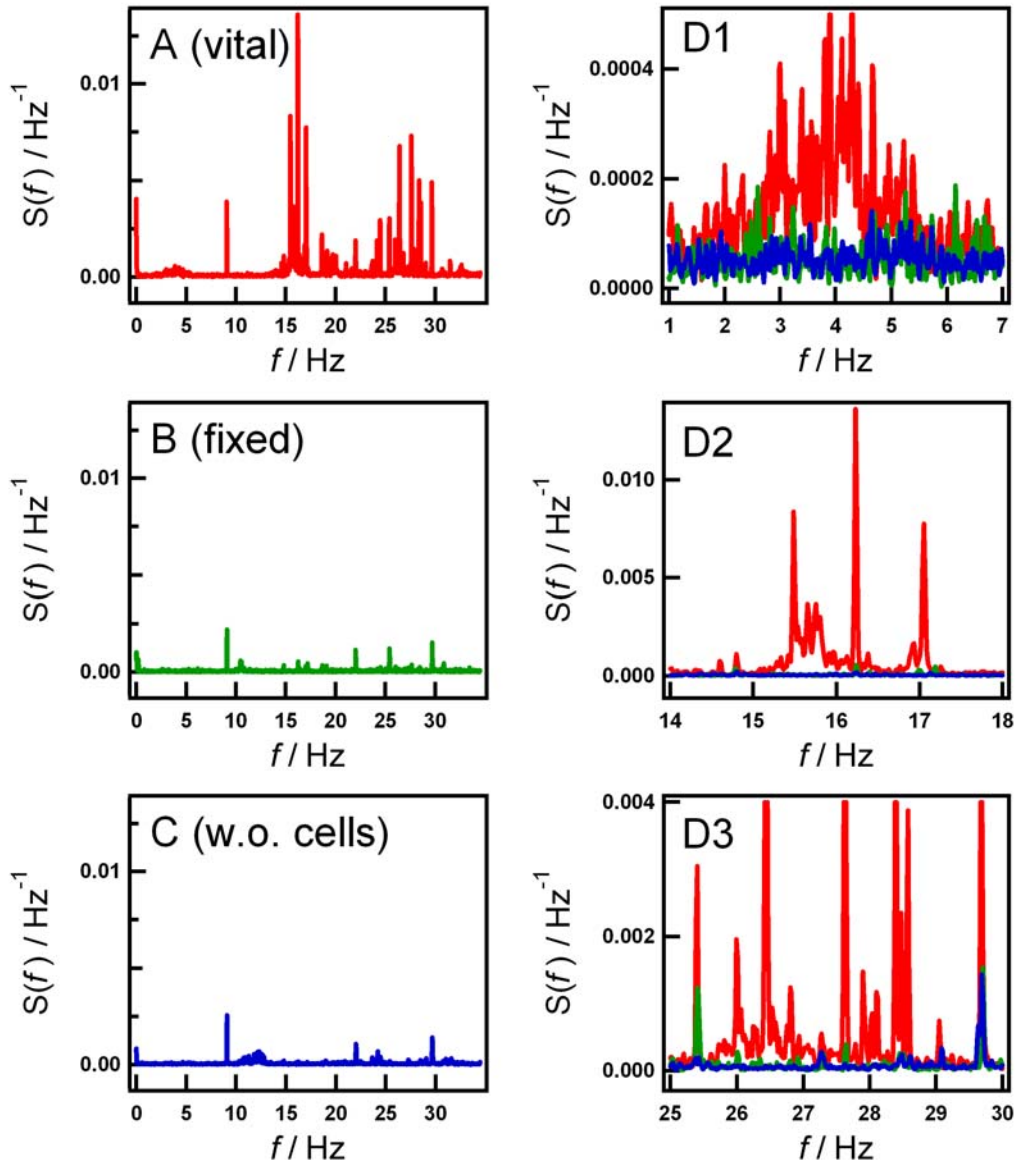

Figure 9.5: Power density spectra of frequency fluctuations recorded with sampling rates of 69 Hz. (A) Vital MDCK-II cells in tissue culture fluid. (B) MDCK-II cells fixed with PFA. (C) Resonator after removal of cells (immersed in tissue culture fluid). (D1-D3) Enlargement of the three broad resonances. (Red) Vital MDCK-II cells. (Green) Fixed MDCK-II cells. (Blue) Resonator after removal of cells.

linking all cell proteins with PFA leads to an obliteration of either resonance (figure 9.5B, green curves in 9.5D1-D3). Finally, the cell layer was removed from the quartz surface mechanically and the electrode was rinsed thoroughly with tissue culture fluid. Figure 9.5C shows the power density spectra of the bare electrode immersed in tissue culture fluid. The power density spectra of vital cells, fixed cells and the bare electrode are compared in figure 9.5D1-D3 (red curve: vital, green curve: fixed, blue curve: without cells). As three resonances are observed in the power density spectra of vital MDCK-II cells, the three different frequency ranges are enlarged (D1: 1-7 Hz, D2: 14-18 Hz, D3: 25-30 Hz). In figure 9.5D1 and D2 the power density spectra of fixed cells as well as the spectrum of the bare quartz show no significant peaks. Around 25-30 Hz two peaks can be observed at 25.4 Hz and 29.8 Hz in each spectra (figure 9.5D3). As the broad resonances found for vital cells around 3-5 Hz, 15-17 Hz and 25-29 Hz (excepted the peaks at 25.4 Hz and 29.8 Hz) vanish after fixation or removal of the cells, it is straightforward to conclude that these resonances are an indication of biological activity of the cells. However coupling of the cells to vibrations of the building can not be ruled out. A monolayer of MDCK-II cells, attached to the surface of the quartz resonator can be modelled as shown in figure 9.6.

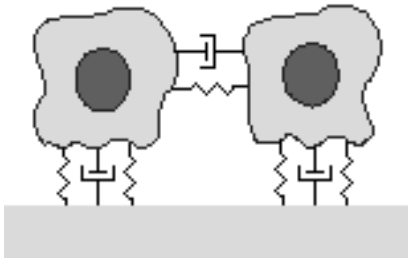

Figure 9.6: Schematic drawing of the cell-cell and cell-substrate coupling via mechanical springs. Energy dissipation is represented by dashpots

Here, cell-substrate as well as cell-cell contacts are represented by mechanical springs and energy dissipation by dashpots. As the cells are coupled via this springs to the substrate it is conceivable that vibrations of the building are transmitted to the cells or a vibrating water column exerts a periodic force to the cells. The elasticity of this springs, i.e. the spring constant, depends on the vitality of the cells. As the vitality is modulated by physiological stimuli the spring constant alters and with it the coupling of the building vibrations to the cells resulting in change of the observed signal. The cell-cell coupling in this model might explain the observed collective

motion of cells.

However, the biological origin of the broad cell resonances remains to be elucidated. Prospective studies might explain this origin and with it the observed collective motion of the cells, which is still poorly understood.

Bibliography

[1] Rodahl, M.; Höök, F.; Krozer, A.; Brzezinski, P.; Kasemo, B. *Rev. Sci. Instrum.* 1995, 66, 3924-3939.

[2] Ramirez, R. W. *The FFT - Fundamentals and Concepts* Prentice-Hall International, Inc., 1985.

[3] Lyons, R. G. *Understanding Digital Signal Processing* Pearson Education, Inc., 2004.

[4] Fliege, N. *Systemtheorie* B. G. Teubner Stuttgart, 1991.

[5] Operating Guide, Frequency Counter HP53181A 225 MHz, 1999, Agilent Technologies, Inc.

[6] Operating Guide, Frequency Counter HP53131A/132A 225 MHz, 2003, Agilent Technologies, Inc.

Chapter 10

Summary and Outlook

The present thesis introduces a novel sensitive technique based on TSM resonators that provides quantitative information about the dynamic properties of biological cells and artificial lipid systems. In order to support and complement results obtained by this method supplementary measurements based on ECIS technique were carried out.

The first part (chapters 3 and 4) deals with artificial lipid systems. In chapter 3 ECIS measurements were used to monitor the adsorption of giant unilamellar vesicles as well as their thermal fluctuations. From dynamic Monte Carlo Simulations the rate constant of vesicle adsorption was determined. Furthermore, analysis of fluctuation measurements reveals Brownian motion reflecting membrane undulations of the adherent liposomes.

In chapter 4 QCM-based fluctuation measurements were applied to quantify nanoscopically small deformations of giant unilamellar vesicles with an external electrical field applied simultaneously. The response of liposomes to an external voltage with shape changes was monitored as a function of cholesterol content and adhesion force.

In the second part (chapters 5 - 8) attention was given to cell motility. It was shown for the first time, that QCM can be applied to monitor the dynamics of living adherent cells in real time. QCM turned out to be a highly sensitive tool to detect the vertical motility of adherent cells with a time resolution in the millisecond regime. The response of cells to environmental changes such as temperature or osmotic stress could be quantified. Furthermore, the impact of cytochalasin D (inhibits actin polymerization) and taxol (facilitate polymerization of microtubules) as well as nocodazole (depolymerizes microtubules) on the dynamic properties of cells was scrutinized. Each drug provoked a significant reduction of the monitored cell shape fluctuations as expected from their biochemical potential. However, not only the abolition of fluctuations was observed but also an increase of motility due

to integrin-induced transmembrane signals. These signals were activated by peptides containing the RGD sequence, which is known to be an integrin recognition motif. Ultimately, two pancreatic carcinoma cell lines, derived from the same original tumor, but known to possess different metastatic potential were studied. Different dynamic behavior of the two cell lines was observed which was attributed to cell-cell as well as cell-substrate interactions rather than motility. Thus one may envision that it might be possible to characterize the motility of different cell types as a function of many variables by this new highly sensitive technique based on TSM resonators.

Finally the origin of the broad cell resonance was investigated. Improvement of the time resolution reveals the "real" frequency of cell shape fluctuations. Several broad resonances around 3-5 Hz, 15-17 Hz and 25-29 Hz were observed and that could unequivocally be assigned to biological activity of living cells. However, the kind of biological process that provokes this synchronized collective and periodic behavior of the cells remains to be elucidated.

Appendix A

Transfer Function of the BVD Equivalent Circuit

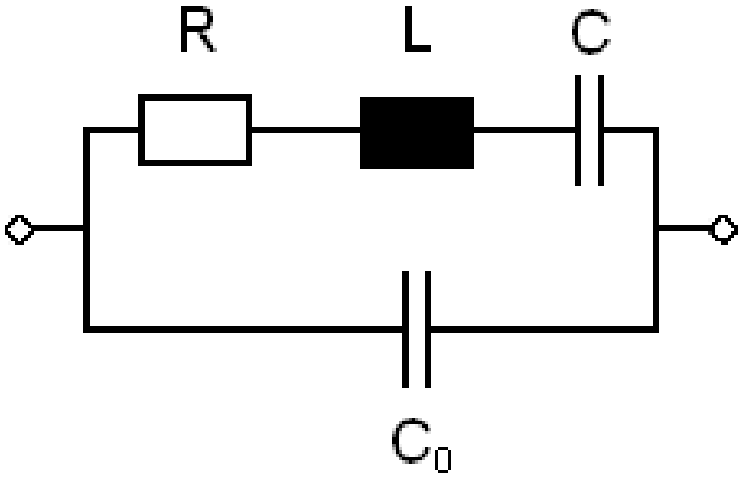

$$|Z| = \left[\left[\frac{R}{R^2 + (\omega L - (\omega C)^{-1})^2}\right]^2 + \left[\frac{\omega C_0 - (\omega L - (\omega C)^{-1})}{R^2 + (\omega L - (\omega C)^{-1})^2}\right]^2\right]^{-\frac{1}{2}} \quad \text{(A.1)}$$

$$\phi = -\frac{180}{\pi} \arctan\left[\frac{\omega C_0 - \omega C - 2\omega^3 C_0 C L - \omega^3 L C^2 + \omega^5 C_0 C^2 L^2 + \omega^3 C_0 C^2 R^2}{\omega^2 R C^2}\right] \quad \text{(A.2)}$$